Dissertation
submitted to the
Combined Faculties of the Natural Sciences and Mathematics
of the Ruperto-Carola-University of Heidelberg. Germany
for the degree of
Doctor of Natural Sciences

Put forward by
Jan Hendrik Stockemer
born in: Cuxhaven
Oral examination: 05.02.2016

Functional renormalization group approach to dynamic critical phenomena

Referees Prof. Dr. Jürgen Berges
Prof. Dr. Jan Martin Pawlowski

Abstract

In this thesis the real time functional renormalization group is applied to investigate dynamic critical phenomena. In the first part, the established method of the functional renormalization group as a tool for the calculation of real time correlation functions is modified to properly incorporate the thermal equilibrium initial conditions.
In the second part, this method is utilized to compute the dynamic critical properties of a system of non-relativistic, bosonic particles. Our result connect to a commonly applied effective description of dynamic critical phenomena.
The third part of the thesis extends these calculations to the relativistic $O(N)$ model. The convergence of parts of the truncation as well as the effects of the chosen cutoff function are tested.
In the last part, the influence of conserved quantities on the dynamic critical properties of a system is discussed. The dynamic universality class of Model C as a simple, effective approximation of the effects of a conserved quantity on the dynamic critical properties of a system is investigated.

Zusammenfassung

Thema dieser Arbeit ist die Untersuchung dynamisch kritischer Phänomene mit Hilfe der Realzeit funktionalen Renomierungsgruppe. Im ersten Abschnitt wird die etablierte Methode der funktionalen Renomierungsgruppe eingeführt und für die Berechnung von Systemen im thermischen Gleichgewicht angepasst.
Der zweite Abschnitt befasst sich mit der Untersuchung der dynamischen Eigenschaften eines nicht-relativitischen, bosonischen Gases in der Nähe eines Phasenübergangs zweiter Ordnung mit besagter Methode.
Im dritten Abschnitt untersuchen wir das relativistische $O(N)$ Model. Wir testen die Konvergenzeigenschaften eines Teiles der angewandten Trunkierungsmethode sowie die Einflüsse verschiedener Regulatorfunktionen.
Der letzte Abschnitt behandelt die Einflüsse der Dynamik von Erhaltungsgrößen auf das kritische Verhalten eines Systems. Wir untersuchen die dynamische Universalitätsklasse Model C als eine effektive Beschreibung der Dynamik gekoppelter Erhaltungsgrößen.

Contents

Chapter 1

Introduction

Second order phase transitions are present in many areas of nature and on the most different scales, from the critical end point in the phase diagram of quantum chromodynamics [81], Bose-Einstein condensation in ultracold atomic gases [60], the critical point in water [78] to early universe inflation [52]. All these transitions share the fact that at the critical point, the average length of correlations spans the whole system. This has the fascinating effect that all internal scales of the system, for example the masses of the involved particles and the range of their interaction, are rendered unimportant compared to this diverging correlation length at the phase transition. Thus, the behaviour of the system is determined by only a few general properties like symmetries and dimensions, manifesting themselves in critical exponents that characterize the power-laws describing most physical properties close to the critical point.
The fascinating consequence is that the critical behavior of physical systems sharing these general properties can be described by the same set of critical exponents despite their possibly very different microscopic properties. This phenomenon is called universality, and systems sharing the same critical exponents are categorized into the same universality class. Investigation of the critical exponents of a universality class will provide information about the critical behavior of all physical systems in class and is therefore generally a rewarding endeavor.
But the diverging correlation length also significantly complicates the analysis of critical phenomena in many common approaches. Infrared divergences and fluctuations on all scales lead to the breakdown of most perturbative approximation methods.

This suggests the application of non-perturbative methods, of which we choose the functional renormalization group [84, 86, 14] in this work. It is based on the concept of successive integration of fluctuations on different scales. Starting at the microscopic description of the system at the ultraviolet scale, fluctuations are included step by step in an effective theory until the infrared scale is reached. This method is very well suited for the description of critical phenomena - not only are the infrared divergences in the critical regime that plague many other approaches regulated by the functional renormalization group, but the scale invariance inherent to second order phase transitions also emerges in a natural way as a fixed point solution in its flow equations.
While the functional renormalization group has been historically employed mainly for the analysis of static properties of critical phase transitions it has recently been adapted to the requirements arising in the investigation of dynamic critical phenomena [12, 20]. The central question in the research of dynamic critical phenomena is that of the value of the dynamic critical exponent z. Similar to the system wide spatial correlations at the critical point indicated by the diverging correlations length, correlations over arbitrary long time scales can be observed at critical phase transitions. These manifest in the divergence of the relaxation time of the system, characterizing the average time span it takes for the system to return back to its equilibrium state after a small perturbation. This phenomenon is called critical slowing down, and the dynamic critical exponent z determines the rate of the divergence of this relaxation time while the system approaches the critical point. so far, research on dynamic critical phenomena has mainly been performed on a phenomenological basis [47, 24, 36]. The dynamic behavior of the system in the vicinity of the critical point is formulated as an effective theory, usually in the form of relaxational dynamics of the order parameter objected to random noise representing the effects of the microscopic modes neglected in this approach. This mesoscopic, effective description of the dynamic characteristics of the system is used as the starting ground for the calculation of its macroscopic critical properties.
In this work, the functional renormalization group is utilized to determine dynamic critical properties based on fundamental, microscopic theories instead of a effective, mesoscopic descriptions thereof.
It will be structured in the following way:

Chapter 2 is opened by a a short introduction to critical phenomena as well as the real time correlation functions we intend to obtain for the examination of dynamic critical properties.

A generating function for said real time correlation functions based on the quantum field theoretical partition function is established as well as the real time functional renormalization group based upon it. We then provide an implementation of the thermal equilibrium initial conditions by utilizing the symmetry properties of correlation functions in thermal equilibrium. This ensures that our functional renormalization group approach incorporates all aspects of the microscopic theory. In the final section, we discuss the manifestation of quantum fluctuations. We are able to show that in thermal equilibrium all effects of quantum fluctuations are encoded in the form of the involved distribution functions, while the so called quantum vertices commonly appearing in these real time approach will have no influence on any of the correlation functions relevant in this work.

In chapter 3, we apply the framework established in the former chapter to a scalar field theory describing a gas of non-relativistic, interacting, bosonic particles [60]. We analyze the dynamic behavior close to the systems second order phase transition associated with Bose-Einsein condensation and compute the related dynamic critical exponent. The calculations of the involved functional renormalization group flow equations as well as their fixed point solutions are discussed in some detail. We find that the relaxational dynamics as well as the random noise usually imposed as an effective theory emerge naturally in our approach, therefore connecting the microscopic theory to the commonly applied mesoscopic descriptions. In the last section of this chapter, the irrelevance of quantum fluctuations for critical phenomena at non-vanishing temperatures is shown on a general level.

Chapter 4 discusses the relativistic $O(N)$ model [71], a theory applicable to a wide range of physical problems from effective descriptions of two flavor QCD [76] to the early universe inflation [52]. We start with the calculation of the functional renormalization group flow equations, their fixed points and the resulting dynamic critical exponent. The convergence of the employed truncation scheme of expansion in the time derivatives is tested, as well as the effects of the application of different cutoff functions on the results. In this context, a frequency dependent cutoff function suitable for the investigation of possible quantum critical regions in the phase diagram of this theory is established. Finally, we propose an ansatz for the examination of the non-relativistic limit and its possible influence on the critical dynamics.

In chapter 5 the effects of the dynamics of conserved quantities on the critical properties of the system are investigated on a mesoscopic level. While

this discussion could support the implementation of said dynamic behavior of conserved quantities on the microscopic approach applied in the former chapters, it is also rewarding in itself. We investigate the critical properties of the dynamic universality class of Model C in the Halperin and Hohenberg classification scheme [47]. Applications of this model are, for example, the description of critical dynamics of mobile impurities [55, 56, 41], structural phase transitions [45] and long wavelength fluctuations near the QCD critical point [6, 80]. Employing the functional renormalization group, we are able to confirm the existence and extend of the so called anomalous scaling region in the plane of order parameter field components and spatial dimensions [70]. While Model C was investigated intensively using perturbative renormalization group approaches [43, 44, 35, 19, 2], no conclusion of this matter could be agreed on. At the end of this chapter, we formulate a mesoscopic action including the dynamics related to the dynamic universality classes of Model A to F in a form viable as a starting point for further functional renormalization group calculation.

This thesis is concluded with a summary of the results and an outlook on possible future extension in chapter 6.

Chapter 2

Real time functional renormalization group

We start this chapter with a short summary of the basic concepts of critical phenomena and the real time correlation functions necessary to investigate dynamic critical properties. A generating functional for these correlation functions in the form of the closed time path functional integral is introduced. The real time functional renormalization group discussed in the next section enables the non-perturbative calculation of said generating functional.
The boundary conditions imposed by thermal equilibrium are included in this functional renormalization group approach by utilizing the symmetry properties of the equilibrium state and their resulting fluctuation dissipation relations. In the final section of this chapter we discuss the manifestation of quantum fluctuations in this approach. We are able to show that in thermal equilibrium states the quantum fluctuations are solely expressed through the distribution functions appearing in the relations between correlation functions, while the so called quantum vertices emerging during the construction of the generating functional for real time correlation functions will have no impact on the calculation of any of the involved physical properties.

2.1 Critical phenomena

The main object of interest in this work are critical phenomena, characterized by the divergence of the correlation length ξ of the system. We will primarily focus on second order phase transitions driven by thermal fluctuations, although we will brush the topic of so the called quantum phase transitions, describing critical phenomena in systems at absolute zero. In

case of said thermally driven second order phase transitions, the system can usually be tuned to a critical point by changing its temperature to a related critical temperature T_C. The rate the correlation length is diverging with while the temperature T of the system approaches the critical temperature T_C is captured by the critical exponent ν:

$$\xi \propto (T - T_C)^{-\nu} . \tag{2.1}$$

According to the scaling hypothesis, several physical observables will follow power law behavior similar to relation (2.1). A very intriguing consequence of the diverging correlation length is the fact that quantitative features of the microscopic theory rendered unimportant by the diverging scale. The properties of the system around the critical point are thoroughly determined by its general, qualitative features, i.e. symmetries, degrees of freedom, dimensions. This hypothesis supported by the observation that very different physical systems can be described by the same set of critical exponents in the vicinity of the critical point. For example, the exponents characterizing the critical point in water are the same as the ones describing the ferromagnetic phase transition.
This phenomenon is called universality, and systems exhibiting the same critical behavior are categorized in the same universality class.
The topic of critical phenomena is covered extensively in the literature, common textbooks are e.g. [67], [59], [50], [87].
So far we focused on the static properties of systems close to the critical temperature, i.e. the length scale on which different parts of the system are correlated at a single point in time, and related equal time properties of the system. The inclusion of dynamic questions, as for example of the propagation and relaxation of a small perturbation to the thermal equilibrium of the system, adds significant complexity to the problem. The static universality classes above split up into different subclasses, called dynamic universality classes.
In addition to the correlation length ξ indicating the average spatial distance on which different parts of the system are correlated at a single point in time, the question after the average time span of correlations in the system arises. This is measured by the relaxation time τ. If the system approaches the critical temperature, this relaxation time is also diverging. This leads to the so called critical slowing down, the fact that perturbations of a system close to the critical temperature relax back to thermal equilibrium on a very large time scale. The rate of divergence of the relaxation time is captured by the

dynamic critical exponent z, which also relates it to the correlation length:

$$\tau \propto (T - T_C)^{-\nu z} \propto \xi^z. \tag{2.2}$$

Our main interest is the calculation of this dynamic critical exponent z. We will extract it from Fourier representation of the spectral function of the system, which is expected to show the scaling behavior

$$\rho(s\,\vec{q}, s^z\,q_0) = s^{\eta-2}\rho(\vec{q}, q_0) \tag{2.3}$$

around the critical point. η is called the anomalous dimension. The exact definition of the spectral function and its Fourier transformation will be shown in the next section.

2.2 Propagators

As they will be at the center of our calculations of critical exponents through this thesis, we will introduce a set of different propagators, their connections and some of their properties here.
First we define the super field $\hat{\zeta}$, which collects any number of fields relevant for our theory, though we limit ourselves to scalar fields in this thesis. Examples for, e.g., the treatment of gauge invariant systems with the functional renormalization group can be found in [37] and [40], for fermionic fields in [26], [38] and [82].
Additionally we will demand the components of ζ to be real. This is not a restriction, as we can formulate any action built from complex field as an action with double the number of real field components.
We start with the spectral function

$$\rho_{ij}(\vec{x}, t_x, \vec{y}, t_y) = i\,\langle\Big[\hat{\zeta}_i(\vec{x}, t_x),\,\hat{\zeta}_j(\vec{y}, t_y)\Big]\rangle\,, \tag{2.4}$$

from which we want to extract the dynamic scaling coefficient z, and the statistical two point function

$$F_{ij}(\vec{x}, t_x, \vec{y}, t_y) = \frac{1}{2}\,\langle\Big\{\hat{\zeta}_i(\vec{x}, t_x),\,\hat{\zeta}_j(\vec{y}, t_y)\Big\}\rangle\,, \tag{2.5}$$

with the commutator $[\,,\,]$ and anti-commutator $\{\,,\,\}$. $\langle . \rangle$ indicates the average of the field operators.
We will use the shorthand notation $x = (\vec{x}, t_x)$ when feasible and convenient, giving $\rho_{ij}(\vec{x}, t_x, \vec{y}, t_y) = \rho_{ij}(x, y)$.

The spectral and statistical correlation functions can be used to calculate the time ordered or Feynman propagator that is used in e.g. perturbative calculations in quantum field theory

$$\begin{aligned} G_{ij}(x,y) &= \langle T\left(\hat{\zeta}_i(x)\hat{\zeta}_j(y)\right)\rangle \\ &= F_{ij}(x,y) - \frac{i}{2}\,\rho_{ij}(x,y)\,\mathrm{sign}(t_x - t_y). \end{aligned} \tag{2.6}$$

We can construct the statistical two point and the spectral function from the propagators

$$G^{>}_{ij}(x,y) = \langle \hat{\zeta}_i(x)\hat{\zeta}_j(y)\rangle\,, \tag{2.7}$$

$$G^{<}_{ij}(x,y) = \langle \hat{\zeta}_j(y)\hat{\zeta}_i(x)\rangle\,, \tag{2.8}$$

in the following way:

$$F_{ij}(x,y) = \frac{1}{2}\left[G^{>}_{ij}(x,y) + G^{<}_{ij}(x,y)\right], \tag{2.9}$$

$$\rho_{ij}(x,y) = G^{>}_{ij}(x,y) - G^{<}_{ij}(x,y). \tag{2.10}$$

The propagators (2.7) and (2.8) have the properties

$$G^{>}_{ij}(x,y)) = G^{<}_{ji}(y,x), \tag{2.11}$$

and, from the fact that we defined our fields to be real and so our field operators to be hermitian,

$$\left(G^{>}_{ij}(x,y)\right)^* = G^{>}_{ji}(y,x) = G^{<}_{ij}(x,y). \tag{2.12}$$

Finally we introduce the retarded and advanced propagator. They are the central objects for linear response calculations around thermal equilibrium [85] and will be relevant in the functional renormalization group calculations throughout this thesis:

$$\begin{aligned} G^{R}_{ij}(x,y) &= i\theta(t_x - t_y)\,\langle\left[\hat{\zeta}_i(x), \hat{\zeta}_i(y)\right]\rangle \\ &= i\theta(t_x - t_y)\left[G^{>}_{ij}(x,y) - G^{<}_{ij}(x,y)\right], \end{aligned} \tag{2.13}$$

$$\begin{aligned} G^{A}_{ij}(x,y) &= -i\theta(t_y - t_x)\,\langle\left[\hat{\zeta}_i(x)\hat{\zeta}_j(y)\right]\rangle \\ &= -i\theta(t_y - t_x)\left[G^{>}_{ij}(x,y) - G^{<}_{ij}(x,y)\right]. \end{aligned} \tag{2.14}$$

$\theta(t)$ is the Heaviside Step Function. The properties (2.11) and (2.12) translate to the retarded and advanced propagator as

$$G^R_{ij}(x,y) = G^A_{ji}(y,x), \tag{2.15}$$

and

$$\left(G^R_{ij}(x,y)\right)^* = G^R_{ij}(x,y), \tag{2.16}$$
$$\left(G^A_{ij}(x,y)\right)^* = G^A_{ij}(x,y). \tag{2.17}$$

The retarded and advanced propagators are real functions for real fields.
We assume translation invariance in space and time here for a moment, as we will work with such exclusively in this thesis. This allows to reformulate our propagators as

$$\begin{aligned} G^R_{ij}(\vec{x},t_x,\vec{y},t_y) &= G^R_{ij}(\vec{x}+\vec{a},t_x+t_a,\vec{y}+\vec{a},t_y+t_a) = G^R_{ij}(\vec{x}-\vec{y},t_x-t_y,0,0) \\ &\equiv G^R_{ij}(\vec{x}-\vec{y},t_x-t_y) \end{aligned} \tag{2.18}$$

and analogous for the other propagators.
We can perform a Fourier transformation with respect to the remaining argument

$$G^R_{ij}(\vec{z},t_z) = \int_{\vec{q},q_0} \exp\left\{i(\vec{z}\vec{q}-t_z q_0)\right\} G^R_{ij}(\vec{q},q_0), \tag{2.19}$$
$$G^R_{ij}(\vec{q},q_0) = \int_{\vec{q},q_0} \exp\left\{-i(\vec{z}\vec{q}-t_z q_0)\right\} G^R_{ij}(\vec{z},t_z). \tag{2.20}$$

For integrations we use the shorthand notations $\int_q = \int_{\vec{q},q_0} = \int \frac{dq_0\, d^d\vec{q}}{(2\pi)^{d+1}}$ and $\int_x = \int_{\vec{x},t} = \int dt\, d^d\vec{x}$. The equations (2.16) and (2.17) cause the following properties for the Fourier transformed propagators

$$G^R_{ji}(-\vec{q},-q_0) = G^A_{ij}(\vec{q},q_0), \tag{2.21}$$
$$\left(G^R_{ij}(\vec{q},q_0)\right)^* = G^R_{ij}(-\vec{q},-q_0) = G^A_{ji}(\vec{q},q_0). \tag{2.22}$$

2.3 Closed time path action

Generating functional

To gain access to the propagators introduced above as well as higher order correlation functions, we construct a generating functional. References discussing the construction of generating functionals for real time correlation

functions are e.g. [58] or [49].
Starting with the partition function for a quantum field theory with general initial conditions

$$Z = \mathrm{Tr}\left[\hat{\rho}\right], \tag{2.23}$$

where ρ is the initial density matrix. This covers all possible equilibrium and nonequilibrium situations.
Correlation functions of N different field operators are defined in quantum field theory as

$$\langle \hat{\zeta}_{i_1}(\vec{x}_1, t_1)...\hat{\zeta}_{i_N}(\vec{x}_N, t_N)\rangle \equiv \mathrm{Tr}\left[\hat{\rho}\,\hat{\zeta}_{i_1}(\vec{x}_1, t_1)...\hat{\zeta}_{i_N}(\vec{x}_N, t_N)\right]. \tag{2.24}$$

To directly extract correlation functions like (2.24) from the partition function (2.23), we introduce source functions:

$$Z_C\left[J\right] = \mathrm{Tr}\left[\hat{\rho}\,\hat{T}_C\,\exp\left\{i\int_{x,C} J_a(x)\hat{\zeta}_a(x)\right\}\right]. \tag{2.25}$$

Here and from here on the summation over equal indices is implicit.
The introduction of sources in the form of the scalar functions $J_i(x)$ allows us to gain correlation functions by functional derivatives of the partition function with respect to these sources:

$$\begin{aligned}\langle T_C\hat{\zeta}_{i_1}(\vec{x}_1, t_1)...\hat{\zeta}_{i_N}(\vec{x}_N, t_N)\rangle &= \frac{\delta^N Z_C\left[J\right]}{i\delta J_{i_1}(\vec{x}_1, t_1)...i\delta J_{i_N}(\vec{x}_N, t_N)}|_{J=0} \\ &= \mathrm{Tr}\left[\hat{\rho}\,\hat{T}_C\,\hat{\zeta}_{i_1}(\vec{x}_1, t_1)...\hat{\zeta}_{i_N}(\vec{x_N}, t_N)\right]. \end{aligned} \tag{2.26}$$

The integration index C marks the integration contour over time, $\int_{x,C} = \int d^d\vec{x}\int_C dt$, and $\hat{T}_C$ orders all following operators according to their position on this time path C.
There are different choices possible for the form of the contour, depending on the type of correlation function we want to calculate. We can only access correlation functions with time arguments on the chosen contour.

As we are interested in real-time correlation functions, we will choose the contour shown in 2.1. This allows us to calculate all time ordered correlation functions with real time arguments from the generating functional (2.25), and in particular the time ordered real-time propagators.

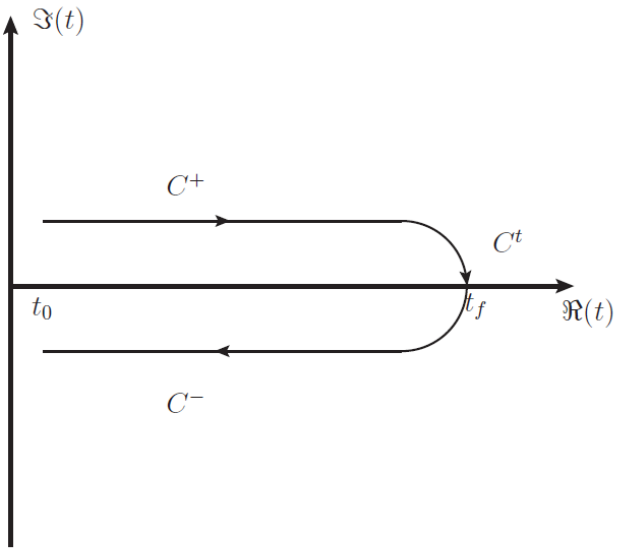

Figure 2.1: Sketch of the time contour the sources are defined on. It is separated into the forward part C^+, running from the initial time t_0 to the final time t_f, the turning part C^t and the backwards part C^- running from t_f back to t_0

We may separate the contour into the three parts seen in figure 2.1

$$\begin{aligned}\int_{x,C} J_a(x)\,\hat{\zeta}_a(x) &= \int_{x,C^+} J_a^+(x)\,\hat{\zeta}_a^+(x) + \int_{x,C^-} J_a^-(x)\,\hat{\zeta}_a^-(x) \\ &= \int_x \left(J_a^+(x)\,\hat{\zeta}_a^+(x) - J_a^-(x)\,\hat{\zeta}_a^-(x) \right) \end{aligned} \tag{2.27}$$

The sources on the turning part C^t of the contour have been set to zero, as we have no interest in correlation functions involving fields living on this part of the contour.
The indices $(+,-)$ indicate the fields and sources only defined on the forward or backward part of the contour. By taking functional derivatives with respect to the sources on the different parts of the contour, we can create different forms of time ordering for the field operators in our correlation

functions. For example, we get the four two-point functions

$$\langle \hat{T}\hat{\zeta}_i(x_1)\hat{\zeta}_j(x_2)\rangle = \frac{\delta^2 Z_C\left[J^+,J^-\right]}{i\delta J_i^+(x_1)\, i\delta J_j^+(x_2)}|_{J^+,J^-=0} \tag{2.28}$$

$$\langle \hat{T}_R\hat{\zeta}_i(x_1)\hat{\zeta}_j(x_2)\rangle = \frac{\delta^2 Z_C\left[J^+,J^-\right]}{i\delta J_i^-(x_1)\, i\delta J_j^-(x_2)}|_{J^+,J^-=0} \tag{2.29}$$

$$\langle \hat{\zeta}_i(x_1)\hat{\zeta}_j(x_2)\rangle = \frac{\delta^2 Z_C\left[J^+,J^-\right]}{i\delta J_i^-(x_1)\, i\delta J_j^+(x_2)}|_{J^+,J^-=0} \tag{2.30}$$

$$\langle \hat{\zeta}_i(x_2)\hat{\zeta}_j(x_1)\rangle = \frac{\delta^2 Z_C\left[J^+,J^-\right]}{i\delta J_i^+(x_1)\, i\delta J_j^-(x_2)}|_{J^+,J^-=0}. \tag{2.31}$$

Connected correlation functions can be created by taking the derivatives of the logarithm of the generating functional instead:

$$\begin{aligned} G_{ij}^{++}(x_1,x_2) &= \langle \hat{T}\hat{\zeta}_i(x_1)\hat{\zeta}_j(x_2)\rangle - \langle\hat{\zeta}_i(x_1)\rangle\langle\hat{\zeta}_j(x_2)\rangle \\ &= \frac{\delta^2 \ln\left(Z_C\left[J^+,J^-\right]\right)}{i\delta J_i^+(x_1)\, i\delta J_j^+(x_2)}|_{J^+,J^-=0} \end{aligned} \tag{2.32}$$

$$\begin{aligned} G_{ij}^{--}(x_1,x_2) &= \langle \hat{T}_R\hat{\zeta}_i(x_1)\hat{\zeta}_j(x_2)\rangle - \langle\hat{\zeta}_i(x_1)\rangle\langle\hat{\zeta}_j(x_2)\rangle \\ &= \frac{\delta^2 \ln\left(Z_C\left[J^+,J^-\right]\right)}{i\delta J_i^-(x_1)\, i\delta J_j^-(x_2)}|_{J^+,J^-=0} \end{aligned} \tag{2.33}$$

$$\begin{aligned} G_{ij}^{-+}(x_1,x_2) &= \langle \hat{\zeta}_i(x_1)\hat{\zeta}_j(x_2)\rangle - \langle\hat{\zeta}_i(x_1)\rangle\langle\hat{\zeta}_j(x_2)\rangle \\ &= \frac{\delta^2 \ln\left(Z_C\left[J^+,J^-\right]\right)}{i\delta J_i^-(x_1)\, i\delta J_j^+(x_2)}|_{J^+,J^-=0} \end{aligned} \tag{2.34}$$

$$\begin{aligned} G_{ij}^{+-}(x_1,x_2) &= \langle \hat{\zeta}_i(x_2)\hat{\zeta}_j(x_1)\rangle - \langle\hat{\zeta}_i(x_1)\rangle\langle\hat{\zeta}_j(x_2)\rangle \\ &= \frac{\delta^2 \ln\left(Z_C\left[J^+,J^-\right]\right)}{i\delta J_i^+(x_1)\, i\delta J_j^-(x_2)}|_{J^+,J^-=0}. \end{aligned} \tag{2.35}$$

Three of these propagators functions can be connected to the propagators (2.7), (2.8) and (2.6):

$$G_{ij}^{++}(x_1,x_2) = G_{ij}(x_1,x_2) \tag{2.36}$$

$$G_{ij}^{-+}(x_1,x_2) = G_{ij}^{>}(x_1,x_2) \tag{2.37}$$

$$G_{ij}^{+-}(x_1,x_2) = G_{ij}^{<}(x_1,x_2). \tag{2.38}$$

The fourth one, $G_{ij}^{--}(x_1,x_2)$ resembles the Feynman propagator (2.6) with inverse time ordering $\hat{T}_R$. If we express the time ordering through Heaviside

Theta functions,

$$\begin{aligned}\langle \hat{T}\hat{\zeta}_i(\vec{x}_1,t_1)\hat{\zeta}_j(\vec{x}_2,t_2)\rangle =&\theta(t_1-t_2)\,\langle \hat{\zeta}_i(\vec{x}_1,t_1)\hat{\zeta}_j(\vec{x}_2,t_2)\rangle \\ &+\theta(t_2-t_1)\,\langle \hat{\zeta}_j(\vec{x}_2,t_2)\hat{\zeta}_i(\vec{x}_1,t_1)\rangle, \qquad (2.39)\\ \langle \hat{T}_R\hat{\zeta}_i(\vec{x}_1,t_1)\hat{\zeta}_j(\vec{x}_2,t_2)\rangle =&\theta(t_1-t_2)\,\langle \hat{\zeta}_j(\vec{x}_2,t_2)\hat{\zeta}_i(\vec{x}_1,t_1)\rangle \\ &+\theta(t_2-t_1)\,\langle \hat{\zeta}_i(\vec{x}_1,t_1)\hat{\zeta}_j(\vec{x}_2,t_2)\rangle, \qquad (2.40)\end{aligned}$$

we can easily see a relation between these propagators:

$$G^{++}(x_1,x_2)+G^{--}(x_1,x_2)=G^{+-}(x_1,x_2)+G^{-+}(x_1,x_2). \qquad (2.41)$$

Functional integral

We now want to express our generating functional as a functional integral. We can represent the trace in the eigenbasis of the $\hat{\zeta}^+$ operator and insert additional unity expressions constructed of eigenvectors of the $\hat{\zeta}^+$ and $\hat{\zeta}^-$ operators at different times to get:

$$\begin{aligned}Z\left[J^+,J^-\right]=\int D\zeta^+(\vec{x};t_i)D\zeta^+(\vec{x};t_f)D\zeta^-(\vec{x};t_i)D\zeta^-(\vec{x};t_f)\,\langle\zeta^+(\vec{x};t_i)|\,\hat{\rho}\,|\zeta^-(\vec{x},t_i)\rangle \\ \times\langle\zeta^-(\vec{x},t_i)|\zeta^-(\vec{x},t_f)\rangle\,\langle\zeta^-(\vec{x},t_f)|\zeta^+(\vec{x},t_f)\rangle\,\langle\zeta^+(\vec{x},t_f)|\zeta^+(\vec{x},t_i)\rangle\,. \qquad (2.42)\end{aligned}$$

The functional integral is performed over all different spatial configurations of the fields, for the intricacies of functional integrals compare e.g. references [30] or [3]. The transition amplitudes can be expressed in the usual way as

$$\langle\zeta^-(\vec{x},t_i)|\zeta^-(\vec{x},t_f)\rangle=\int_{t_i}^{t_f}D\zeta^-(\vec{x},t)\exp\left\{-iS[\zeta^-]-i\int_{\vec{x},t}\zeta^-(\vec{x},t)J^-(\vec{x},t)\right\}, \qquad (2.43)$$

$$\langle\zeta^+(\vec{x},t_f)|\zeta^+(\vec{x},t_i)\rangle=\int_{t_i}^{t_f}D\zeta^+(\vec{x},t)\exp\left\{iS[\zeta^+]+i\int_{\vec{x},t}\zeta^+(\vec{x},t)J^+(\vec{x},t)\right\}. \qquad (2.44)$$

The functional integral is now performed over all field configurations in time and space that match the boundary conditions set by the transition amplitude. Inserting this in the partition function:

$$
\begin{aligned}
Z\left[J^+,J^-\right] &= \int D\zeta^+(\vec{x},t)D\zeta^-(\vec{x},t)\left\langle\zeta^+(\vec{x};t_i)\right|\hat{\rho}\left|\zeta^-(\vec{x},t_i)\right\rangle\left\langle\zeta^-(\vec{x},t_f)|\zeta^+(\vec{x},t_f)\right\rangle \\
&\quad\times\exp\left\{i\left(S[\zeta^+]-S[\zeta^-]+\int_{\vec{x},t}\left(\zeta^+(\vec{x},t)J^+(\vec{x},t)-\zeta^-(\vec{x},t)J^-(\vec{x},t)\right)\right)\right\} \\
&= \int D\zeta^+(\vec{x},t)D\zeta^-(\vec{x},t) \\
&\quad\times\exp\left\{i\left(F[\zeta^+,\zeta^-,\hat{\rho}]+S[\zeta^+]-S[\zeta^-]\right)\right\} \\
&\quad\times\exp\left\{i\int_{\vec{x},t}\left(\zeta^+(\vec{x},t)J^+(\vec{x},t)-\zeta^-(\vec{x},t)J^-(\vec{x},t)\right)\right\} \qquad (2.45)
\end{aligned}
$$

In the last step we expressed the initial conditions and the transition amplitude at the turning point of the contour as an exponential

$$
\left\langle\zeta^-(\vec{x},t_f)|\zeta^+(\vec{x},t_f)\right\rangle\left\langle\zeta^+(\vec{x};t_i)\right|\hat{\rho}\left|\zeta^-(\vec{x},t_i)\right\rangle = \exp\left\{iF[\zeta^+,\zeta^-,\hat{\rho}]\right\}. \qquad (2.46)
$$

Keldysh action

We define new fields

$$
\zeta(x) = \frac{1}{2}\left(\zeta^+(x)+\zeta^-(x)\right), \qquad (2.47)
$$

$$
\tilde{\zeta}(x) = \left(\zeta^+(x)-\zeta^-(x)\right). \qquad (2.48)
$$

These will prove to be more convenient and physically intuitive, as we will see below.
The inverse of this transformation is

$$
\zeta^+(x) = \zeta(x)+\frac{1}{2}\tilde{\zeta}(x), \qquad (2.49)
$$

$$
\zeta^-(x) = \zeta(x)-\frac{1}{2}\tilde{\zeta}(x). \qquad (2.50)
$$

In our functional integral (2.45), the action appears in the combination $S[\zeta^+]-S[\zeta^-]$. If we assume a polynomial form of the action, the individual terms transform straightforwardly. For terms involving only one type

of field we get

$$\begin{aligned}\left(\zeta_i^+(x)\right)^n - \left(\zeta_i^-(x)\right)^n &= \left(\zeta_i(x) + \frac{1}{2}\tilde{\zeta}_i(x)\right)^n - \left(\zeta_i(x) - \frac{1}{2}\tilde{\zeta}_i(x)\right)^n \\ &= \sum_{k=0}^{n} \binom{n}{k} \left[(\zeta_i(x))^{n-k} \left(\frac{\tilde{\zeta}_i(x)}{2}\right)^k - (\zeta_i(x))^{n-k} \left(\frac{-\tilde{\zeta}_i(x)}{2}\right)^k \right] \\ &= \sum_{k=0,\text{k odd}}^{n} 2\binom{n}{k} (\zeta_i(x))^{n-k} \left(\frac{\tilde{\zeta}_i(x)}{2}\right)^k . \end{aligned} \tag{2.51}$$

We can generalize this to terms constructed from N different types of fields

$$\begin{aligned}&\prod_{i=1}^{N} \left(\zeta_i^+(x)\right)^{n_i} - \prod_{i=1}^{N} \left(\zeta_i^-(x)\right)^{n_i} \\ =&\prod_{i=1}^{N} \sum_{k_i=0,\sum_i k_i \text{odd}}^{n_i} 2\binom{n_i}{k_i} (\zeta_i(x))^{n_i-k_i} \left(\frac{\tilde{\zeta}_i(x)}{2}\right)^{k_i} . \end{aligned} \tag{2.52}$$

Again, we see that only terms with an overall odd number of response fields ζ_i appear.
If we expand the term constructed from a single field (2.51) to first order in the response fields, we get the simple expression

$$\left(\zeta_i^+(x)\right)^n - \left(\zeta_i^-(x)\right)^n = \tilde{\zeta}_i(x)\partial_{\zeta_i} \left(\zeta_i(x)\right)^n + O\left(\tilde{\zeta}_i^2(x)\right) \tag{2.53}$$

and an analogous expression for the term composed of multiple fields :

$$\prod_{i=1}^{N} \left(\zeta_i^+(x)\right)^{n_i} - \prod_{i=1}^{N} \left(\zeta_i^-(x)\right)^{n_i} = \sum_{j=1}^{N} \tilde{\zeta}_j(x)\partial_{\zeta_j} \prod_{i=1}^{N} \left(\zeta_i(x)\right)^{n_i} + O\left(\tilde{\zeta}_i^2(x)\right). \tag{2.54}$$

Instead of repeating the procedure for gradient dependent terms, we will just declare the different types of field derivatives as separate fields in our field vector. This finally leads us to the expression

$$S[\zeta^+] - S[\zeta^-] = \int_x \sum_{i=1}^{N} \tilde{\zeta}_i(x) \frac{\delta S[\zeta]}{\delta \zeta_i(x)} + + O\left(\tilde{\zeta}_i^2(x)\right). \tag{2.55}$$

This matches exactly the action we would get from a classical approach, where the generating functional is constructed by averaging over the solutions of the classical equations of motion. For this reasons, all terms in the keldysh action with a combined power in the tilde fields of three and higher are considered quantum contributions, as they do not appear in the corresponding classical action. More details on this matter can be found in reference [9].
The source terms transform as

$$\begin{aligned}&\int_x \left(\zeta_i^+(x)J_i^+(x) - \zeta_i^-(x)J_i^-(x)\right)\\ =&\int_x \left[\zeta_i(x)\tilde{J}_i(x) + \tilde{\zeta}_i(x)J_i(x)\right].\end{aligned} \tag{2.56}$$

where we defined new sources similar to the fields:

$$J(x) = \frac{1}{2}\left(J^+(x) + J^-(x)\right), \tag{2.57}$$

$$\tilde{J}(x) = \left(J^+(x) - J^-(x)\right). \tag{2.58}$$

Another advantage of the field transformation (2.47) will reveal if we examine the behavior of the system physical choices of the sources. It is necessary to distinguish between the sources on the upper and lower part of the time path shown in figure 2.1 for purposes of time ordering in our generating functional. But for all physically relevant situations J^+ and J^- have to be the same. So after all functional derivatives have been taken, we will always set the sources to a physical form $J^+ = J^- = J^P$. In this thesis, this will usually be $J^P = 0$, as we are interested in calculating equilibrium correlation functions.
For physical values of the sources though, we see that the expectation values of the plus fields $\chi_i^+(x) \equiv \langle\zeta_i^+(x)\rangle$ and minus fields $\chi_i^-(x) \equiv \langle\zeta_i^-(x)\rangle$ have to be the same, as for one point functions there is no time ordering relevant:

$$\chi_i^+(x)|_{J^-=J^P}^{J^+=J^P} = \mathrm{Tr}\left[\hat{\rho}\hat{\zeta}(x)e^{i\int_x \hat{\zeta}_i(x)J_i^P(x)}\right] = \chi_i^-(x)|_{J^-=J^P}^{J^+=J^P}. \tag{2.59}$$

As a consequence, the expectation values of the fields (2.47) for physical sources are

$$\chi_i(x)|_{\tilde{J}=0}^{J=J^P} = \frac{1}{2}\left[\chi_i^+(x)|_{J^-=J^P}^{J^+=J^P} + \chi_i^-(x)|_{J^-=J^P}^{J^+=J^P}\right] \tag{2.60}$$

$$\tilde{\chi}_i(x)|_{\tilde{J}=0}^{J=J^P} = \chi_i^+(x)|_{J^-=J^P}^{J^+=J^P} - \chi_i^-(x)|_{J^-=J^P}^{J^+=J^P} = 0. \tag{2.61}$$

One field delivers the actual physical field expectation value while the other one vanishes. We have effectively separated our field degrees of freedom into the physical field content and the degrees of freedom merely needed for organizing our time ordering. The field χ_i is therefore called the physical field, and for the same reason our notation does not distinguish it from the field in the original action. The field denoted with a tilde is usually called the response field, for its role in linear response calculations, the quantum field as it differentiates between classical and quantum systems in its higher vertices and sometimes it is just named as bookkeeping field.

2.4 Effective action

As we now have brought our fields to a more convenient and physically intuitive form, we will proceed to do the same with the whole generating functional (2.25). To get connected correlation functions like (2.32) directly, we modify it as

$$W[J, \tilde{J}] = -i \ln Z[J, \tilde{J}]. \tag{2.62}$$

This produces the field expectation values

$$\chi(x) = \langle \zeta(x) \rangle = \frac{\delta W[J, \tilde{J}]}{\delta \tilde{J}(x)}, \tag{2.63}$$

$$\tilde{\chi}(x) = \langle \tilde{\zeta}(x) \rangle = \frac{\delta W[J, \tilde{J}]}{\delta J(x)}, \tag{2.64}$$

and the propagators

$$G^R_{ij}(x_1, x_2) = \frac{\delta W[J, \tilde{J}]}{\delta \tilde{J}_i(x_1) \delta J_j(x_2)}, \tag{2.65}$$

$$G^A_{ij}(x_1, x_2) = \frac{\delta W[J, \tilde{J}]}{\delta J_i(x_1) \delta \tilde{J}_j(x_2)}, \tag{2.66}$$

$$F_{ij}(x_1, x_2) = -i \frac{\delta W[J, \tilde{J}]}{\delta \tilde{J}_i(x_1) \delta \tilde{J}_j(x_2)}. \tag{2.67}$$

We can perform a Legendre transformation of this generating functional (2.62) to obtain the so called effective action

$$\begin{aligned} \Gamma[\chi, \tilde{\chi}] =& W[J(\chi, \tilde{\chi}), \tilde{J}(\chi, \tilde{\chi})] \\ & - \int_x \left[\chi_i(x) \tilde{J}_i(\chi(x), \tilde{\chi}(x)) + \tilde{\chi}_i(x) J_i(\chi(x), \tilde{\chi}(x)) \right]. \end{aligned} \tag{2.68}$$

The functions $J(\chi, \tilde{\chi})$ and $\tilde{J}(\chi, \tilde{\chi})$ can be determined by inversion of (2.63) and (2.64). The effective action is a very intuitive functional, as it resembles the classical, microscopic action used in our path integral but already includes all fluctuations. It gives access to several thermodynamic quantities as well as still functioning as the generating functional for connected correlation functions.
The equations of motions for the macroscopic fields χ and $\tilde{\chi}$ are obtained by

$$\frac{\delta \Gamma[\chi, \tilde{\chi}]}{\delta \tilde{\chi}_i(x)} = -J_i(x) \tag{2.69}$$

$$\frac{\delta \Gamma[\chi, \tilde{\chi}]}{\delta \chi_i(x)} = -\tilde{J}_i(x) \tag{2.70}$$

and thus analogous to the classical equations of motion produced by the microscopic action.
Before we start to construct the propagators from the effective action, we will introduce the functional renormalization group, and with that a modified, scale dependent form of the effective action.

2.5 Functional renormalization group on the closed time path

While we theoretically established a framework to obtain all needed correlation functions by the generating functional (2.68), the calculation of the

functional integral is possible only for a very limited and specific number of systems. At some point approximations have to be made. The Functional Renormalization Group, while an exact and with a few exceptions again not solvable formulation of the problem in itself, offers different efficient and intuitive approximation methods for the field of critical phenomena.
There are plenty of extensive reviews covering the euclidean [25, 53, 14, 4], and the closed time path [10, 12, 39, 48, 51] functional renormalization group.
The main idea of the functional renormalization group is the step by step inclusion of the fluctuations in the functional integral. For this purpose, we add an additional, artificial term to the action:

$$S_k[\zeta, \tilde{\zeta}] = S[\zeta, \tilde{\zeta}] + \Delta S_k[\zeta, \tilde{\zeta}]. \tag{2.71}$$

The index k is the Functional Renormalization Group scale or parameter, controlling the amount of integrated out fluctuations. Its exact meaning will be specified by the choice of the artificial term. For its general form we choose

$$\Delta S_k[\zeta, \tilde{\zeta}] = -\int_{x_1,x_2} \tilde{\zeta}_i(x_1) R_k^{ij}(x_1, x_2) \zeta_j(x_2). \tag{2.72}$$

Different combinations of fields in the bilinear form would also be allowed, but this specific choice will be sufficient for our purposes.
R_k is the (scale dependent) cutoff function. It can be chosen from a variety of functions, with the restrictions

$$\lim_{k\to 0} R_k \to 0, \tag{2.73}$$

$$\lim_{k\to \Lambda} R_k \to \infty. \tag{2.74}$$

Λ is the ultraviolet cutoff of the theory. The reason for this conditions becomes clear if we examine the effects of the cutoff term (2.72) on the effective action
If we define a new, scale dependent effective action similar to (2.68) called the effective average action,

$$\begin{aligned}\Gamma_k[\chi, \tilde{\chi}] =& W_k[J(\chi, \tilde{\chi}), \tilde{J}(\chi, \tilde{\chi})] - \Delta S_k[\chi, \tilde{\chi}] \\ &- \int_x \left[\chi_i(x)\tilde{J}_i(\chi(x), \tilde{\chi}(x)) + \tilde{\chi}_i(x) J_i(\chi(x), \tilde{\chi}(x))\right],\end{aligned} \tag{2.75}$$

we will see that the restrictions on the cutoff function translate to the following properties of the effective action

$$\lim_{k\to 0} \Gamma_k[\chi,\tilde{\chi}] \to \Gamma[\chi,\tilde{\chi}], \tag{2.76}$$

$$\lim_{k\to \Lambda} \Gamma_k[\chi,\tilde{\chi}] \to S[\chi,\tilde{\chi}]. \tag{2.77}$$

So any cutoff function with the properties (2.73) ans (2.74) will interpolate smoothly between the classical, microscopic action we base our calculations on and the full effective action with all fluctuations included.
As we can not calculate the full path integral with or without a cutoff function for most systems, we need a method of following the changes on the action produced by changes of the scale parameter. We will observe the effects of an infinitesimal change by taking the scale derivative of the effective action:

$$\partial_k \Gamma_k[\chi,\tilde{\chi}] = \frac{-i}{2} \operatorname{Tr}\left[G_k^R\, \partial_k R_k + G_k^A\, \partial_k R_k\right] \tag{2.78}$$

This is the real time version of the Wetterich equation. The trace here acts on all indices of the object, coordinates as well as the field indices. As an example, a trace of three propagators or similar objects could be resolved as:

$$\operatorname{Tr}\left[ABC\right] = \sum_{ijk} \int_{q,q_1,q_2} A_{ij}(q,q_1) B_{jk}(q_1,q_2) C_{ki}(q_2,q). \tag{2.79}$$

For translational invariant systems these objects will typically contain Dirac delta functions, reducing the number of integrations in such a trace to one.

Scale dependent propagators

The scale dependent propagators can be calculated directly from the effective average action (2.75):

$$G_k^R = -\left[\left(\Gamma_k^{\tilde{\chi}\chi} + R_k\right) - \Gamma_k^{\tilde{\chi}\tilde{\chi}} \left(\Gamma_k^{\chi\tilde{\chi}} + R_k\right)^{-1} \Gamma_k^{\chi\chi}\right]^{-1}, \tag{2.80}$$

$$G_k^A = -\left[\left(\Gamma_k^{\chi\tilde{\chi}} + R_k\right) - \Gamma_k^{\chi\chi} \left(\Gamma_k^{\tilde{\chi}\chi} + R_k\right)^{-1} \Gamma_k^{\tilde{\chi}\tilde{\chi}}\right]^{-1}, \tag{2.81}$$

$$iF_k = -\left[\Gamma_k^{\chi\chi} - \left(\Gamma_k^{\chi\tilde{\chi}} + R_k\right) \left(\Gamma_k^{\tilde{\chi}\tilde{\chi}}\right)^{-1} \left(\Gamma_k^{\tilde{\chi}\chi} + R_k\right)\right]^{-1}, \tag{2.82}$$

$$i\tilde{F}_k = -\left[\Gamma_k^{\tilde{\chi}\tilde{\chi}} - \left(\Gamma_k^{\tilde{\chi}\chi} + R_k\right) \left(\Gamma_k^{\chi\chi}\right)^{-1} \left(\Gamma_k^{\chi\tilde{\chi}} + R_k\right)\right]^{-1}. \tag{2.83}$$

Here the shorthand notation $\Gamma_k^{\tilde{\chi}\chi} = \frac{\delta^2\Gamma_k[\chi,\tilde{\chi}]}{\delta\tilde{\chi}\delta\chi}$ has been introduced.
If we evaluate these for physical sources, i.e. vanishing response fields, we get the much simpler expressions

$$G_k^R = -\frac{1}{\Gamma_k^{\tilde{\chi}\chi} + R_k} \tag{2.84}$$

$$G_k^A = -\frac{1}{\Gamma_k^{\chi\tilde{\chi}} + R_k} \tag{2.85}$$

$$iF_k = G_k^R \Gamma_k^{\tilde{\chi}\tilde{\chi}} G_k^A \tag{2.86}$$

$$i\tilde{F}_k = 0 \tag{2.87}$$

this is due to the fact that all functional derivatives of the effective average only with respect to the physical fields χ vanish if evaluated for physical sources, i.e., evaluated for vanishing response fields $\tilde{\chi} = 0$ [22]:

$$\frac{\delta^n \Gamma_k[\chi,\tilde{\chi}]}{\delta\chi \dots \delta\chi}\Big|^{\tilde{\chi}=0} = 0. \tag{2.88}$$

Flow equations

We can get the flow equations for the second derivatives of the effective action, which build the propagators (2.80) - (2.83), by taking the respective functional derivatives of the flow equation (2.78). For example, evaluated for vanishing response fields:

$$
\begin{aligned}
\partial_t \Gamma_k^{\tilde{\chi}\chi} =& \frac{-i}{2} \{ Tr \left[\frac{\delta^2 \Gamma_k^{\tilde{\chi}\chi}}{\delta\tilde{\chi}\delta\chi} \, G_k^R \, \partial_t R_k \, G_k^R \right] + Tr \left[\frac{\delta^2 \Gamma_k^{\chi\tilde{\chi}}}{\delta\tilde{\chi}\delta\chi} \, G_k^A \, \partial_t R_k \, G_k^A \right] \\
&+ Tr \left[\frac{\delta^2 \Gamma_k^{\chi\chi}}{\delta\tilde{\chi}\delta\chi} \, iF_k \, \partial_t R_k \, G_k^A \right] + Tr \left[\frac{\delta^2 \Gamma_k^{\chi\chi}}{\delta\tilde{\chi}\delta\chi} \, G_k^R \, \partial_t R_k \, iF_k \right] \\
&+ Tr \left[\frac{\delta \Gamma_k^{\tilde{\chi}\chi}}{\delta\chi} \, G_k^R \, \frac{\delta \Gamma_k^{\tilde{\chi}\chi}}{\delta\tilde{\chi}} \, G_k^R \, \partial_t R_k \, G_k^R \right] + Tr \left[\frac{\delta \Gamma_k^{\tilde{\chi}\chi}}{\delta\tilde{\chi}} \, G_k^R \, \frac{\delta \Gamma_k^{\tilde{\chi}\chi}}{\delta\chi} \, G_k^R \, \partial_t R_k \, G_k^R \right] \\
&+ Tr \left[\frac{\delta \Gamma_k^{\tilde{\chi}\chi}}{\delta\chi} \, iF_k \, \frac{\delta \Gamma_k^{\chi\chi}}{\delta\tilde{\chi}} \, G_k^R \, \partial_t R_k \, G_k^R \right] + Tr \left[\frac{\delta \Gamma_k^{\chi\chi}}{\delta\tilde{\chi}} \, G_k^R \, \frac{\delta \Gamma_k^{\tilde{\chi}\chi}}{\delta\chi} \, G_k^R \, \partial_t R_k \, iF_k \right] \\
&+ Tr \left[\frac{\delta \Gamma_k^{\tilde{\chi}\tilde{\chi}}}{\delta\chi} \, G_k^A \, \frac{\delta \Gamma_k^{\chi\chi}}{\delta\tilde{\chi}} \, G_k^R \, \partial_t R_k \, G_k^R \right] + Tr \left[\frac{\delta \Gamma_k^{\chi\tilde{\chi}}}{\delta\chi} \, G_k^A \, \frac{\delta \Gamma_k^{\chi\chi}}{\delta\tilde{\chi}} \, G_k^R \, \partial_t R_k \, iF_k \right] \\
&+ Tr \left[\frac{\delta \Gamma_k^{\chi\tilde{\chi}}}{\delta\chi} \, G_k^A \, \frac{\delta \Gamma_k^{\chi\tilde{\chi}}}{\delta\tilde{\chi}} \, G_k^A \, \partial_t R_k \, G_k^A \right] + Tr \left[\frac{\delta \Gamma_k^{\chi\tilde{\chi}}}{\delta\chi} \, G_k^A \, \frac{\delta \Gamma_k^{\chi\chi}}{\delta\tilde{\chi}} \, iF_k \, \partial_t R_k \, G_k^A \right] \\
&+ Tr \left[\frac{\delta \Gamma_k^{\chi\chi}}{\delta\tilde{\chi}} \, G_k^R \, \frac{\delta \Gamma_k^{\tilde{\chi}\chi}}{\delta\chi} \, iF_k \, \partial_t R_k \, G_k^A \right] + Tr \left[\frac{\delta \Gamma_k^{\chi\chi}}{\delta\tilde{\chi}} \, G_k^R \, \frac{\delta \Gamma_k^{\tilde{\chi}\tilde{\chi}}}{\delta\chi} \, G_k^A \, \partial_t R_k \, G_k^A \right] \\
&+ Tr \left[\frac{\delta \Gamma_k^{\chi\chi}}{\delta\tilde{\chi}} \, iF_k \, \frac{\delta \Gamma_k^{\chi\tilde{\chi}}}{\delta\chi} \, G_k^A \, \partial_t R_k \, G_k^A \right] + Tr \left[\frac{\delta \Gamma_k^{\chi\tilde{\chi}}}{\delta\tilde{\chi}} \, G_k^A \, \frac{\delta \Gamma_k^{\chi\tilde{\chi}}}{\delta\tilde{\chi}} \, G_k^A \, \partial_t R_k \, G_k^A \right] \} \qquad (2.89)
\end{aligned}
$$

The derivative on the left hand site is with respect to the dimensionless scale parameter $t = \ln(\frac{k}{\Lambda})$. Formulating our flow equations as derivatives with respect to the dimensionless scale parameter t instead of the dimensionful one k will be helpful for constructing dimensionless forms of the flow equations later on.

We can write down all flow equations diagrammatically using the diagrammatic representations of the involved objects as shown in 2.2. Expressed in diagrams, the Wetterich equation (2.78) is shown in figure 2.3. The flow equation for the second derivative (2.89) of the effective action will have the diagrammatic form shown in figure 2.4. We see that the flow equations include all allowed one loop diagrams with the corresponding number of external legs.

Furthermore, we can simplify the flow equations by introducing the operator $\tilde{\partial}_t = \partial_t R_k \, \frac{\delta}{\delta R_k}$. Using this, the flow equation for the second derivative (2.89) can be brought in the more clear form:

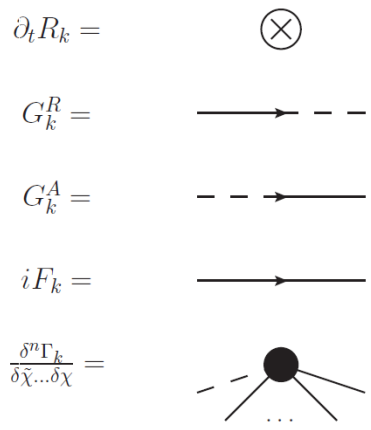

Figure 2.2: Diagramatic representation of the objects involved in the flow equations.

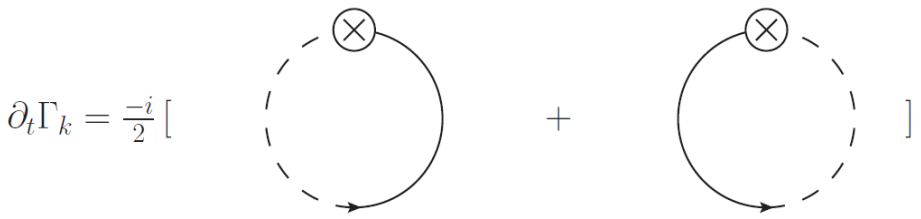

Figure 2.3: Diagramatic representation of the closed time path Wetterich equation.

$$\begin{aligned}\partial_t \Gamma_k^{\tilde{\chi}\chi} =& \tilde{\partial}_t \frac{-i}{2} \{Tr\left[\frac{\delta^2\Gamma_k^{\chi\chi}}{\delta\tilde{\chi}\delta\chi} iF_k\right] + Tr\left[\frac{\delta^2\Gamma_k^{\chi\tilde{\chi}}}{\delta\tilde{\chi}\delta\chi} G_k^A\right] + Tr\left[\frac{\delta^2\Gamma_k^{\tilde{\chi}\chi}}{\delta\tilde{\chi}\delta\chi} G_k^R\right] \\ &+Tr\left[\frac{\delta\Gamma_k^{\chi\tilde{\chi}}}{\delta\chi} G_k^A \frac{\delta\Gamma_k^{\chi\chi}}{\delta\tilde{\chi}} iF_k\right] + Tr\left[\frac{\delta\Gamma_k^{\tilde{\chi}\chi}}{\delta\chi} iF_k \frac{\delta\Gamma_k^{\chi\chi}}{\delta\tilde{\chi}} G_k^R\right] \\ &+Tr\left[\frac{\delta\Gamma_k^{\chi\tilde{\chi}}}{\delta\chi} G_k^A \frac{\delta\Gamma_k^{\chi\tilde{\chi}}}{\delta\tilde{\chi}} G_k^A\right] + Tr\left[\frac{\delta\Gamma_k^{\tilde{\chi}\chi}}{\delta\chi} G_k^R \frac{\delta\Gamma_k^{\tilde{\chi}\chi}}{\delta\tilde{\chi}} G_k^R\right] \\ &+Tr\left[\frac{\delta\Gamma_k^{\tilde{\chi}\tilde{\chi}}}{\delta\chi} G_k^A \frac{\delta\Gamma_k^{\chi\chi}}{\delta\tilde{\chi}} G_k^R\right] \}. \end{aligned} \tag{2.90}$$

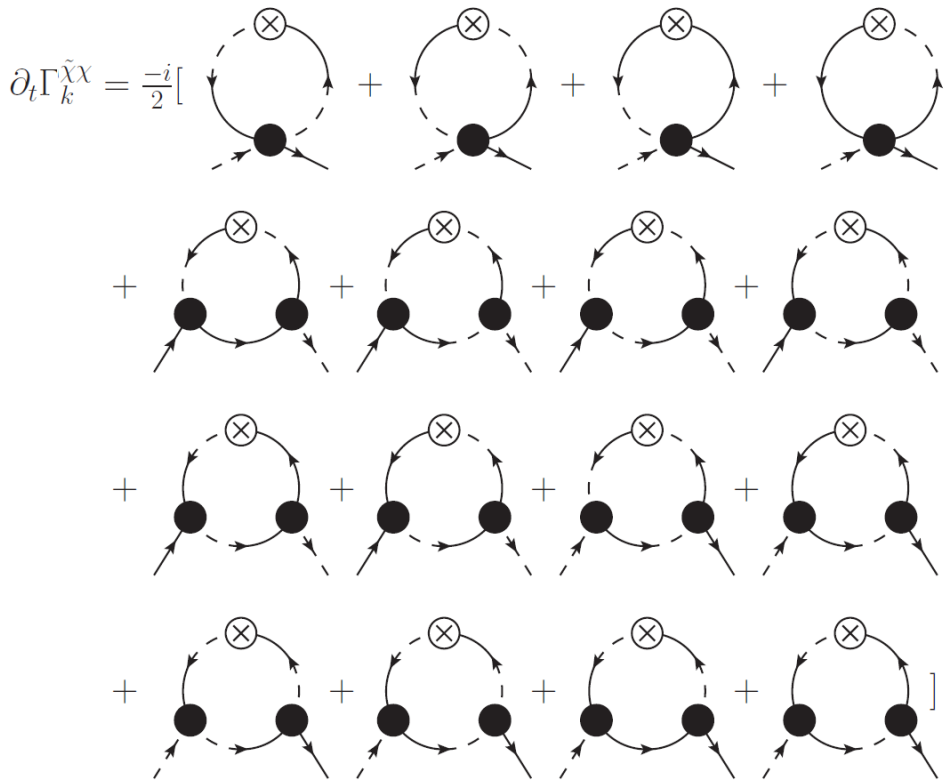

Figure 2.4: Diagramatic representation of the flow equation for the second functional derivative of the effective action.

Note that this operator $\tilde{\partial}_t$ depends still on e.g. the momenta and frequencies, so while we place the operator outside of the trace, we have to act it on the objects inside before we can perform the trace. Its main purpose is simplifying the representation of our diagrams, although under certain circumstances parts of the trace can be taken before applying the operator $\tilde{\partial}_t$. The such simplified flow equation (2.90) can be seen in figure 2.5.

A remark concerning terminology: we will call all derivatives of the effective action of order three or higher "vertex functions" or "vertices", as they will act as such in the loop diagrams appearing in our flow equations. Vertex functions with only one derivative with respect to the response field and arbitrary derivatives with respect to the physical field will be called "classical vertices". Functions with two derivatives with respect to the response field will be called "noiselike vertices" and those with three will be called "quan-

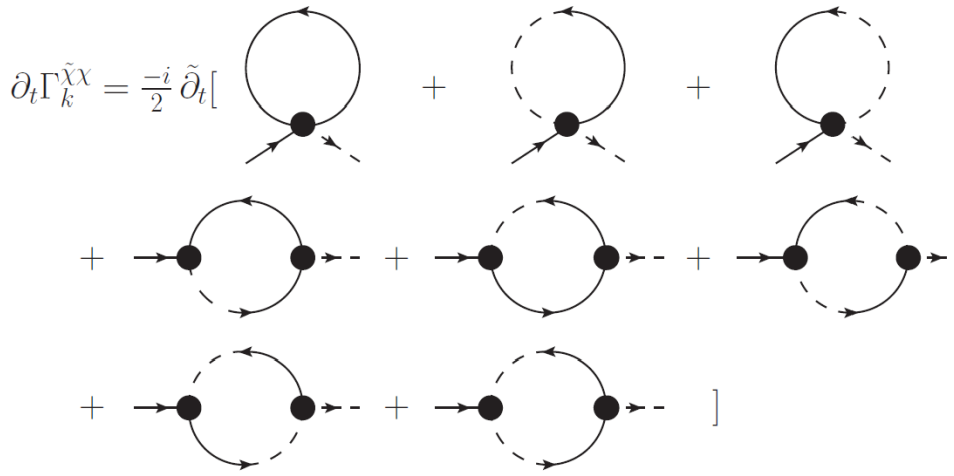

Figure 2.5: Diagramatic representation of the simplified flow equation for the second functional derivative of the effective action.

tum vertices". The reason for the naming of the classical and the quantum vertices was explained in section 2.3, the motivation for the description of vertices with two derivatives with respect to the response field as noiselike will come clear in section 3.8.

Hierarchy of flow equations and truncations

The flow equations for the second derivatives of the effective average action (2.89) depend on its third and fourth derivatives, while the Wetterich equation itself depends on the second derivatives through the propagators. This pattern will proceed for higher flow equations, the equation for $\Gamma^{(n)}$ will depend on vertex functions up to $\Gamma^{(n+2)}$. This will lead to an infinite series of coupled equations, which we will usually not be able to solve exactly.
So far we have switched the problem of performing the functional integral to solving this infinite set of coupled functional differential equations. The advantage of this representation is the variety of approximation methods applicable to truncate this infinite order of equations.
The most common methods of truncation are the field expansion and the gradient expansion where all contributions to the effective action with order of gradients or fields respectively above a certain order are neglected. They are explained, e.g., in the references at the beginning of this section. A com-

bination of both these expansions is used throughout this thesis, as it has shown to provide accurate results for the critical exponents already at low orders of the expansion, compare for example the references [21] or [66].
An example for a more sophisticated truncation scheme is the so called Blaizot-Mendez-Wschebor (BMW) approximation, where full momentum and field dependencies for vertex functions up to a certain order are maintained. This scheme is explained in references [16] and [5].

2.6 Boundary conditions

In this section, we discuss the effects of the boundary conditions summarized in the functional F defined in (2.46).
We first specify the initial density matrix. Our main object of interest are systems in thermal equilibrium, and the density matrix corresponding to thermal equilibrium is

$$\hat{\rho} = \exp\left\{-\hat{H}\beta\right\}, \tag{2.91}$$

with the hamilton operator of the system $\hat{H}$ and the inverse temperature $\beta = \frac{1}{T}$.
Here we choose natural units so that the Boltzmann constant k_b equals one. We will do the same for the speed of light, $c = 1$, and the Planck constant, $\hbar = 1$. From now on we will exclusively discuss systems in thermal equilibrium, so we will not introduce additional notation to distinguish equilibrium quantities, and will always assume equation (2.91) to hold.

Kubo-Martin-Schwinger condition and the fluctuation dissipation relation

The initial conditions (2.91) fulfill the so called Kubo-Martin-Schwinger (KMS) condition, which will result in fluctuation dissipation relations (FDR) between different correlation functions. We will demonstrate this on the level of the two point functions.
The equilibrium density matrix (2.91) matches the time evolution operator

$$\hat{U}(t) = \exp\left\{-i\hat{H}t\right\}, \tag{2.92}$$

with an imaginary time argument

$$\hat{U}(-i\beta) = \exp\left\{-\hat{H}\beta\right\}. \tag{2.93}$$

If we use this to rewrite the propagator (2.7), we see that it is in equilibrium directly related to (2.8):

$$\begin{aligned} G^{>}_{ij}(t_1,\vec{x}_1,t_2,\vec{x}_2) &= \mathrm{Tr}\left[\exp\left\{-\hat{H}\beta\right\}\zeta_i(t_1,\vec{x}_1)\zeta_j(t_2,\vec{x}_2)\right] \\ &= \mathrm{Tr}\left[\exp\left\{-\hat{H}\beta\right\}\zeta_i(t_1,\vec{x}_1)\exp\left\{-\hat{H}\beta\right\}\zeta_j(t_2-i\beta,\vec{x}_2)\exp\left\{\hat{H}\beta\right\}\right] \\ &= \mathrm{Tr}\left[\exp\left\{-\hat{H}\beta\right\}\zeta_j(t_2-i\beta,\vec{x}_2)\zeta_i(t_1,\vec{x}_1)\right] \\ &= G^{<}_{ij}(t_1,\vec{x}_1,t_2-i\beta,\vec{x}_2), \end{aligned} \tag{2.94}$$

where we used the cyclic invariance of the trace. In thermal equilibrium the system is translation invariant in space as well as time,

$$G^{>}_{ij}(t_1,\vec{x}_1,t_2,\vec{x}_2) = G^{>}_{ij}(t_1-t_2,\vec{x}_1-\vec{x}_2), \tag{2.95}$$

$$G^{<}_{ij}(t_1,\vec{x}_1,t_2,\vec{x}_2) = G^{<}_{ij}(t_1-t_2,\vec{x}_1-\vec{x}_2), \tag{2.96}$$

which allows to perform a Fourier transformation with respect to a single argument, as shown in (2.19) and (2.20). In Fourier space relation (2.94) becomes

$$G^{>}_{ij}(q_0,\vec{q}) = \exp\{\beta q_0\}\, G^{<}_{ij}(q_0,\vec{q}). \tag{2.97}$$

We can insert this into the definition of the spectral function (2.10) to get the relations

$$G^{<}_{ij}(q_0,\vec{q}) = \rho_{ij}(q_0,\vec{q})\, n_{BE}(q_0), \tag{2.98}$$

$$G^{>}_{ij}(q_0,\vec{q}) = \rho_{ij}(q_0,\vec{q})\ (n_{BE}(q_0)+1)\,, \tag{2.99}$$

$$\tag{2.100}$$

introducing the Bose-Einstein distribution

$$n_{BE}(q_0) = \frac{1}{e^{\beta q_0}-1}. \tag{2.101}$$

Inserting this into the definition of the statistical function (2.9) we finally get the fluctuation dissipation relation

$$F_{ij}(q_0,\vec{q}) = -i\left(n_{BE}(q_0)+\frac{1}{2}\right)\rho_{ij}(q_0,\vec{q}). \tag{2.102}$$

This relation will be very useful in our treatment of the thermal initial conditions through this work.

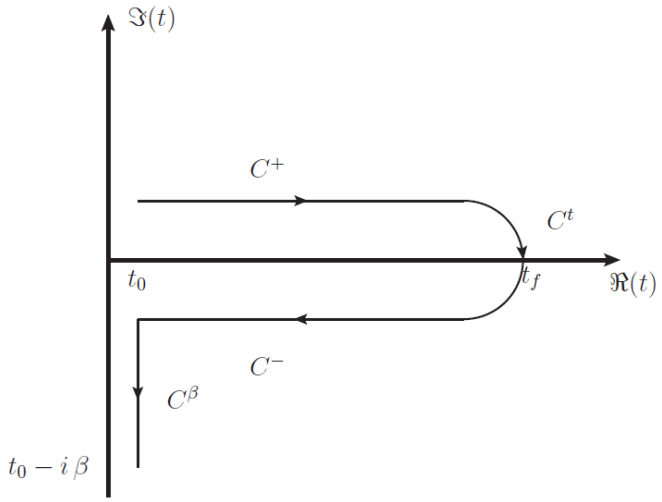

Figure 2.6: Here the contour already seen in figure 2.1 is extended for an additional part C^β, running from t_0 to $t_0 - i\,\beta$. The additional part represents the initial equilibrium density matrix.

If we evaluate this relation for our scale dependent propagators and for physical sources, we get the simple relation

$$\Gamma_k^{\tilde{\chi}\chi}(q_0,\vec{q}) = -i\left(n_{BE}(q_0)+\frac{1}{2}\right)\left(\Gamma_k^{\tilde{\chi}\chi}(q_0,\vec{q}) - \Gamma_k^{\chi\tilde{\chi}}(q_0,\vec{q})\right) \tag{2.103}$$

between the second derivatives of the effective action that do not vanish for physical sources.

Contribution of the initial conditions

To examine the contribution of the initial conditions term in (2.46), we use again the fact that the initial density matrix in thermal equilibrium (2.91) can be interpreted as a time evolution operator with an imaginary argument. The initial density matrix effectively acts as an additional part of the time contour shown in figure 2.1 then, extending it into the imaginary time plane as shown in figure 2.6.

We will show now that this additional part of the contour C^β does not affect our spectral function (2.10) directly, but only via the consequences of the symmetry condition (2.94). In order to do this, we will examine the

equations of motion for the propagators calculated from the two particle irreducible effective action. The derivation of these equations of motions can be found e.g. [15], [8] or [7]. The equation of motion of the time ordered propagator (2.6) for vanishing sources is:

$$\int_{z,C} \left(G^0_{ac}(x,z)\right)^{-1} G_{cb}(z,y) - \int_{z,C} \Sigma_{ac}(x,z) G_{cb}(z,y) = \delta_C(x,y). \quad (2.104)$$

Here we have used the inverse classical propagator $\left(G^0_{ab}(x,y)\right)^{-1} = \frac{\delta^2 S[\chi^+,\chi^-]}{\delta\chi^+_a(x)\delta\chi^+_b(y)}$ and the proper self energy $\Sigma_{ab}(x,y)$, which we will separate equivalently to the time ordered propagator:

$$G_{ab}(x,y) = \theta_C(t_x - t_y) G^>_{ab}(x,y) + \theta_C(t_y - t_x) G^<_{ab}(x,y) \quad (2.105)$$

$$\Sigma_{ab}(x,y) = \delta_C(t_x - t_y)\Sigma^\delta_{ab}(x,y) + \theta_C(t_x - t_y)\Sigma^>_{ab}(x,y) + \theta_C(t_y - t_x)\Sigma^<_{ab}(x,y), \quad (2.106)$$

where the Heaviside and Dirac delta functions are defined on the time path shown in 2.1, and we allow for a singular part Σ^δ in the proper self energy. For details on the involved functions we refer again to e.g. [8].
To simplify the calculations, we assume the classical action to be of a local form $S[\chi^+,\chi^-] = \int_x f(\chi^+(x),\chi^-(x))$, where the function f may also contain arbitrary derivatives of the fields $\chi^+(x)$ and $\chi^-(x)$.
This will result in a inverse classical propagator proportional to a Dirac delta function $\left(G^0_{ac}(x,z)\right)^{-1} = \delta_C(x-y)\left(G^0_{ac}(x)\right)^{-1}$. Using this, we can get from equation (2.104) to the equations of motion for the propagator $G^<$ by choosing the time arguments as $x_0 \in C^+$ and $y_0 \in C^-$. Inserting then the equations (2.105) and (2.106) into equation (2.104), we get:

$$\begin{aligned}\left(G^0_{ac}(x)\right)^{-1} G^<_{cb}(x,y) = &\int_{\vec{z}} \int_{t_0}^{t_x} \left(\Sigma^>_{ac}(x,z) - \Sigma^<_{ac}(x,z)\right) G^<_{cb}(z,y) \\ &- \int_{\vec{z}} \int_{t_0}^{t_y} \Sigma^<_{ac}(x,z)\left(G^>_{cb}(z,y) - G^<_{cb}(z,y)\right) \\ &+ \int_{\vec{z}} \int_{t_0}^{t_0 - i\beta} \Sigma^<_{ac}(x,z) G^>_{cb}(z,y). \end{aligned} \quad (2.107)$$

The equation of motion for $G^>$ can be derived in a similar way with the choices $x_0 \in C^-$ and $y_0 \in C^+$ or by complex conjugation of (2.107), yielding:

$$\begin{aligned}\left(G^0_{ac}(x)\right)^{-1} G^>_{cb}(x,y) = &\int_{\vec{z}} \int_{t_0}^{t_x} \left(\Sigma^>_{ac}(x,z) - \Sigma^<_{ac}(x,z)\right) G^>_{cb}(z,y) \\ &- \int_{\vec{z}} \int_{t_0}^{t_y} \Sigma^>_{ac}(x,z) \left(G^>_{cb}(z,y) - G^<_{cb}(z,y)\right) \\ &- \int_{\vec{z}} \int_{t_0}^{t_0+i\beta} \Sigma^>_{ac}(x,z) G^<_{cb}(z,y). \end{aligned} \tag{2.108}$$

Defining the proper self energy for the spectral function $\Sigma^\rho_{ab}(x,y) = \Sigma^>_{ab}(x,y) - \Sigma^<_{ab}(x,y)$, we can now combine the equations (2.107) and (2.108) to get the equation of motion for the spectral function:

$$\begin{aligned}\left(G^0_{ac}(x)\right)^{-1} \rho_{cb}(x,y) = &\int_{\vec{z}} \int_{t_y}^{t_x} \Sigma^\rho_{ac}(x,z) \rho_{cb}(z,y) \\ &- \int_{\vec{z}} \int_{t_0}^{t_0+i\beta} \Sigma^>_{ac}(x,z) G^<_{cb}(z,y) \\ &- \int_{\vec{z}} \int_{t_0}^{t_0-i\beta} \Sigma^<_{ac}(x,z) G^>_{cb}(z,y). \end{aligned} \tag{2.109}$$

At this point we can use the equilibrium properties (2.94) of the propagators $G^<$ and $G^>$ as well as their invariance to time translations in thermal equilibrium to find the contributions of the imaginary part of the contour to the equation of motion of the spectral function to vanish:

$$\begin{aligned} &- \int_{\vec{z}} \int_{t_0}^{t_0+i\beta} \Sigma^>_{ac}(x,z) G^<_{cb}(z,y) - \int_{\vec{z}} \int_{t_0}^{t_0-i\beta} \Sigma^<_{ac}(x,z) G^>_{cb}(z,y) \\ &= - \int_{\vec{z}} \int_{t_0-i\beta}^{t_0} \Sigma^>_{ac}(\vec{x},t_x,\vec{z},t_z+i\beta) G^<_{cb}(\vec{z},t_z+i\beta,\vec{y},t_y) - \int_{\vec{z}} \int_{t_0}^{t_0-i\beta} \Sigma^<_{ac}(x,z) G^>_{cb}(z,y) \\ &= \int_{\vec{z}} \int_{t_0}^{t_0-i\beta} \Sigma^<_{ac}(x,z) G^>_{cb}(z,y) - \int_{\vec{z}} \int_{t_0}^{t_0-i\beta} \Sigma^<_{ac}(x,z) G^>_{cb}(z,y) \\ &= 0. \end{aligned} \tag{2.110}$$

So we see that the vertical path C^β and therefore the thermal initial density matrix does not contribute to the spectral function directly, as long as the symmetry condition (2.94) is fulfilled for all the involved propagators. As all physical properties we are interested in can be extracted from the spectral function, we can therefore drop the imaginary part of the contour in all our calculations as long as we ensure that the symmetry (2.94) holds, or equivalently the fluctuation dissipation relations following from it.

Contribution of the turning point

Instead of explicitly calculating the effect of the turning point matrix element

$$\langle \zeta^-(\vec{x}, t_f) | \zeta^+(\vec{x}, t_f) \rangle \tag{2.111}$$

we will approximate its effects. The Keldysh action is just a convenient form of representing the system, while containing the same physics as the original action. This concerns in particular the symmetries of the system. If we look at the action expressed in the "plus/minus" fields appearing in the path integral shown in equation (2.45) though, we see that any internal symmetry of the system would be doubled if we would only include the actions $S[\zeta^+]$ and $S[\zeta^-]$ on the upper and lower part of the contour. If the original action would be, for example, symmetric under change of signs of the fields, $\zeta \to -\zeta$, the resulting plus/minus action would be symmetric under change of signs of the plus fields, $\zeta^+ \to -\zeta^+$, and the minus fields, $\zeta^- \to -\zeta^-$, separately. A Z_2 symmetry of the fields would become a $Z_2 \times Z_2$ symmetry, a $O(N)$ symmetry would become a $O(N) \times O(N)$ symmetry and so on.
For this reason, the turning point element has to introduce a mixing between the ζ^+ and ζ^- fields of the upper and lower contour parts, to break any unphysical enhanced symmetry of our Keldysh action. To achieve this we approximate the turning point element (2.111) as

$$\langle \zeta^-(\vec{x}, t_f) | \zeta^+(\vec{x}, t_f) \rangle \approx \epsilon \int_{\vec{x},t} \tilde{\zeta}(\vec{x}, t) \partial_t \zeta(\vec{x}, t), \tag{2.112}$$

written already in the Keldysh fields. If we replace these with the plus and minus fields, it can be seen that this will indeed introduce a mixing between the fields of the forward and backward part of the contour:

$$\begin{aligned}
\int_{\vec{x},t} \tilde{\zeta}(\vec{x}, t) \partial_t \zeta(\vec{x}, t) =& \frac{1}{2} \int_{\vec{x},t} \left(\zeta^+(\vec{x}, t) - \zeta^-(\vec{x}, t) \right) \partial_t \left(\zeta^+(\vec{x}, t) + \zeta^-(\vec{x}, t) \right) \\
=& \frac{1}{2} \int_{\vec{x},t} [\zeta^+(\vec{x}, t) \partial_t \zeta^+(\vec{x}, t) - \zeta^-(\vec{x}, t) \partial_t \zeta^-(\vec{x}, t) \\
& + \zeta^+(\vec{x}, t) \partial_t \zeta^-(\vec{x}, t) - \zeta^-(\vec{x}, t) \partial_t \zeta^+(\vec{x}, t)] \\
=& \int_{\vec{x},t} \zeta^+(\vec{x}, t) \partial_t \zeta^-(\vec{x}, t)
\end{aligned} \tag{2.113}$$

where we partially integrated in the last step and used the fact that terms of the form $\int_{\vec{x},t} \zeta^i(\vec{x}, t) \partial_t \zeta^i(\vec{x}, t)$ can be represented as the integral over a total

derivative and will vanish due to our assumption of vanishing fields at the integration boundary:

$$\begin{aligned}\int_{\vec{x},t} \zeta^i(\vec{x},t)\partial_t\zeta^i(\vec{x},t) &= \frac{1}{2}\int_{\vec{x},t} \partial_t \left[\zeta^i(\vec{x},t)\right]^2 \\ &= \frac{1}{2}\int_{\vec{x}} \left[\left(\zeta^i(\vec{x},t_f)\right)^2 - \left(\zeta^i(\vec{x},t_i)\right)^2\right] \approx 0. \end{aligned} \tag{2.114}$$

As the turning point is shifted to infinite times, we assume that aside from the breaking of the enhanced symmetry, its effects will be vanishing. This motivates the infinitesimal ϵ in front of (2.112).
The turning point element (2.112) will also produce the expected forms of the retarded and advanced propagators as well as the spectral function at the ultra violet cutoff.

2.7 Quantum vertices and the fluctuation dissipation relation

We want to discuss the role of the quantum vertices, i.e. derivatives of the effective action with an odd number of tilde legs equal to or larger than three. It can be shown that these will never appear in the flow equation for any classical function, i.e. derivative of the effective action with only one tilde leg. In the specific case of the second derivative we see that in equation (2.90) or figure 2.5 respectively. In general this can be seen by taking one derivative with respect to the response field and an arbitrary number of derivatives with respect to the physical field of the flow equation (2.78), then set the sources to physical values. Writing out the propagators, (2.78) looks like

$$\begin{aligned}\partial_k\Gamma_k[\chi,\tilde{\chi}] = \frac{i}{2}\,\mathrm{Tr}[&\left[\left(\Gamma_k^{\tilde{\chi}\chi}+R_k\right) - \Gamma_k^{\tilde{\chi}\tilde{\chi}}\left(\Gamma_k^{\chi\tilde{\chi}}+R_k\right)^{-1}\Gamma_k^{\chi\chi}\right]^{-1}\dot{R}_k \\ &+\left[\left(\Gamma_k^{\chi\tilde{\chi}}+R_k\right) - \Gamma_k^{\chi\chi}\left(\Gamma_k^{\tilde{\chi}\chi}+R_k\right)^{-1}\Gamma_k^{\tilde{\chi}\tilde{\chi}}\right]^{-1}\dot{R}_k].\end{aligned} \tag{2.115}$$

The only terms that potentially could contain a quantum vertex are those where the tilde derivative acts on $\Gamma_k^{\tilde{\chi}\tilde{\chi}}$. But these will always appear in combination with $\Gamma_k^{\chi\chi}$, or a derivative of this with respect to only physical fields. These will vanish when the flow equation is evaluated for physical sources . It is established now that flow equations for derivatives of the effective action with only one tilde leg will only depend on vertices with at most two tilde

legs. Generally, to solve these we would have to calculate the flow equations for the noiselike vertices with two tilde legs as well, and here quantum vertices with three or more tilde legs would contribute.
In thermal equilibrium though, we can express all noiselike vertices through combinations of classical vertices. As we have seen before, the fluctuation dissipation relation (2.102) will connect the lowest order noiselike function $\Gamma_k^{\tilde{\chi}\tilde{\chi}}$ to the functions $\Gamma_k^{\tilde{\chi}\chi}$ and $\Gamma_k^{\chi\tilde{\chi}}$ if evaluated for constant fields, as displayed in (2.103). There are connections between higher order correlation functions that can be deduced analogous to the derivation of the fluctuation dissipation relation in section 2.6.
As these calculations are however quite involved, a direct application of the symmetry properties of thermal equilibrium as described in the reference [79] might provide a more convenient way to obtain the relations between the higher order classical and noise vertices.
If the applied truncation scheme assumes a gradient structure for the noiselike vertex functions that fulfills the relation

$$\frac{\delta^n \Gamma_k^{\tilde{\chi}\tilde{\chi}}}{\delta\,\chi ... \delta\,\chi} = \partial_\chi^n \Gamma_k^{\tilde{\chi}\tilde{\chi}}, \tag{2.116}$$

for vertex functions evaluated at constant fields, the higher order vertex functions can be calculated in a straightforward manner from the fluctuation dissipation relation (2.102). Writing out the propagators in the fluctuation dissipation relation yields:

$$\begin{aligned}
&\left(\Gamma_k^{\tilde{\chi}\chi} + R_k\right)^{-1} \left(\Gamma_k^{\tilde{\chi}\tilde{\chi}}\right) \left(\Gamma_k^{\chi\tilde{\chi}} + R_k\right)^{-1} \\
&= \left(n_{BE}(q_0) + \frac{1}{2}\right) \left[\left(\Gamma_k^{\tilde{\chi}\chi} + R_k\right)^{-1} - \left(\Gamma_k^{\chi\tilde{\chi}} + R_k\right)^{-1}\right].
\end{aligned} \tag{2.117}$$

Taking the derivative with respect to the constant field values on both sides of the equation results in the relation:

$$\begin{aligned}
&G_k^R\, \partial_\chi \Gamma_k^{\tilde{\chi}\chi}\, iF_k + iF_k\, \partial_\chi \Gamma_k^{\chi\tilde{\chi}}\, G_k^A + G_k^R\, \partial_\chi \Gamma_k^{\tilde{\chi}\tilde{\chi}}\, G_k^A \\
&= \left(n_{BE}(q_0) + \frac{1}{2}\right) \left[G_k^R\, \partial_\chi \Gamma_k^{\tilde{\chi}\chi}\, G_k^R - G_k^A\, \partial_\chi \Gamma_k^{\chi\tilde{\chi}}\, G_k^A\right].
\end{aligned} \tag{2.118}$$

This can be resolved for $\partial_\chi \Gamma_k^{\tilde{\chi}\tilde{\chi}}$:

$$\begin{aligned}
\partial_\chi \Gamma_k^{\tilde{\chi}\tilde{\chi}} = &\left(n_{BE}(q_0) + \frac{1}{2}\right) \left[\partial_\chi \Gamma_k^{\tilde{\chi}\chi}\, G_k^R\, \left(G_k^A\right)^{-1} - \left(G_k^R\right)^{-1} G_k^A\, \partial_\chi \Gamma_k^{\chi\tilde{\chi}}\right] \\
&- \partial_\chi \Gamma_k^{\tilde{\chi}\chi}\, iF_k\, \left(G_k^A\right)^{-1} - \left(G_k^R\right)^{-1}\, iF_k\, \partial_\chi \Gamma_k^{\chi\tilde{\chi}}.
\end{aligned} \tag{2.119}$$

So we see that the third order noise vertex can be expressed solely through classical vertices, and the lower order noise function $\Gamma_k^{\tilde{\chi}\tilde{\chi}}$ - which we can in turn express through classical functions via the original fluctuation dissipation relation (2.103).
This can be repeated to arbitrary order, returning the nth order noiselike vertex $\frac{\delta^{n-2}\Gamma^{\tilde{\chi}\tilde{\chi}}}{\delta\chi\ldots\delta\chi}$ as a function of classical vertices up to order n and noiselike vertices of order $(n-1)$ and lower. All truncation schemes applied in this theses will allow for this direct calculations.
In summary, we have shown that the flow equations of all classical functions are completely independent of the quantum vertices in thermal equilibrium. The result is valid without any form of truncation or approximation.
This, however, does not mean that quantum effects are not relevant in thermal equilibrium. The effects of the quantum fluctuation are just completely included in the form of the distribution function $n_{BE}(q_0) + \frac{1}{2}$.
There are situations where the system behaves completely classicaly indeed, and the quantum effects included in $n_{BE}(q_0) + \frac{1}{2}$ can be neglected too. An example for such a situation will be discussed in chapter 3.

Chapter 3

Dynamic critical phenomena for non-relativistic, interacting bosons

In this chapter we will apply the framework established in chapter 2 to a gas of non-relativistic, interacting bosons and examine its dynamic critical behavior in the vicinity of the second order phase transition associated with Bose-Einstein condensation [60]. After introducing a truncation for the effective average action and the cutoff function used in the functional renormalization group approach, we discuss in some detail the calculation of the involved renormalization group flow equations.
The discussion of the fixed points and the explicit calculation of these flow equations reveals that, in the vicinity of the phase transition, the dynamic behavior of the system fundamentally changes form unitary propagation at the microscopic scale to a relaxational type of dynamic. We then reformulate our closed time path functional integral as the average over the solutions of Langevin type equation, driven by a gaussian distributed random noise. This provides insight into the physical meanings of the coefficients involved in our truncation as well as allows to connect our approach to the mesoscopic approaches to critical dynamics discussed in chapter 5.
In the last section of this chapter we confirm the fact that quantum fluctuations will have no influence on the critical properties of systems undergoing phase transitions at non-vanishing temperatures.

3.1 Action

The action for a non-relativistic, interacting, bosonic system is

$$S[\psi,\psi^*] = \int_x \left\{ \frac{-i}{2}\left[\psi^*(x)\,\partial_t\psi(x) - \psi(x)\,\partial_t\psi^*(x)\right] - \psi^*(x)\,\frac{1}{2m}\,\nabla^2\psi(x) + V(\psi(x)\psi^*(x)) \right\}. \tag{3.1}$$

We will assume a contact interaction for the bosonic particles on the microscopic scale, i.e. a potential of the form:

$$V(\psi(x)\psi^*(x)) = -\sigma\,\psi^*(x)\,\psi(x) + \frac{\lambda}{2}\left(\psi(x)\,\psi^*(x)\right)^2. \tag{3.2}$$

The parameters involved in this action are the mass m, the interaction strength λ and the chemical potential σ.
As a classical equation of motion, it produces the Gross-Pitaevskii equation [42], [57]:

$$i\partial_t\psi(x) = \left[-\frac{1}{2m}\nabla^2 - \sigma + \lambda|\psi(x)|^2\right]\psi(x) \tag{3.3}$$

The system is symmetric under change of phase of the complex field, $\psi(x) \to e^{i\theta}\psi(x)$ for a real constant θ. The conserved quantity related to this continuous symmetry via Noethers Theorem [74] is the particle number

$$N = \int_{\vec{x}} \psi(x)\,\psi^*(x). \tag{3.4}$$

In depth discussions of the thermodynamic properties and functional renormalization group calculations in imaginary time can be found in [32], [33], [31] and [17]. We will focus on the real-time analysis and the resulting dynamic critical behavior in this chapter.
To get an action compatible with the framework build up in chapter 2, we will perform the field transformations

$$\psi(x) = \psi_1(x) + i\,\psi_2(x), \tag{3.5}$$
$$\psi^*(x) = \psi_1(x) - i\,\psi_2(x), \tag{3.6}$$

where the real fields ψ_1 and ψ_2 represent the real and imaginary part of the original field ψ.

This will produce an action containing real fields only:

$$\begin{aligned} S[\psi_1,\psi_2] = \int_x \big\{ &\psi_1(x)\partial_t\psi_2(x) - \psi_2(x)\partial_t\psi_1(x) \\ &- \psi_1(x)\frac{1}{2m}\nabla^2\psi_1(x) - \psi_2(x)\frac{1}{2m}\nabla^2\psi_2(x) \\ &- \sigma\psi_1(x)^2 - \sigma\psi_2(x)^2 + \frac{\lambda}{2}\left(\psi_1(x)^2+\psi_2(x)^2\right)^2 \big\}. \end{aligned} \tag{3.7}$$

The invariance under phase transformation translates to an O(2) symmetry of the action.
To calculate realtime propagators like the spectral function (2.10), we would like to write this action in the keldysh form described in section 2.3. As we have established in section 2.7 that the quantum vertices will not contribute to our equilibrium calculations, we can discard the terms of third order in the response field and use equation (2.55) to get the following keldysh action:

$$\begin{aligned} S[\psi_i,\tilde{\psi}_i] =& 2\int_x \big\{ \tilde{\psi}_1(x)\,\partial_t\psi_2(x) - \tilde{\psi}_2(x)\,\partial_t\psi_1(x) \\ &- \tilde{\psi}_i(x)\,\frac{1}{2m}\,\nabla^2\psi_i(x) - \sigma\,\tilde{\psi}_i(x)\psi_i(x) \\ &+ \lambda\,\tilde{\psi}_i(x)\psi_i(x)\,\left(\psi_1(x)^2+\psi_2(x)^2\right)\big\}. \end{aligned} \tag{3.8}$$

Including the effects of the turning point element as described in 2.6, we get the additional time derivative terms:

$$\epsilon\,\tilde{\psi}_1(x)\,\partial_t\psi_1(x) + \epsilon\,\tilde{\psi}_2(x)\,\partial_t\psi_2(x). \tag{3.9}$$

To ensure that the equilibrium initial density matrix (2.91) is taken into account as described in section 2.6, we have to include all terms necessary to fulfill the fluctuation-dissipation relation (2.102):

$$\begin{aligned} S^{\tilde{\psi}\tilde{\psi}}(q_0,\vec{q}) &= -i\left(n_{BE}(q_0)+\frac{1}{2}\right)\,\left(S^{\tilde{\psi}\psi}(q_0,\vec{q}) - S^{\psi\tilde{\psi}}(q_0,\vec{q}))\right) \\ &= -i\left(n_{BE}(q_0)+\frac{1}{2}\right)\,(-2\,i\,\epsilon\,q_0)\,. \end{aligned} \tag{3.10}$$

This altogether leads us to the action:

$$
\begin{aligned}
S[\psi_i, \tilde{\psi}_i] = \int_x \big\{ & \tilde{\psi}_1(x)\, \partial_t \psi_2(x) - \tilde{\psi}_2(x)\, \partial_t \psi_1(x) \\
& - \tilde{\psi}_i(x)\, \frac{1}{2m}\, \nabla^2 \psi_i(x) - \sigma\, \tilde{\psi}_i(x) \psi_i(x) \\
& + \lambda\, \tilde{\psi}_i(x) \psi_i(x)\, \left(\psi_1(x)^2 + \psi_2(x)^2\right) \\
& + \epsilon\, \tilde{\psi}_i(x)\, \partial_t \psi_i(x) - 2\, i\, \epsilon\, \tilde{\psi}_i(x)\, \left(n_{BE}(-i\partial_t) + \frac{1}{2} \right)\, \partial_t \tilde{\psi}_i(x) \big\}.
\end{aligned}
\tag{3.11}
$$

We absorbed an overall factor of two into the fields.
It can be easily checked that the higher order fluctuation-dissipation relations like (2.119) are identically fulfilled for this action.

3.2 Ansatz and regulator

As mentioned in section 2.5, we need to truncate the hierarchy of equations following from the Wetterich equation (2.78). We choose here an expansion in gradients and fields to lowest nontrivial order, resulting in the ansatz for the effective average action:

$$
\begin{aligned}
\Gamma_k[\phi_i, \tilde{\phi}_i] = \int_x \big\{ & X_k\, \tilde{\phi}_1(x)\, \partial_t \phi_2(x) - X_k\, \tilde{\phi}_2(x)\, \partial_t \phi_1(x) \\
& - Z_k\, \tilde{\phi}_i(x)\, \nabla^2 \phi_i(x) + \tilde{\phi}_i\, \phi_i(x)\, \partial_\rho U_k(\rho) \\
& + Y_k\, \tilde{\phi}_i(x)\, \partial_t \phi_i(x) - 2\, i\, Y_k\, \tilde{\phi}_i(x)\, \left(n_{BE}(-i\partial_t) + \frac{1}{2} \right)\, \partial_t \tilde{\phi}_i(x) \big\}.
\end{aligned}
\tag{3.12}
$$

We introduced the effective potential $U_k(\rho)$ depending on the particle density $\rho(x) = \frac{1}{2}\phi_i(x)\phi_i(x)$.
For our truncation, we will choose

$$
U_k(\rho) = \frac{\lambda_k}{2} \left(\rho(x) - \rho_k^0\right)^2 . \tag{3.13}
$$

We expanded the potential around its minimum ρ_k^0, which is a running coupling of our FRG flow. The other running couplings in our ansatz are the unitary dynamic coefficient X_k, the damping coefficient Y_k the anomalous

dimension Z_k and the interaction strength λ_k. Details about this choice of potential can be found e.g. in [14] or [25].
Using the minimum of the potential ρ_k^0 as a running coupling instead of the chemical potential allows not only for a more accurate expansions of the potential, see reviews above, but also is more convenient in the calculation of the functional renormalization group flow. The equations of motion determining the average field values are derived by taking the first derivatives of the effective average action with respect to the fields. As we have already established in 2.3, the average of the response field has to vanish for physical sources. For this reason, all equations of motion resulting from derivatives with respect to the physical field will be automatically fulfilled. The remaining equation of motion for our ansatz is

$$\left.\frac{\delta\,\Gamma_k[\phi_i,\tilde{\phi}_i]}{\delta\,\tilde{\phi}_1(x)}\right|^{\tilde{\phi}(x)=0} = X_k\,\partial_t\phi_2(x) + Y_k\,\partial_t\phi_1(x) - Z_k\,\nabla^2\,\phi_1(x) + \phi_1(x)\,\partial_\rho U_k(\rho) = J_1(x), \tag{3.14}$$

$$\left.\frac{\delta\,\Gamma_k[\phi_i,\tilde{\phi}_i]}{\delta\,\tilde{\phi}_2(x)}\right|^{\tilde{\phi}(x)=0} = -X_k\,\partial_t\phi_1(x) + Y_k\,\partial_t\phi_2(x) - Z_k\,\nabla^2\,\phi_2(x) + \phi_2(x)\,\partial_\rho U_k(\rho) = J_2(x). \tag{3.15}$$

As we are interested in equilibrium situations only, we will from now on always evaluate for vanishing sources $J(x) = 0$ after all derivatives. As our system is translational invariant in space and time, the field average has to be independent of the spatial and temporal coordinates:

$$\phi(x) = \langle\psi(x)\rangle = \phi. \tag{3.16}$$

This reduces the equations of motion (3.14) to

$$\phi_1(x)\,\partial_\rho U_k(\rho) = 0 \tag{3.17}$$

$$\phi_2(x)\,\partial_\rho U_k(\rho) = 0. \tag{3.18}$$

So the field expectation value is determined by the minimum ϕ^0 of the potential U_k, which is one of the reasons for our choice of ρ_k^0 as a running coupling.
Depending on the initial values of the coupling and chemical potential, the

minimum of the potential can either be a positive real constant or zero. These are the two different phases our critical point separates: the "symmetry broken phase", where $\lim_{k\to 0} \rho_k^0 > 0$ and so breaks the $O(2)$ symmetry of the system spontaneously, and the "symmetric phase", where $\lim_{k\to 0} \rho_k^0 = 0$ and so the $O(2)$ is restored after integration of all fluctuations. The minimum ρ_k^0 does not necessarily have to vanish for all scales k in this case, however. An initial value of $\rho_\Lambda^0 > 0$ can still lead to a symmetric expectation value for $k \to 0$.
All our calculations in this thesis will focus on the symmetry broken phase of the system, as a truncation on the level of the ansatz (3.12) would generate only trivial results for the coefficients of the gradient terms Z_k, Y_k and X_k due to the momentum and frequency independence of the four point vertices it produces.

Projections

To construct explicit flow equations for the scale dependent coefficients in our ansatz (3.12) we need to project the general derivatives of the effective action onto the specific terms in our truncation. For the first derivative we do this as follows:

$$\partial_t U_k'(\rho) = \frac{1}{\sqrt{2\rho}} \lim_{p\to 0} \partial_t \frac{\delta \Gamma_k}{\delta \tilde{\phi}_1(p)}. \tag{3.19}$$

From this we can extract the interaction coefficient

$$\partial_t \lambda_k = \left[\partial_\rho \partial_t U_k'(\rho)\right] |^{\rho=\rho_k^0} \tag{3.20}$$

and the running minimum of the potential, using its definition as

$$\partial_t U_k'(\rho_k^0) = \left[\partial_t U_k'(\rho)\right] |^{\rho=\rho_k^0} + U_k''(\rho_k^0)\, \partial_t \rho_k^0, \tag{3.21}$$

resulting in the equation

$$\partial_t \rho_k^0 = -\frac{1}{\lambda_k}\, \partial_t U_k'(\rho)|^{\rho=\rho_k^0}. \tag{3.22}$$

The wave function renormalization can be extracted from the second derivative of the effective action as

$$\partial_t Z_k = \lim_{p\to 0} \partial_{\vec{p}^2}\, \partial_t \frac{\delta \Gamma_k}{\delta \tilde{\phi}_2(-p) \delta \phi_2(p)} |^{\rho=\rho_k^0}, \tag{3.23}$$

as well as the damping coefficient

$$\partial_t Y_k = -i \lim_{p\to 0} \partial_{p_0} \partial_t \frac{\delta\Gamma_k}{\delta\tilde{\phi}_2(-p)\delta\phi_2(p)}|^{\rho=\rho_k^0}. \tag{3.24}$$

For the unitary coefficient we have to take the second derivative with respect to fields with mixed indices

$$\partial_t X_k = i \lim_{p\to 0} \partial_{p_0} \partial_t \frac{\delta\Gamma_k}{\delta\tilde{\phi}_2(-p)\delta\phi_1(p)}|^{\rho=\rho_k^0}. \tag{3.25}$$

Regulator

In addition to choosing an ansatz, we have to specify a cutoff function R_k to perform any explicit calculation. If we would solve the full theory, every choice fulfilling the conditions (2.73) and (2.74) would lead to the same effective action at the end of the flow - we would just choose different ways through the theory space leading from the same starting point to the same end point. As soon as we approximate the effective action though, different choices of the cutoff function can lead to results of different precision. We will choose the optimized cutoff

$$R_k(q) = R_k(\vec{q}) = Z_k \left(k^2 - \vec{q}^2\right) \theta(k^2 - \vec{q}^2), \tag{3.26}$$

as discussed in [62] and [64]. It has been found to produce accurate results for static critical exponents already at the low orders of the polynomial expansions of the effective action which we used for our ansatz (3.12), compare for example [63] and [65].
It is important to note that we choose a purely spatial cutoff function. This means that only the spatial fluctuations are regularized during the renormalization flow, while we theoretically integrate over all possible frequency fluctuations in all steps. In practice we will see that the frequencies contributing at a fixed k are usually limited by the dispersion relation of the system though. A recent discussion of frequency dependent cutoff functions in the framework of the real-time FRG can be found in [75].
The cutoff function (3.26) has the additional advantage of greatly simplifying the momentum integrations during the calculation of the loop diagrams in the flow equations.
Another popular choice is the exponential cutoff

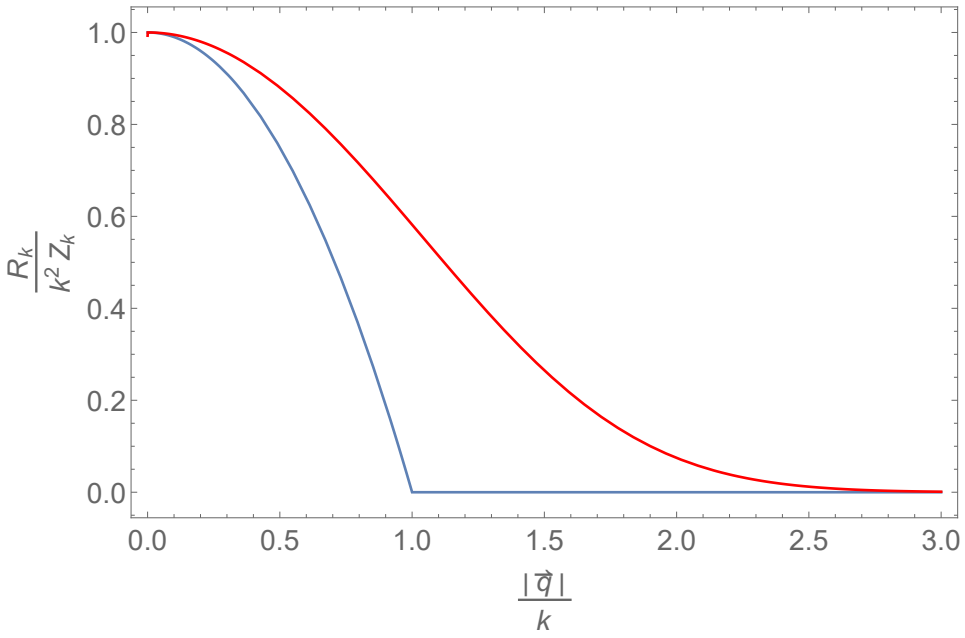

Figure 3.1: The optimized cutoff function (3.26) plotted in blue and the exponential cutoff (3.27) plotted in red.

$$R_k(\vec{q}) = Z_k \, \vec{q}^2 \, \frac{e^{-\frac{\vec{q}^2}{k^2}}}{1 - e^{-\frac{\vec{q}^2}{k^2}}}, \tag{3.27}$$

as it is e.g. more suited for numerical integrations than the optimized cutoff (3.26). Examples of FRG calculations applying the exponential cutoff can be found in the references [86] and [84].
The exponential and the optimized cutoff function can be seen for fixed k in figure 3.1.

3.3 Scale dependent propagators and vertex functions

The ansatz (3.12) will produce the following scale dependent retarded and advanced propagator:

$$G_k^R(q) = -\frac{1}{\omega_1^2(\vec{q})\,\omega_2^2(\vec{q}) + i\,q_0\,Y_k\,\left(\omega_1^2(\vec{q}) + \omega_2^2(\vec{q})\right) - q_0^2\,\left(Y_k^2 + X_k^2\right)} \times \begin{pmatrix} \omega_2^2(\vec{q}) + i\,q_0\,Y_k & i\,q_0\,X_k \\ -i\,q_0\,X_k & \omega_1^2(\vec{q}) + i\,q_0\,Y_k \end{pmatrix}, \tag{3.28}$$

$$G_k^A(q) = -\frac{1}{\omega_1^2(\vec{q})\,\omega_2(\vec{q}) - i\,q_0\,Y_k\,\left(\omega_1^2(\vec{q}) + \omega_2^2(\vec{q})\right) - q_0^2\,\left(Y_k^2 + X_k^2\right)} \times \begin{pmatrix} \omega_2^2(\vec{q}) - i\,q_0\,Y_k & i\,q_0\,X_k \\ -i\,q_0\,X_k & \omega_1^2(\vec{q}) - i\,q_0\,Y_k \end{pmatrix}. \tag{3.29}$$

We used the shorthand notation:

$$\omega_1^2(\vec{q}) = Z_k\vec{q}^2 + \partial_\rho U_k(\rho) + 2\rho\partial_\rho^2 U_k(\rho) + R_k(\vec{q}), \tag{3.30}$$

$$\omega_2^2(\vec{q}) = Z_k\vec{q}^2 + \partial_\rho U_k(\rho) + R_k(\vec{q}). \tag{3.31}$$

They will produce the spectral function and the statistical propagator:

$$\rho_k(q) = \frac{1}{\omega_1^4(\vec{q})\,\omega_2^4(\vec{q}) + q_0^2\,\left[Y_k^2\,\left(\omega_1^4(\vec{q}) + \omega_2^4(\vec{q})\right) - X_k^2\,\omega_1^2\,\omega_2^2\right] - q_0^4\,\left(Y_k^2 + X_k^2\right)} \times \begin{pmatrix} 2\,i\,q_0\,Y_k\left[\omega_2^4(\vec{q}) + q_0^2\,\left(Y_k^2 + X_k^2\right)\right] & -2\,q_0^2\,\left[\omega_1^2(\vec{q}) + \omega_2^2(\vec{q})\right]\,Y_k\,X_k \\ 2\,q_0^2\,\left[\omega_1^2(\vec{q}) + \omega_2^2(\vec{q})\right]\,Y_k\,X_k & 2\,i\,q_0\,Y_k\left[\omega_1^4(\vec{q}) + q_0^2\,\left(Y_k^2 + X_k^2\right)\right] \end{pmatrix}, \tag{3.32}$$

$$iF_k(q) = \left(n_{BE}(q_0) + \frac{1}{2}\right) \times \frac{1}{\omega_1^4(\vec{q})\,\omega_2^4(\vec{q}) + q_0^2\,\left[Y_k^2\,\left(\omega_1^4(\vec{q}) + \omega_2^4(\vec{q})\right) - X_k^2\,\omega_1^2\,\omega_2^2\right] - q_0^4\,\left(Y_k^2 + X_k^2\right)} \times \begin{pmatrix} 2\,i\,q_0\,Y_k\left[\omega_2^4(\vec{q}) + q_0^2\,\left(Y_k^2 + X_k^2\right)\right] & -2\,q_0^2\,\left[\omega_1^2(\vec{q}) + \omega_2^2(\vec{q})\right]\,Y_k\,X_k \\ 2\,q_0^2\,\left[\omega_1^2(\vec{q}) + \omega_2^2(\vec{q})\right]\,Y_k\,X_k & 2\,i\,q_0\,Y_k\left[\omega_1^4(\vec{q}) + q_0^2\,\left(Y_k^2 + X_k^2\right)\right] \end{pmatrix}. \tag{3.33}$$

The classical vertices appearing in the flow equations are

$$\frac{\delta^2\Gamma_k^{\phi\phi}}{\delta\phi_1(p_1)\delta\tilde{\phi}_1(p_2)} = \begin{pmatrix} 3\,\partial_\rho^2 U_k(\rho) & 0 \\ 0 & \partial_\rho^2 U_k(\rho) \end{pmatrix}, \tag{3.34}$$

$$\begin{aligned} \frac{\delta\Gamma_k^{\phi\phi}}{\delta\tilde{\phi}_1(p_1)} &= \frac{\delta\Gamma_k^{\tilde{\phi}\phi}}{\delta\phi_1(p_1)} = \frac{\delta\Gamma_k^{\phi\tilde{\phi}}}{\delta\phi_1(p_1)} \\ &= \begin{pmatrix} 3\sqrt{2\rho}\,\partial_\rho^2 U_k(\rho) & 0 \\ 0 & \sqrt{2\rho}\,\partial_\rho^2 U_k(\rho) \end{pmatrix}, \end{aligned} \tag{3.35}$$

$$\begin{aligned} \frac{\delta\Gamma_k^{\phi\phi}}{\delta\tilde{\phi}_2(p_1)} &= \frac{\delta\Gamma_k^{\tilde{\phi}\phi}}{\delta\phi_2(p_1)} = \frac{\delta\Gamma_k^{\phi\tilde{\phi}}}{\delta\phi_2(p_1)} \\ &= \begin{pmatrix} 0 & \sqrt{2\rho}\,\partial_\rho^2 U_k(\rho) \\ \sqrt{2\rho}\,\partial_\rho^2 U_k(\rho) & 0 \end{pmatrix}. \end{aligned} \tag{3.36}$$

$$\tag{3.37}$$

The noiselike vertices all vanish in this truncation:

$$\frac{\delta^2\Gamma_k^{\phi\tilde{\phi}}}{\delta\phi_1(p_1)\delta\tilde{\phi}_1(p_2)} = \frac{\delta^2\Gamma_k^{\tilde{\phi}\phi}}{\delta\phi_1(p_1)\delta\tilde{\phi}_1(p_2)} = 0 \tag{3.38}$$

$$\frac{\delta\Gamma_k^{\phi\tilde{\phi}}}{\delta\tilde{\phi}_1(p_1)} = \frac{\delta\Gamma_k^{\tilde{\phi}\tilde{\phi}}}{\delta\phi_1(p_1)} = \frac{\delta\Gamma_k^{\phi\tilde{\phi}}}{\delta\tilde{\phi}_2(p_1)} = \frac{\delta\Gamma_k^{\tilde{\phi}\tilde{\phi}}}{\delta\phi_2(p_1)} = 0. \tag{3.39}$$

This will considerably reduce the number of contributing diagrams, as we will see in section 3.5.

3.4 Dimensionless quantities

The flow equations based on equation (2.78) basically indicate the change of the effective average action Γ_k induced by the change of the scale k of momentum fluctuations already included. The critical point is characterized by the divergence of the correlation length ξ, as described in section 2.1. The presence of a divergent length scale will render all other scales unimportant, including the renormalization group scale k. Therefore we expect the effective average action to be invariant to small changes of the scale k and all other involved scales in the vicinity of the critical point. If we express all scales trough the renormalization group scale k, this will result in an invariance of our scale dependent quantities to variations of the scale, i.e. the critical point will appear as a fixed point in the flow equations of these

quantities.
For this reason, we will bring our scaling coefficients in a dimensionless form. For the static coefficients ρ_k and λ_k this means:

$$\rho_k^0 = k^{d-2+\eta_Z}\rho, \tag{3.40}$$

$$\lambda_k = k^{4-d-2\,\eta_Z}\lambda. \tag{3.41}$$

As we will mainly focus on the dimensionless quantities from here on, we will drop the scale index k and not further distinguish them from any quantities introduced before.
The exponent η_Z is the scaling exponent related to the wave function renormalization Z_k:

$$\eta_Z = -\partial_t \ln(Z_k). \tag{3.42}$$

At the critical point it will be independent of the scale k, so the wave function renormalization will have the scaling form $Z_k \propto k^{-\eta_Z}$. Its exponent η_Z is identical to the exponent η in the scaling equation for the spectral function (2.10), and is called the anomalous dimension of the system as it is the modification of the dimension of the renormalized field.
The momenta in the propagators will be rescaled by

$$\vec{q}^2 = y\,k^2. \tag{3.43}$$

The frequency in the propagators is a bit more complicated, as it is supposed to scale as $q_0 \to s^z q_0$ around the critical point. We will rescale it as

$$x = Y q_0, \tag{3.44}$$

with the rescaled damping coefficient:

$$Y_k = k^{2-\eta_Z}\,Y. \tag{3.45}$$

For the unitary coefficient we define a similar rescaled form:

$$X_k = k^{2-\eta_Z}\,X. \tag{3.46}$$

The rescaleing of the frequency is a choice which in a certain sense predicts some of the behavior around the critical point already. In the retarded (3.28) and advanced propagator (3.29) as well as in the spectral function (3.32) from which we intend to deduce the scaling behavior, the frequency

appears either paired with the damping coefficient Y_k or the unitary coefficient X_k. After rescaleing the frequency, they will therefore only appear in the ratio:

$$\alpha = \frac{X}{Y} = \frac{X_k}{Y_k}. \tag{3.47}$$

The two dynamic coefficient will have the scaling form

$$Y \propto k^{-\eta_Y} \tag{3.48}$$
$$X \propto k^{-\eta_X} \tag{3.49}$$
$$\tag{3.50}$$

around the critical point, where the scaling exponents η_X and η_Y are constant. In general, their scaling exponents are defined similar to the anomalous dimension η_Z:

$$\eta_Y = -\partial_t \ln(Y), \tag{3.51}$$
$$\eta_X = -\partial_t \ln(X). \tag{3.52}$$

The new defined coefficient α will therefore behave as

$$\alpha \propto k^{\eta_Y - \eta_X}. \tag{3.53}$$

So around the critical point, there are only three possible options for the behavior of α:

$$\eta_Y > \eta_X \ : \ \alpha \xrightarrow{k\to 0} 0, \tag{3.54}$$
$$\eta_Y = \eta_X \ : \ \alpha \xrightarrow{k\to 0} \text{const}, \tag{3.55}$$
$$\eta_Y < \eta_X \ : \ \alpha \xrightarrow{k\to 0} \infty. \tag{3.56}$$

If the third case would be true, the rescaling of the frequency with Y would be an inconvenient choice as α would diverge through our calculations. In this case we should rather rescale with X and work with the inverse ratio, which then would disappear.
So war we did not encounter a situation where the damping Y_k was dominated by any other dynamic coefficient, so rescaling with Y_k is a rather safe first choice in general. As we will see in section 3.8 the damping is usually directly related to the critical slowing down. If any of the dynamic ratios like α diverges, the choice of rescaling should be reconsidered.

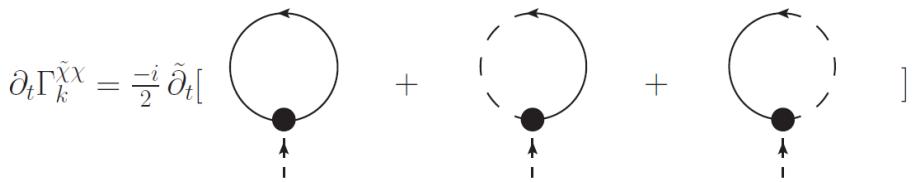

Figure 3.2: The diagrams in the full flow equation for the first order derivative of the effective action.

In the first two cases of (3.54)- (3.56), the dynamic critical exponent z is then defined by the scaling exponent of the damping Y:

$$z = \eta_Y. \tag{3.57}$$

In the third case, it would be defined by the scaling of the unitary coefficient X:

$$z = \eta_X. \tag{3.58}$$

This has a very direct physical meaning: the dynamic critical exponent z determines the divergence of the relaxation time as explained in section 2.1. If the critical exponent related to one dynamic coefficient is larger then the exponent of another, this means the related time scale diverges faster around the critical point. Approaching the critical temperature, the long time behavior of the dynamics will be completely dictated by the dynamics related to this coefficient then.

3.5 Diagrams and flow equations

We will focus on a classical, high temperature approximation first, where the temperature is larger then all involved frequencies $T >> q_0$. In this approximation, the Bose-Einstein distribution (2.101) simplifies to:

$$\left(n_{BE}(q_0) + \frac{1}{2}\right) \approx \frac{T}{q_0}. \tag{3.59}$$

We will extend the calculations to the full distribution function and discuss the effects of the quantum fluctuations on the critical and non-critical behavior of the system in section 3.9.

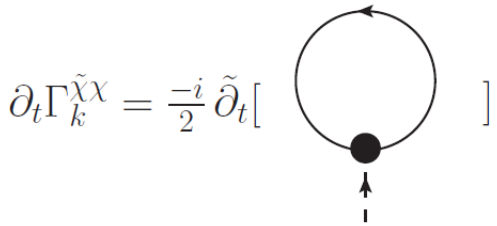

Figure 3.3: The remaining diagrams in the flow equation for the first order derivative of the effective action with the ansatz (3.12) applied.

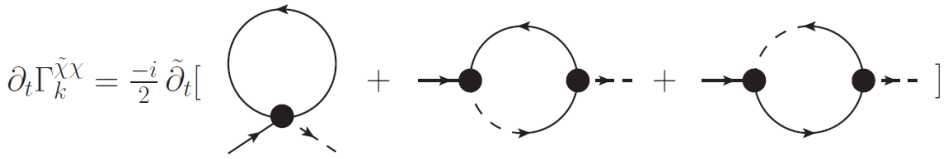

Figure 3.4: The remaining diagrams in the flow equation for the second order derivative of the effective action with the ansatz (3.12) applied.

All flow equations are of the two basic forms shown in figure 3.2 and figure 2.5. As several of the involved vertices vanish, as seen in section 3.3, our flow equations will simplify considerably. The flow equation for the first order derivative now has the diagrammatic form shown in figure 3.3, the one for the second order derivative the one shown in figure 3.4.
If we write out, for example, the remaining diagram of the first derivative flow equation shown in 3.3 in momentum space we get the following expressions to calculate:

$$\lim_{p\to 0}\partial_t \frac{\delta\Gamma_k}{\delta\tilde{\phi}(p)} = \sqrt{2\,\rho}\,T\,Y_k\,U''(\rho)\,\tilde{\partial}_t \times \int_q \frac{\left[\omega_1^2(\vec{q}) + 3\,\omega_2^2(\vec{q}) + 4\,q_0^2\,\left(X_k^2+Y_k^2\right)\right]}{\omega_1^2(\vec{q})\,\omega_2^2(\vec{q}) + q_0^2\,\left[Y_k\left(\omega_1^2(\vec{q})+\omega_2^2(\vec{q})\right) - 2\,X_k\omega_1(\vec{q})\,\omega_2(\vec{q})\right] + q_0^4\,\left(X_k^2+Y_k^2\right)^2}. \tag{3.60}$$

After bringing this into the dimensionless form described in section 3.4 and performing the derivative $\tilde{\partial}_t$ introduced in section 2.5, we can perform the spatial and frequency integrations.
The spatial integration can easily be performed after changing to spherical

coordinates,due to the rotational invariance of the system and the Heaviside theta functions in our chosen cutoff function (3.26). The frequency integration can be performed by using the residue theorem, see e.g. [72], resulting in the final flow equations for the dimensionless static coefficients:

$$\partial_t \rho = (2 - d - \eta_Z)\,\rho + T\,v_d \frac{(2 + d - \eta_Z)\left(1 + \lambda\rho + \lambda^2\rho^2\right)}{(1 + 2\rho\lambda)^2}, \tag{3.61}$$

$$\partial_t \lambda = (d - 4 + 2\eta_Z)\,\lambda + T\,v_d \lambda^2 \frac{(2 + d - \eta_Z)\left(5 + 3\lambda\rho + 6\lambda^2\rho^2 + 4\lambda^3\rho^3\right)}{(1 + 2\rho\lambda)^3}, \tag{3.62}$$

$$\eta_Z = T\,v_d \frac{(2 + d)\,\lambda^2\rho}{(1 + 2\rho\lambda)^2}. \tag{3.63}$$

The dynamic exponents and flow equations are:

$$\eta_Y = (2 - \eta_Z) + T\,v_d \lambda^2 \rho \frac{(2 + d - \eta_Z)\left(3 + 6\lambda\rho + 2\lambda^2\rho^2\right)}{(1 + \rho\lambda)^2\,(1 + 2\rho\lambda)^2}, \tag{3.64}$$

$$\eta_X = (2 - \eta_Z) + T\,v_d \lambda^2 \rho \frac{(2 + d - \eta_Z)\,(2 + d - \eta_Z)\left(-3 + 4\lambda\rho + 24\lambda^2\rho^2 + 24\lambda^3\rho^3 + 8\lambda^4\rho^4\right)}{(1 + \rho\lambda)^2\,(1 + 2\rho\lambda)^3}, \tag{3.65}$$

$$\partial_t \alpha = \alpha\,(\eta_Y - \eta_X)\,. \tag{3.66}$$

The prefactor v_d is

$$v_d = \frac{2^{1-d}\pi^{-\frac{d}{2}}}{\Gamma(2 + \frac{d}{2})}, \tag{3.67}$$

with the Euler gamma function $\Gamma(x)$.
We see a decoupling of the equations of the static coefficients from those of the dynamic ones, as we would expect in our classical approximation [15].

3.6 Fixed points and stability

Static Fixed Points

As the static sector decouples form the dynamic one, we can search for a fixed point in these equations independently. We find the static fixed point values for a temperature set to one in three and four spatial dimensions shown in table (3.1).

d	ρ	λ	η_z
3	0.0355	7.6887	0.0593
3	0.0675	0	0
4	0.0063	0	0

Table 3.1: Fixed point values of density ρ, coupling λ and anomalous dimension η_Z in three and four spatial dimensions d.

As usual, we see the Gaussian and the Wilson-Fisher fixed points for $d = 3$, whereas the theory becomes trivial in a macroscopically non interacting sense for dimensions equal to or larger than 4, i.e. only the gaussian fixed point with vanishing interactions is present.
For spatial dimensions of one or two we will not find any fixed points solutions for the equations (3.61) to (3.63) as predicted by the Mermin-Wagner Theorem [69], [46]. In these spatial dimensions no second order phase transition occurs, but there is still a divergence in the correlation length to be found in the sense of a Kosterlitz-Thouless transition [54].
If we analyze the stability of the fixed points in three dimensions by expanding the flow equations (3.61) and (3.62) for values of the density ρ and the interaction λ separately and calculating the eigenvalues of the resulting matrix, we find two repulsive directions for the Gaussian fixed point and one attractive and one repulsive direction for the Wilson-Fisher fixed point. Out of these two, the latter is the stable one. We still have to tune one parameter to reach the critical region around this fixed point due to the repulsive direction. This corresponds to tuning the Temperature to the critical value. We can visualize the flow to these fixed points by plotting the flow equations (3.61) and (3.62), with the anomalous dimensions (3.63) inserted, in a vector diagram as shown in figure 3.5 for the three dimensional and figure 3.6 for the four dimensional case.

If we modify our approximation for demonstrative purposes by setting $\eta_Z = 0$, the analytic solutions for the stable fixed points are simply

$$\rho_c = \frac{T}{3\,\pi^2}, \tag{3.68}$$

$$\lambda_c = \frac{3\,\pi^2\,\left(\sqrt{3}-1\right)}{2\,T}, \tag{3.69}$$

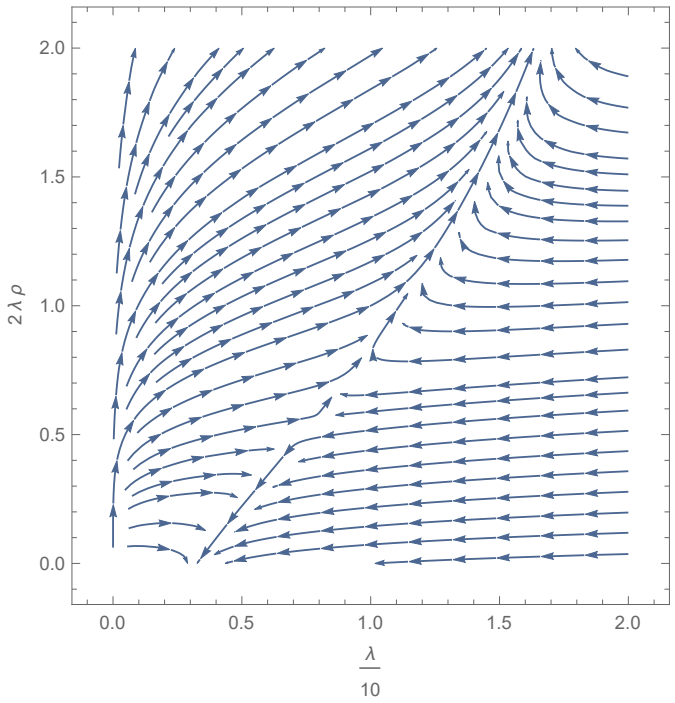

Figure 3.5: The flow of ρ and λ in three spatial dimensions for $T = 1$. We can see the two repulsive directions for the Gaussian fixed point at $(0, 0)$ and one attractive and one repulsive one for the Wilson-Fisher fixed point at $(0.55, 7.7)$. The arrows point in the direction of $-t$.

in three spatial dimensions and

$$\rho_c = \frac{T}{16\,\pi^2}, \tag{3.70}$$

$$\lambda_c = 0 \tag{3.71}$$

in four.

The stability properties of the fixed points can be determined by an expansion of the flow equations around the corresponding fixed point values of ρ and λ. If we abbreviate the right hand side of the flow equations (3.61) and (3.62) as $f_\rho(\rho, \lambda)$ and $f_\lambda(\rho, \lambda)$, an expansion to linear order around the fixed point values yields:

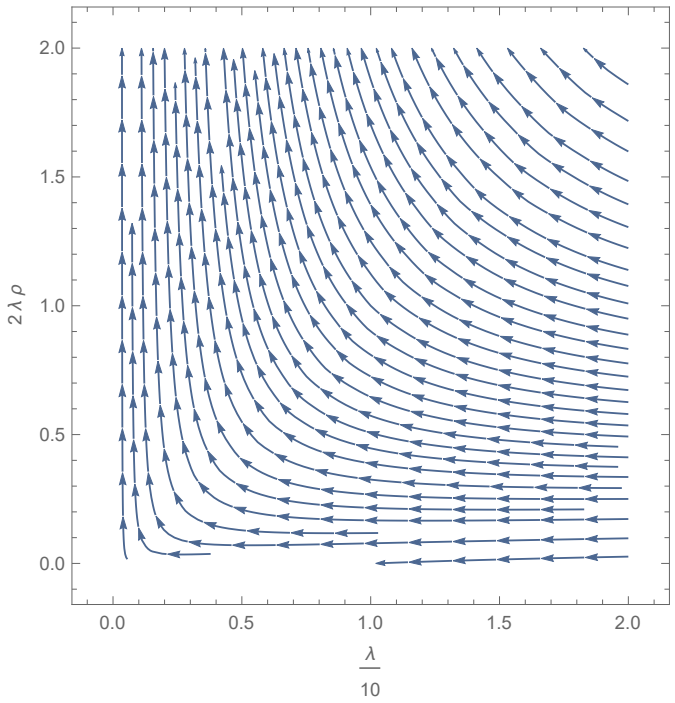

Figure 3.6: The flow of ρ and λ in four spatial dimensions for $T = 1$. Only the Gaussian fixed point at $(0, 0)$ can be found. The arrows point in the direction of $-t$.

$$\partial_t \rho \approx \partial_\rho f_\rho(\rho_c, \lambda_c)\,(\rho - \rho_c) + \partial_\lambda f_\rho(\rho_c, \lambda_c)\,(\lambda - \lambda_c)\,, \tag{3.72}$$

$$\partial_t \lambda \approx \partial_\rho f_\lambda(\rho_c, \lambda_c)\,(\rho - \rho_c) + \partial_\lambda f_\lambda(\rho_c, \lambda_c)\,(\lambda - \lambda_c)\,. \tag{3.73}$$

Then functions $f_\rho(\rho, \lambda)$ and $f_\lambda(\rho, \lambda)$ are usually called the beta functions for ρ and λ. We denote them by f instead of β to avoid confusion with the dynamic coefficient β introduced below.
As the fixed point values ρ_c and λ_c are independent of the renormalization group parameter t, we can reformulate equation (3.72) in matrix form as

$$\partial_t \begin{pmatrix} \delta\rho \\ \delta\lambda \end{pmatrix} = \begin{pmatrix} \partial_\rho f_\rho(\rho_c, \lambda_c) & \partial_\lambda f_\rho(\rho_c, \lambda_c) \\ \partial_\rho f_\lambda(\rho_c, \lambda_c) & \partial_\lambda f_\lambda(\rho_c, \lambda_c) \end{pmatrix} \begin{pmatrix} \delta\rho \\ \delta\lambda \end{pmatrix} \tag{3.74}$$

$$= \hat{A} \begin{pmatrix} \delta\rho \\ \delta\lambda \end{pmatrix}, \tag{3.75}$$

with $\delta\rho = \rho - \rho_c$ and $\delta\lambda = \lambda - \lambda_c$.
If we find the unitary matrix $\hat{S}$ that diagonalizes the matrix $\hat{A}$ on the right hand side of equation (3.74),

$$\hat{S}\hat{A}\hat{S}^{-1} = \begin{pmatrix} \kappa_1 & 0 \\ 0 & \kappa_2 \end{pmatrix}, \tag{3.76}$$

with the eigenvalues κ_i of $\hat{A}$, we can solve the diagonalized form of equation (3.74) by using an exponential ansatz for each of the components of the vector $\vec{s} = \begin{pmatrix} s_1 \\ s_2 \end{pmatrix} = \hat{S} \begin{pmatrix} \delta\rho \\ \delta\lambda \end{pmatrix}$. Equation (3.74) decouples into two linear differential equations if we diagonalize the matrix $\hat{A}$:

$$\partial_t s_1 = \kappa_1 \, s_1 \tag{3.77}$$
$$\partial_t s_2 = \kappa_2 \, s_2. \tag{3.78}$$

The equations (3.77) and (3.78) are solved by

$$\vec{s} = \begin{pmatrix} a_1 \, e^{\kappa_1 t} \\ a_2 \, e^{\kappa_2 t} \end{pmatrix}. \tag{3.79}$$

So we see that the eigenvalues of $\hat{A}$ indicate the stability of the fixed point. A positive eigenvalue marks a stable or irrelevant direction, a negative eigenvalue an unstable or relevant direction. Note that the renormalization group parameter runs from zero to minus infinity.
In general, we call the fixed point with the least relevant directions the stable one. For our second order phase transition, we expect one relevant direction for the stable fixed point, as we have to tune to one parameter, usually the temperature, to its critical value to reach the fixed point.
Calculating the eigenvalues for the Wilson fisher fixed point in three dimensions shown in equation (3.68) and (3.69), we find

$$\kappa_1 = -1.61 \tag{3.80}$$
$$\kappa_2 = 0.38. \tag{3.81}$$

Note that the exponents are universal as they are independent of temperature or initial conditions of the flow. As predicted, one exponent is positive and one negative, so the flow is attracted to the fixed point in the direction of

the first eigenvector and repulsed in the direction of the second eigenvector. If the coefficient a_1 in the solution (3.79) is chosen to be much smaller than one, the flow will be attracted towards the fixed point and stay in its vicinity until the exponential factor becomes large enough to drive it away.
We can apply the inverse of the matrix $\hat{S}$ to the solution $\vec{s}$ of the diagonalized equations to gain the solutions for $\delta\rho$ and $\delta\lambda$:

$$\delta\rho = 7\,T^2\,\left[a_1\,10^{-3}\,e^{\kappa_1 t} - a_2\,10^{-4}\,e^{\kappa_2 t}\right] \tag{3.82}$$

$$\delta\lambda = a_1\,e^{\kappa_1 t} + a_2\,e^{\kappa_2 t}. \tag{3.83}$$

We can connect the coefficient a_1 to the initial values of $\delta\rho$ and $\delta\lambda$:

$$a_1 = \frac{9}{T^2}\left[10^{-2}\,T^2\,\delta\lambda_0 + 14\,\delta\rho_0\right]. \tag{3.84}$$

Setting $a_1 = 0$, this allows us to calculate relations between the initial density and coupling and the critical temperature. These relations are of course only valid for initial conditions in the vicinity of the fixed point.

Dynamic Fixed Points

The fixed point of the dynamic equation (3.66), evaluated at the static Wilson-Fisher fixed point in three spatial dimensions, is zero. To actually capture a possible diverging behavior of α as shown in (3.56), we define a new quantity β:

$$\beta = \frac{\alpha}{1+\alpha}. \tag{3.85}$$

For the three different, possible fixed point behaviors of α shown in (3.54) -(3.56), it will become:

$$\beta \xrightarrow{\alpha\to 0} 0, \tag{3.86}$$

$$\beta \xrightarrow{\alpha\to \text{const}} \text{const}, \tag{3.87}$$

$$\beta \xrightarrow{\alpha\to \infty} 1. \tag{3.88}$$

Examining the flow equation for β, we indeed find a fixed point for $\beta = 0$ as well as $\beta = 1$. As shown in figure 3.7, the fixed point at $\beta = 0$ is the stable one of the two, therefore justifying our choice of rescaling for the frequencies in equation (3.44).

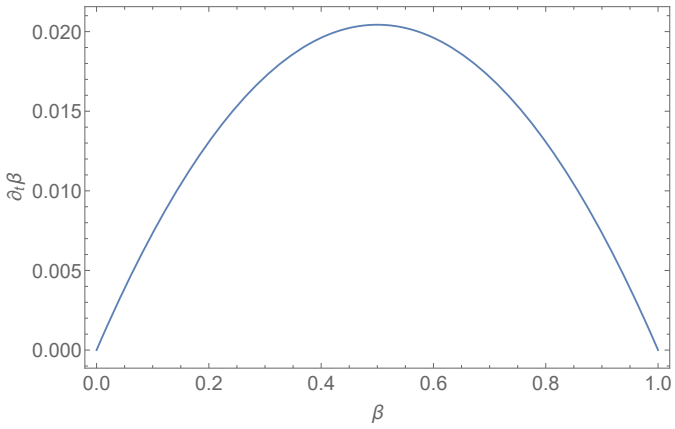

Figure 3.7: The flow of β in three dimensions, evaluated at the ρ and λ values of the Wilson-Fisher fixed point. We can see the two fixed points at $\beta = 0$ and $\beta = 1$. The flow will lead to $\beta = 0$ for all values of β between 0 and 1.

We see that the unitary coefficient X_k becomes irrelevant at the critical point. This corresponds to the universality class of Model A in the categorization scheme of Halperin and Hohenberg [47]. The different dynamic universality classes will be discussed further in chapter 5. The universality class of Model A has been studied in the framework of the functional renormalization group in reference [20].
The dynamic critical exponent for the stable fixed point in three dimensions is

$$z = \eta_X = 2.027. \tag{3.89}$$

More sophisticated truncations could include the dynamics of conserved quantities like the particle number in the approximation. These are generally believed to be relevant for the critical dynamics of non-relativistic bosonic systems, assuming their univerality class to be actually Model E in the Halperin and Hohenberg classification scheme. Compare for example reference [47] or [36].

3.7 Numerical solutions of the flow equations

After all integrations are performed, the resulting flow equations (3.61) - (3.66) can be solved easily applying standard numerical methods. As we

have seen, the static equations (3.61) - (3.63) decouple from the dynamic coefficients, so we can treat them independently of the dynamics. To find the critical exponents we have to tune the system close to its phase transition. It is convenient to fix the temperature and initial coupling and vary the initial density close to the point were the system switches its macroscopic density $\lim_{k\to 0} \rho_k^0$ from a non-vanishing value in the spontaneous symmetry breaking phase to zero in the symmetric phase.
This corresponds to following a fixed λ line in the flow diagram shown in figure 3.5 until we reach the intersection with the attractive line leading directly to the fixed point. If we start our flow close to this line, it will follow it towards the critical point and stay in its vicinity for a certain amount of renormalization group time t, depending on how precise we tuned the initial conditions. This is equivalent to choosing the initial coefficient of the repulsive direction as small as possible, as discussed in section 3.6. Afterwards the repulsive term will grow large and the system will flow either to an infinite value of the dimensionless density ρ, corresponding to the symmetry broken phase, or it will reach $\rho = 0$. At this point we have to stop the flow and switch to the flow equations of the symmetric phase.
In figures 3.8 - 3.10 we show examples of solutions of the flow for different initial conditions. We fixed the temperature to $T = 1$ and the initial coupling to $\lambda|^{t=0} = 0.1$ and tuned the initial density to values slightly larger (blue and orange lines) and smaller (green and red lines) than the value of ρ at the intersection with the attractive line for these parameters.
The difference between the initial density of the two initial values in the symmetric and in the symmetry broken phases lies at roughly $\Delta\rho \approx 10^{-14}$ each. The amounts of renormalization group time the systems stay in the vicinity of the critical point are already very different here, which emphasizes the importance of numerical fine tuning in the search for the critical point.
We can see in the plot of the density in figure 3.8 how the flow approaches the fixed point value calculated in section 3.6, and stays almost constant for an amount of renormalization group time depending on the precision of the tuning of the initial values. The same is true for the coupling, seen in figure 3.9. In this region, the flow effectively adopts the fixed point values, so the critical exponents can be read off here. The anomalous dimension seen in figure 3.10 is an example, it approaches the value found in fixed point analysis in section 3.6.

The dynamic flow equation (3.66) can be solved for the different static solutions discussed above. In figure 3.11 we see solutions for the same initial value of α for the different static solutions discussed, indicated by the color

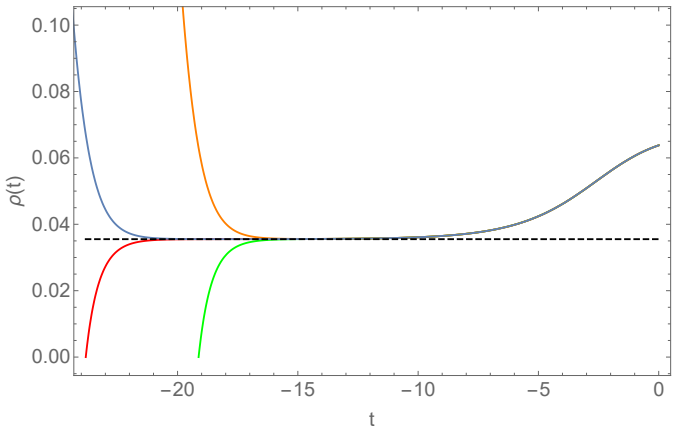

Figure 3.8: The flow of the dimensionless density ρ in three dimensions for initial values slightly above (blue, orange) and below (red, green) the critical initial values, as well as the exact fixed point value (black, dashed) from section 3.6

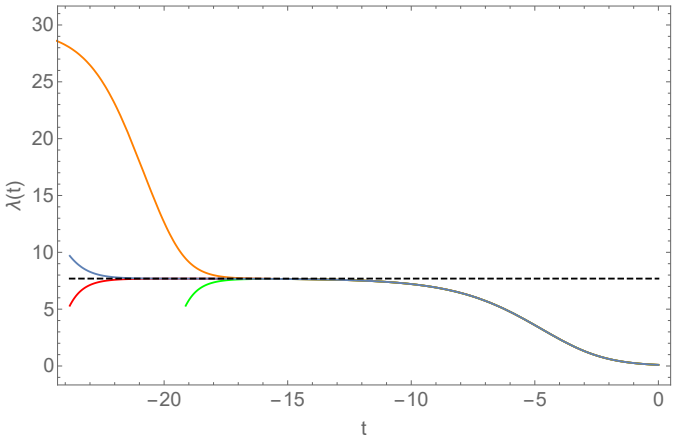

Figure 3.9: The flow of the dimensionless interaction λ in three dimensions for initial values slightly above (blue, orange) and below (red, green) the critical initial values, as well as the exact fixed point value (black, dashed) from section 3.6

of the plots. They all approach the $\alpha = 0$ fixed point in the critical region, as predicted in section 3.6. The corresponding scaling exponents η_Y and η_X can be seen in figure 3.12 and 3.13. Their critical values can be read off as the flow approaches the fixed point, and the dynamic critical exponent z can

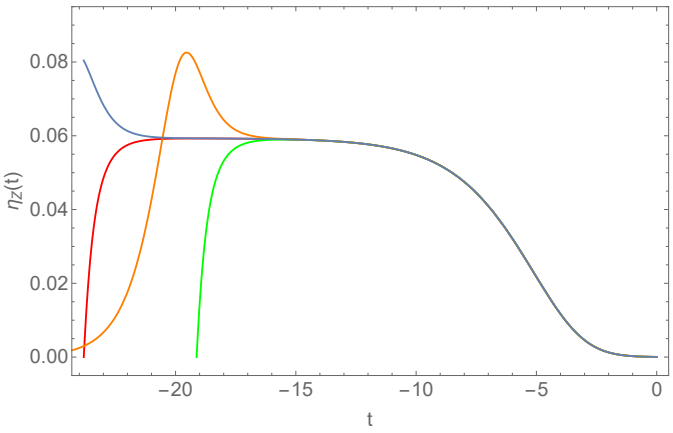

Figure 3.10: The flow of the anomalous dimension η_Z in three dimensions for initial values slightly above (blue, orange) and below (red, green) the critical initial values, as well as the exact fixed point value (black, dashed) from section 3.6

be extracted from the value of η_Y simply by $z = \eta_Y$ for the case of $\alpha = 0$, as explained in section 3.4.
The flow of the dimensionful unitary coefficient X_k and the damping coefficient Y_k compared to their initial values can be seen in figures 3.12 and 3.13. In the critical regime the damping grows exponentially. This can be confirmed if we solve the dynamic equations for ρ and λ evaluated at the fixed point values, assuming the static sector has been tuned to the critical point exactly. Then the equation for α simplifies to

$$\partial_t \alpha = 0.091\, \alpha, \tag{3.90}$$

for a system in three spatial dimensions at the Wilson Fisher fixed point and at a temperature of $T = 1$. Its solved by a simple exponential decay of alpha. The solutions for X_k and Y_k at this fixed point are:

$$Y_k = Y_\Lambda\, e^{-2.027\, t}, \tag{3.91}$$
$$X_k = X_\Lambda\, e^{-1.936\, t}. \tag{3.92}$$

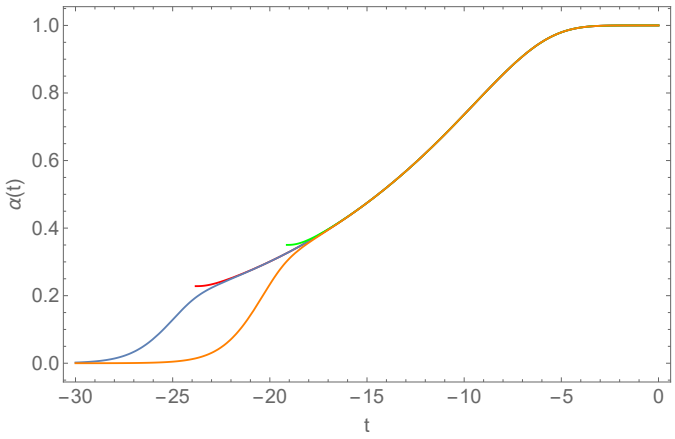

Figure 3.11: The flow of the dynamic coefficient α in three dimensions for static initial values slightly above (blue, orange) and below (red, green) the critical initial values. The initial value of α is one for all plots.

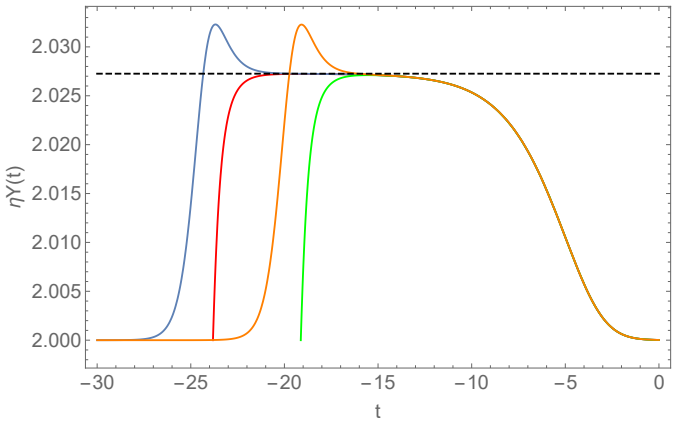

Figure 3.12: The flow of the dynamic exponent η_Y in three dimensions for static initial values slightly above (blue, orange) and below (red, green) the critical initial values, as well as the exact fixed point value (black, dashed) from section 3.6. The initial value of α is one for all plots.

3.8 Stochastic differential equations and interpretation of the dynamic coefficients

In this section we connect our keldysh path integral approach to the field of stochastic differential equations to get an additional perspective on the

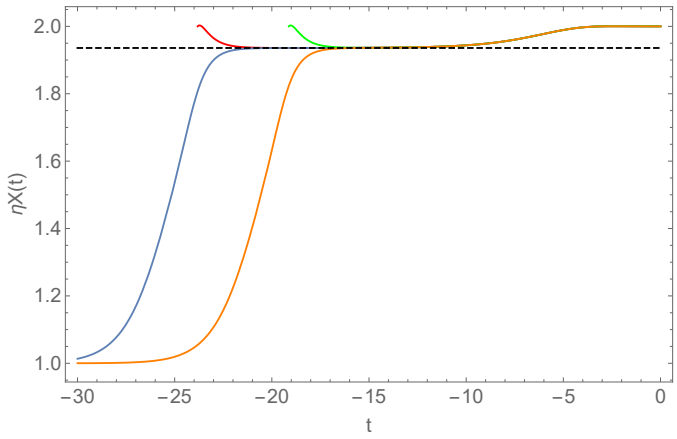

Figure 3.13: The flow of the dynamic exponent η_X in three dimensions for static initial values slightly above (blue, orange) and below (red, green) the critical initial values, as well as the exact fixed point value (black, dashed) from section 3.6. The initial value of α is one for all plots.

interpretation of the coefficients in our ansatz (3.12).

Path integral representation of stochastic differential equations

To do this, we first show that solving the path integral for our action (3.1) is equivalent to averaging over the stochastic differential equation

$$\partial_t \psi_i(x) = -D \frac{\delta F[\psi]}{\delta \psi_i(x)} + \xi_i(x), \tag{3.93}$$

which is called the Langevin equation. More general information about Langevin type equations can be found, e.g., in the references [61] and [23]. We assume the fields to be real here, and the role of the functional F and the coefficient D will be specified later. A detailed discussion about the functional integral representation of stochastic differential equations can be found in reference [68].
The real function $\xi(x)$ appearing in equation (3.93) is a gaussian distributed random noise function:

$$\langle \xi_i(x) \rangle = 0, \tag{3.94}$$

$$\langle \xi_i(x) \xi_j(y) \rangle = 2\,T\,D\,\delta_{ij}\,\delta^4(x-y). \tag{3.95}$$

For a classical equation of motion, we would produce average values of observables by averaging over the solutions to the equation for all possible initial values of the fields, weighted by a factor representing the initial preparation of the system:

$$\langle O \rangle_C = \frac{1}{Z_C} \int D\psi\, O(\psi(x))\, \rho_0(\psi(0,\vec{x}))\, \Pi_i\, \delta(\frac{\delta S[\psi]}{\delta \psi_i(x)}), \tag{3.96}$$

$$Z_C = \int D\psi\, \rho_0(\psi(0,\vec{x}))\, \Pi_i\, \delta(\frac{\delta S[\psi]}{\delta \psi_i(x)}). \tag{3.97}$$

S is the classical action, the function ρ_0 is the classical analog to the initial density matrix in the quantum field theoretical partition function shown in equation (2.23).
In the case of the Langevin equation, there is no additional statistical weight factor like ρ_0. Instead, we average over the solutions of the equation (3.93) for all initial conditions of the fields and all possible realizations of the noise function $\xi(x)$. The average over the noise function is weighted with a factor $e^{-\int_x \frac{1}{4\,T\,D} \xi(x)^2}$ to ensure its gaussian distribution as shown in equations (3.94) and (3.95). For a stochastic differential equation of the form (3.93), the average of an observable is then

$$\langle O \rangle_S = \frac{1}{Z_S} \int D\psi\, D\xi(x)\, O(\psi(x))\, e^{-\int_x \frac{1}{4\,T\,D} \xi_i(x)^2}\, \Pi_i\, \delta(\partial_t \psi_i(x) + D \frac{\delta\, F[\psi]}{\delta \psi_i(x)} - \xi_i(x)), \tag{3.98}$$

$$Z_S = \int D\psi\, D\xi(x)\, e^{-\int_x \frac{1}{4\,T\,D} \xi(x)^2}\, \Pi_i\, \delta(\partial_t \psi_i(x) + D \frac{\delta\, F[\psi]}{\delta \psi_i(x)} - \xi_i(x)). \tag{3.99}$$

As before, we can construct a generating functional for these observables by introducing external sources to the partition functions Z_C and Z_S, as explained in section 2.3.
We can represent the delta distributions in the stochastic path integral as a functional integral over an auxiliary field each:

$$\delta(\partial_t \psi_i(x) + D \frac{\delta\, F[\psi]}{\delta \psi_i(x)} + \xi_i(x)) = \int D\tilde{\psi}\, e^{i \int_x \tilde{\psi}(x) \left[\partial_t \psi_i(x) + D \frac{\delta\, F[\psi]}{\delta \psi_i(x)} - \xi_i(x)\right]}. \tag{3.100}$$

This allows us to perform the integration over the different realizations of the noise function:

$$Z_S = \int D\psi\, D\tilde{\psi}\, D\xi(x)\, e^{-\int_x \frac{1}{4\,T\,D}\xi_i(x)^2}\, e^{i\int_x \left\{\tilde{\psi}_i\left[\partial_t\psi_i(x)+D\frac{\delta\,F[\psi]}{\delta\psi_i(x)}-\xi_i(x)\right]\right\}} \tag{3.101}$$

$$= N\int D\psi\, D\tilde{\psi}\; e^{i\int_x \left\{\tilde{\psi}_i\left[\partial_t\psi_i(x)+D\frac{\delta\,F[\psi]}{\delta\psi_i(x)}\right]-T\,D\,\tilde{\psi}^2(x)\right\}}. \tag{3.102}$$

N is a factor produced by the gaussian integration over the noise functions, which is irrelevant for any correlation functions.
So the stochastic partition function can be represented as a path integral over the physical and auxiliary fields, which is similar in form to our keldysh path integral introduced in section 2.3:

$$Z_S = N\int D\psi\, D\tilde{\psi}\, e^{iS_S[\psi,\tilde{\psi}]}, \tag{3.103}$$

with the stochastic action

$$S_S[\psi,\tilde{\psi}] = \int_x \left\{\tilde{\psi}_i\,\left[\partial_t\psi_i(x) + D\frac{\delta\,F[\psi]}{\delta\psi_i(x)}\right] -\, T\,D\,\tilde{\psi}^2(x)\right\}. \tag{3.104}$$

The auxiliary field introduced through the delta functions plays the role of the quantum field in the keldysh approach.
We can now fix the number of fields to two, and choose an appropriate functional $F[\psi]$:

$$F[\psi] = \int_x X_k\,\left[\psi_2(x)\,\partial_t\psi_1(x) + \psi_1(x)\,\partial_t\psi_2(x)\right] +\, H_k^{GL}[\psi], \tag{3.105}$$

with the effective Ginzburg-Landau Hamiltonian

$$H_k^{GL}[\psi] = \int_x \left[\frac{1}{2}\,Z_k\,\left(\nabla\psi_i(x)\right)\,\left(\nabla\psi_i(x)\right) + U_k(\psi_i(x))\right], \tag{3.106}$$

$$U_k(\psi_i(x)) = \frac{\lambda_k}{2}\,\left(\frac{\psi_i^2(x)}{2} - \rho_k^0\right)^2, \tag{3.107}$$

redefine the factor D as $D = \frac{1}{Y_k}$ and rescale it into the auxiliary field to finally get a stochastic action

$$S_S[\psi,\tilde{\psi}] = \int_x \left\{X_k\,\left[\tilde{\psi}_2(x)\,\partial_t\psi_1(x) + \tilde{\psi}_1(x)\,\partial_t\psi_2(x)\right] + \tilde{\psi}_i\,\left[Y_k\,\partial_t\psi_i(x) + \frac{\delta H_k^{GL}[\psi]}{\delta\psi_i(x)}\right] -\, T\,Y_k\,\tilde{\psi}^2(x)\right\}. \tag{3.108}$$

So with this choice for the functional F and the factor D, the averaging procedure over the Langevin equation (3.93) will produce the exact same path integral as our Keldysh approach for the Gross-Pietaevskii action (3.11) if we set the k dependent coefficients to its cutoff values as in the classical action (3.1).

Linearized equations of motion and interpretation of the dynamic coefficients

This equivalence of representations gives us insight in the meaning of the coefficients involved in our ansatz (3.12). At any scale k during our renormalization group flow, instead of following the flow further to $k = 0$ we can instead translate the problem to the equivalent task of solving the equations

$$Y_k\,\partial_t\psi_1(x) + X_k\,\partial_t\psi_2(x) = -\frac{\delta\,H_{GL}[\psi]}{\delta\psi_1(x)} + \xi_1(x), \tag{3.109}$$

$$Y_k\,\partial_t\psi_2(x) + X_k\,\partial_t\psi_1(x) = -\frac{\delta\,H_{GL}[\psi]}{\delta\psi_2(x)} + \xi_2(x), \tag{3.110}$$

for all initial condition of the fields and realizations of the noise function with a new ultraviolet cutoff $\tilde{\Lambda} = k \leq \Lambda$. For the following calculations it is more convenient to express the equations of motion again in the complex fields, compare section 3.1:

$$Y_k\,\partial_t\psi(x) + X_k\,i\,\partial_t\psi(x) = -\frac{\delta\,H_{GL}[\psi]}{\delta\psi^*(x)} + \xi(x). \tag{3.111}$$

And its complex conjugate. The noise function is now the complex valued function $\xi(x) = \xi_1(x) + i\,\xi_2(x)$.
We see that the first term on the right hand side will vanish if the field is at the minimum of the Ginzburg-Landau Hamiltonian H_{GL}, reducing the right hand side of the equation to the noise function. To get an impression of the dynamic behavior of the system for field configurations close to this minimum, we expand the Ginzburg-Landau Hamiltonian to first order around it:

$$Y_k\,\partial_t\delta\psi(x) + X_k\,i\,\partial_t\delta\psi(x) \approx -\left(-Z_k\,\nabla^2 + 2\,\rho_0^k\,\lambda_k\right)\,\delta\psi(x) + \xi(x). \tag{3.112}$$

Here the function $\delta\psi(x)$ describes the difference of the field configuration from the minimum of the Ginzburg-Landau Hamiltonian.
If we define a dimensionless noise function $\tilde{\xi}(x) = \frac{\xi(x)}{T_k\,k^2}$, we can switch to

a dimensionless form of the equation using the dimensionless coefficients defined in section 3.4:

$$Y\,\partial_t\delta\psi(x) + X\,i\,\partial_t\delta\psi(x) = -\left(-\nabla^2 + 2\,\rho_0\,\lambda\right)\,\delta\psi(x) + \tilde{\xi}(x). \tag{3.113}$$

If we ignore the noise function for a moment, we can solve this equation by performing a spatial Fourier transformation

$$Y\,\partial_t\delta\psi(t,\vec{p}) + X\,i\,\partial_t\delta\psi(t,\vec{p}) = -\omega(\vec{p})\,\delta\psi(t,\vec{p}) + \tilde{\xi}(t,\vec{p}). \tag{3.114}$$

with $\omega(\vec{p}) = \vec{p}^2 + 2\,\rho_0\,\lambda$, and using the exponential ansatz

$$\delta\psi(t,\vec{p}) = \delta\psi_0(\vec{p})\,e^{-\frac{\omega(\vec{p})}{Y+iX}\,(t-t_0)}. \tag{3.115}$$

Here $\delta\psi_0(\vec{p})$ is the initial field configuration in momentum space at the time $t = t_0$. We can rewrite this solution using the comparison coefficient $\alpha = \frac{X}{Y}$ introduced in section 3.4 and the dimensionless time $\tau = \frac{t-t_0}{Y}$:

$$\delta\psi(t,\vec{p}) = \delta\psi_0(\vec{p})\,e^{-\frac{\omega(\vec{p})}{1+i\alpha}\,\tau}. \tag{3.116}$$

Solutions for different values of $\omega(\vec{p})$ and α can be seen in figure 3.14. All solutions show damped oscillations over time. The smaller the coefficient α becomes, the stronger the solution is damped.

In the limiting case $Y_k \to 0$, as we have it at the ultraviolet cutoff Λ, any perturbation to the equilibrium field configuration will propagate indefinitely. The noise term will vanish completely in this limit, as its weight factor $e^{-\int_x \frac{1}{4T}\xi(x)^2}$ will suppress any noise configurations in the path integral except $\xi(x) = 0$. So the Langevin equation (3.111) will reduce to the classical Gross-Pietaevskii equation in this limit.

If we start to integrate out high momentum mode, the damping coefficient Y_k will built up. So will the noise function, as its strength is proportional to $Y_k\,T$. The noise function will not have an impact on the general form of the dynamics but in general only put static noise on the solutions. The linearized form of the equation can still easily be solved by:

$$\delta\psi(t,\vec{p}) = \left[\delta\psi_0(\vec{p}) + \int_{t_0}^{t} dt'\,\eta(t',\vec{p})\,e^{\frac{\omega(\vec{p})}{Y+iX}\,(t'-t_0)}\right]\,e^{-\frac{\omega(\vec{p})}{Y+iX}\,(t-t_0)}. \tag{3.117}$$

These solutions basically have two phases. While the first term in the amplitude factor, the initial field configuration $\psi_0(\vec{p})$, is larger than the second, noise related term the system will relaxate towards the minimum of H_{GL}. This is always the case at $t = t_0$, where the second term vanishes. As the

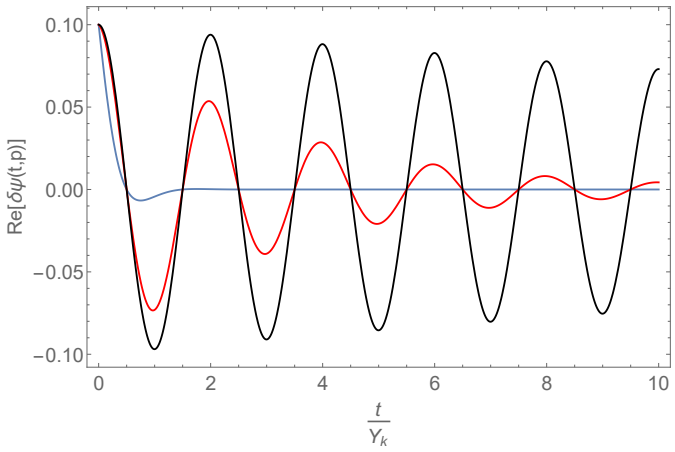

Figure 3.14: Solutions to the linearized Langevin equation (3.114) for the initial field configuration $\delta\psi_0(\vec{p}) = 1$ shown for the spatial momenta chosen such that $\omega(\vec{p}) = 1$. The plots show solutions for $\alpha = 1$ (blue), $\alpha = 10$ (red) and $\alpha = 100$ (black). The smaller the value of α the stronger is the damping of the oscillations of the perturbation.

system approaches this equilibrium state, the initial configuration becomes irrelevant. The noise function will randomly drive the system away from the equilibrium configuration, while the damping relaxates it back towards it. The larger the temperature T of the system, the stronger is the system driven away by the noise.
In summary we see that the fast, i.e high momentum modes we integrated out during our functional renormalization group flow will act as a heat bath for the slower modes that are yet to include.
The other limiting case $X \to 0$ or, more general $\alpha \to 0$, reduces equation (3.111) to a pure Langevin equation. This is the case at the critical point, where we have seen that α vanishes in sections 3.6 and 3.5. The critical dynamic is therefore purely relaxational, without a unitarily propagating component. Additionally, we found the coefficient Y to be divergent in the vicinity of the critical point. As we can see in equation (3.93), this will lead to a vanishing relaxation coefficient D and therefore a diverging relaxation time, as we would expect around the critical point. So while the dynamic of the field is still relaxational, any perturbation will nevertheless persist indefinitely in the system as the time scale of the relaxation back to the equilibrium configuration is diverging. This dynamic property of a system at a second order phase transition is called critical slowing down. The re-

lation between the noise and damping expressed in (3.95) is called Einstein relation, see [28], and is equivalent to the Fluctuation-Dissipation relation in the classical limit of the distribution function n. We can easily generalize this relation for a full quantum system by taking the full noise term as seen in (3.11) into account and calculate back to the Langevin equation. The form of equation (3.93) will be the same, but the weight of the gaussian noise function will adopt a more complicated form, including additional time derivatives.

3.9 Quantum effects

To highlight the differences between the classical and full quantum system, we will go back to a more general truncation for this section. If we drop all indices except the frequencies, all diagrams used in projections on static coefficients, i.e. without derivatives with respect to the external frequencies necessary for projections, will be of the form:

$$\lim_{p_0 \to 0} D(p_0) = \int_{q_0,\vec{q}} \left(n_{BE}(q_0) + \frac{1}{2} \right) f(a_i q_0^{n_i}). \tag{3.118}$$

The coefficients a_i are the dimensionless forms of the dynamic coefficients appearing in the effective action, n_i is the order of the time derivative the accompany. Note that this coefficients can in general depend on spatial momenta and field expectation value.
As discussed in section 3.4, we will now rescale the frequencies with the dynamic coefficient a_j with the largest scaling exponent at the fixed point compared to the power of frequencies it appears with:

$$\frac{\eta_{a_j}}{n_j} \geq \frac{\eta_{a_i}}{n_i}, \tag{3.119}$$

$$x = a_j^{\frac{1}{n_j}} q_0. \tag{3.120}$$

As usual, the scaling exponents ηa_i are defined as

$$\partial_t \log(a_i) = -\eta_{a_i}. \tag{3.121}$$

The diagrams relevant for the static projections now are of the form:

$$\lim_{p_0 \to 0} D(p_0) = \int_{x,\vec{q}} a_j^{-\frac{1}{n_j}} \left(n_{BE}(x\, a_j^{-\frac{1}{n_j}}) + \frac{1}{2} \right) f(\alpha_i\, x^{n_i}). \tag{3.122}$$

Here the α_i are the generalized comparison coefficients as introduced before for X and Y:

$$\alpha_i = a_i \, a_j^{-\frac{n_i}{n_j}}. \tag{3.123}$$

It is worth mentioning here again that only dynamic coefficients with scaling exponents fulfilling

$$\frac{\eta_{a_j}}{n_j} = \frac{\eta_{a_i}}{n_i} \tag{3.124}$$

are relevant for the dynamics at the critical point. The comparison coefficients of all other dynamic coefficients will vanish at the fixed point.
If we look at equation (3.122), we see that it depends on $i-1$ comparison coefficients α_i, as $\alpha_j = 1$ by definition, and one dynamic coefficient a_j. In a classical situation, where the distribution function reduces to

$$\left(n_{BE}(q_0) + \frac{1}{2}\right) \approx \frac{T}{q_0}, \tag{3.125}$$

the diagrams will only depend on the $i-1$ comparison coefficients:

$$\lim_{p_0 \to 0} D(p_0) = \int_{x,\vec{q}} \frac{T}{x} \, f(\alpha_i \, x^{n_i}). \tag{3.126}$$

We can see that at a critical point at non-zero temperature $T > 0$, the diagrams will reduce to the same form and the system will therefore always behave classically by examining the behavior of a_j.
The dynamic coefficient a_j will diverge as

$$a_j = c \left(\frac{k}{\Lambda}\right)^{-\eta_{a_j}} \tag{3.127}$$

as the renormalization group scale k goes to zero. We can always assume its scaling exponent η_{a_j} to be positive here, as it is connected to the dynamic critical exponent z by

$$\eta_{a_j} = n_j \, z. \tag{3.128}$$

The dynamic critical exponent z will always be positive for a second order phase transition with a diverging relaxation time by definition.
Through this divergence of the dynamic coefficient a_j at the critical point,

we see that in the limit of vanishing renormalization group scale k the distribution function as it appears in the rescaled diagrams will always behave like

$$\lim_{k\to 0} a_j^{-\frac{1}{n_j}} \left(n_{BE}(x\, a_j^{-\frac{1}{n_j}}) + \frac{1}{2} \right) = \frac{T}{x}, \tag{3.129}$$

for non-vanishing temperatures.
The projections onto the dynamic coefficients will include derivatives with respect to the external frequencies:

$$\partial_t a_i \propto \lim_{p_0\to 0} \partial_{p_0}^{n_j} D(p_0). \tag{3.130}$$

We can rescale these external frequencies similar to the internal loop frequencies q_0:

$$x_p = a_j^{\frac{1}{n_j}} p_0. \tag{3.131}$$

Through shifts of the integration of the internal frequencies in the loops we can ensure that the distribution function is independent of the external frequencies, which allows us to bring the resulting diagrams again in a form similar to the one in equation (3.126):

$$\partial_t a_i \propto \lim_{p_0\to 0} \partial_{p_0}^{n_j} D(p_0) = a_j^{\frac{n_i}{n_j}} \lim_{x_p\to 0} \partial_{x_p}^{n_j} \tilde{D}(x_p) \tag{3.132}$$

$$= \int_{x,\vec{q}} a_j^{\frac{n_i}{n_j}}\, a_j^{-\frac{1}{n_j}} \left(n_{BE}(x\, a_j^{-\frac{1}{n_j}}) + \frac{1}{2} \right) \tilde{f}(\alpha_i\, x^{n_i}). \tag{3.133}$$

If we calculate the scaling exponents η_i related to the dynamic coefficients a_i, which is in turn all we need to get the flow equations for the comparison coefficients α_i, the additional factor of $a_j^{\frac{n_i}{n_j}}$ is reduced to another dependence on the α_i:

$$\eta_i = -\frac{\partial_t \alpha_i}{a_i} \quad \propto \int_{x,\vec{q}} \frac{1}{\alpha_i}\, a_j^{-\frac{1}{n_j}} \left(n_{BE}(x\, a_j^{-\frac{1}{n_j}}) + \frac{1}{2} \right) \tilde{f}(\alpha_i\, x^{n_i}). \tag{3.134}$$

So we find that the dynamic equations will also reduce to a classical form, as we can apply the same arguments to this equations as for the static ones of the form (3.126).
As we have established that all effects of quantum fluctuations are included

in the distribution function $n_{BE}(q_0)+\frac{1}{2}$ in section 2.7, and that it will reduce to its classical form at the fixed point, we can conclude that quantum effects are not relevant at second order phase transitions for non-zero temperatures.

Chapter 4

Dynamic critical phenomena for the relativistic $O(N)$ model

In this chapter we will employ the framework established in chapter 2 to examine the critical dynamic behavior of a relativistic, scalar field theory describing generally a gas of interacting, relativistic bosonic particles. The relativistic $O(N)$ theory has a wide range of applications, it can be seen as a low energy chiral effective theory for two flavor QCD [76] and is applied in the description of early universe inflation [52].
While it is commonly assumed that the relativistic O(N) model falls in the dynamic universality class of Model C in the classification scheme of Halperin and Hohenberg [47], discussed for example in the references [13] and [73], the question of its dynamic universality class is not conclusively resolved yet. Though our truncation scheme will not be sufficient to distinguish the different dynamic universality classes, the discussion in this chapter may serve as the basis for further calculations able to do so. Possible extensions of the truncation to cover these dynamic universality classes will be discussed in chapter 5, as well as treatment of the universality class of Model C.
Here we will first introduce the action of the relativistic $O(N)$ model and adapt it to the closed time path. The fixed point solutions of the functional renormalization group flow for a low order truncation of the effective average action in derivatives and fields are discussed. We focus here on the case of a one component scalar field as this covers all qualitative features of interest for the discussion. An extension of the results to an arbitrary number of field components can be found in our publication [71].
Furthermore, we examine different choices of cutoff functions as well as the convergence of the results with respect to the expansion of the effective

average action in time derivatives by extending the prior truncation by three additional orders of time derivatives.
In the last section, a possible ansatz for the investigation of the effects of the non-relativistic limit and the related emerging conservation of the particle number on the critical dynamics is proposed.

4.1 Action and ansatz

We introduce the action for relativistc, interacting system of bosonic particles:

$$S[\psi] = \int_x \left\{ \frac{1}{2}\,\psi(x)\,\partial_t^2\psi(x) - \frac{1}{2}\,\psi(x)\,\nabla^2\psi(x) + V(\psi(x)) \right\}. \tag{4.1}$$

The field ψ is a real field with a single component. The related equation of motion is the Klein-Gordon equation:

$$\left[\partial_t^2 - \nabla^2 + V'(\psi(x))\right]\psi(x) = 0. \tag{4.2}$$

The action (4.1) is symmetric under a change of the sign of the field $\psi(x)$. As this is a discrete symmetry, it is not related to a conserved quantity. So contrary to the non-relativistic system, particle number is not conserved in the relativistic one described by the action (4.1).
Even if we would formulate an action similar to (4.1) for a complex instead of a real field, so the system would show a $U(1)$ symmetry like the non-relativistic system, the related conserved quantity would not be the particle number as seen in equation (3.4). Instead, the action would represent a system of charged particles, and the conserved quantity related to the $U(1)$ symmetry would be the overall charge of the system.
We will focus in the following section on a one component real field, as the main properties discussed in the following sections are not changed qualitatively by the number of field components. An extension of the action and the flow equations derived in the next section to an arbitrary number of field components as well as a discussion of their key dynamic features can be found in the reference [71].
As before in the case of the non-relativistic bosons, we will assume a contact interaction on the microscopic scale:

$$V(\psi(x)) = -\sigma\,\psi^2(x) + \frac{\lambda}{4!}\,\psi^4(x). \tag{4.3}$$

Following the procedure described in chapter 2.3, we arrive at the Keldysh action related to the action (4.1)

$$S[\psi,\tilde{\psi}] = \int_x \{\tilde{\psi}(x)\,\partial_t^2\psi(x) - \tilde{\psi}(x)\,\nabla^2\psi(x) + \tilde{\psi}(x)\,\partial_\psi V(\psi(x)) \tag{4.4}$$

$$+ \epsilon\,\tilde{\psi}(x)\,\partial_t\psi(x) - 2\,i\,\epsilon\,\tilde{\psi}(x)\,\left(n_{BE}(-i\partial_t) + \frac{1}{2}\right)\,\partial_t\tilde{\psi}(x)\}. \tag{4.5}$$

As we have established in section 3.9 that at the critical point, the system will always behave classicaly, we can use the classical distribution function

$$\left(n_{BE}(q_0) + \frac{1}{2}\right) \approx= \frac{T}{q_0} \tag{4.6}$$

for the calculation of critical properties without approximation.
As an ansatz for the effective action Γ_k, we again expand it in the gradients up to second order and additionally limit the gradients to terms second order in the fields:

$$\Gamma_k[\psi,\tilde{\psi}] = \int_x \{\tilde{X}_k\,\tilde{\psi}(x)\,\partial_t^2\psi(x) - Z_k\,\tilde{\psi}(x)\,\nabla^2\psi(x) + \tilde{\psi}(x)\,\sqrt{2\rho(x)}\,\partial_\rho U_k(\rho(x))$$

$$+ \epsilon\,\tilde{\psi}(x)\,\partial_t\psi(x) - 2\,i\,\epsilon\,\tilde{\psi}(x)\,\left(n_{BE}(-i\partial_t) + \frac{1}{2}\right)\,\partial_t\tilde{\psi}(x)\} \tag{4.7}$$

For the potential term, we apply a local potential approximation, expanding it up to fourth order in the fields:

$$U_k(\rho(x)) = \frac{\lambda}{2}\left(\rho(x) - \rho_k^0\right). \tag{4.8}$$

We once more dismissed the appearing quantum vertices, as they will not influence the flow equations of any of the coefficients relevant for the propagators, as established in section 2.7. We distinguish the relativistic coefficient $\tilde{X}_k$ from the non-relativistic unitary coefficient X_k in the former chapter by the tilde. The remaining coefficients in the ansatz (4.7) have the same physical meaning as described in chapter 3.

Scale dependent propagators and vertex functions

The propagators following from the ansatz (4.7), evaluated at physical field values $\tilde{\psi}(x) = 0$ and $\rho(x) = \rho$, which are relevant for the calculations in the next section are

$$G_k^R(q_0,\vec{q}) = -\frac{1}{-\tilde{X}_k\, q_0^2 + \omega^2(\vec{q}) + i\, Y_k\, q_0}, \tag{4.9}$$

$$G_k^A(q_0,\vec{q}) = -\frac{1}{-\tilde{X}_k\, q_0^2 + \omega^2(\vec{q}) - i\, Y_k\, q_0}, \tag{4.10}$$

$$\rho_k(q_0,\vec{q}) = \frac{2\, i\, q_0\, Y_k}{\left[-\tilde{X}_k\, q_0^2 + \omega^2(\vec{q})\right]^2 + Y_k^2\, q_0^2}, \tag{4.11}$$

$$iF_k(q_0,\vec{q}) = \frac{2\, i\, T\, Y_k}{\left[-\tilde{X}_k\, q_0^2 + \omega^2(\vec{q})\right]^2 + Y_k^2\, q_0^2}, \tag{4.12}$$

using the shorthand notation

$$\omega^2(\vec{q}) = Z_k\, \vec{q}^2 + \partial_\rho U_k(\rho) + 2\,\rho\,\partial_\rho^2 U_k(\rho) + R_k(\vec{q}). \tag{4.13}$$

Analogous to the calculation in chapter 3, we will again use the optimized cutoff function (3.26). The classical vertices appearing in the diagrams relevant for the calculation of the flow of the involved coefficients are

$$\frac{\delta^2\Gamma_k^{\phi\phi}}{\delta\phi(p_1)\delta\tilde{\phi}(p_2)} = 3\,\partial_\rho^2 U_k(\rho), \tag{4.14}$$

$$\frac{\delta\Gamma_k^{\phi\phi}}{\delta\tilde{\phi}(p_1)} = 3\,\sqrt{2\rho}\,\partial_\rho^2 U_k(\rho), \tag{4.15}$$

$$\frac{\delta\Gamma_k^{\phi\tilde{\phi}}}{\delta\phi(p_1)} = 3\,\sqrt{2\rho}\,\partial_\rho^2 U_k(\rho). \tag{4.16}$$

Projections

We can project on the flow equations of the coefficients appearing in the ansatz (4.7) using the following equations. Do gain access to the static coefficients, we first project on the first derivative of the ρ dependent effective potential:

$$\partial_t U_k'(\rho) = \frac{1}{\sqrt{2\rho}} \lim_{p\to 0} \partial_t \frac{\delta\Gamma_k}{\delta\tilde{\phi}(p)}. \tag{4.17}$$

This equations leads to the flow of the interaction coefficient

$$\partial_t \lambda_k = \left[\partial_\rho \partial_t U_k'(\rho)\right] |^{\rho=\rho_k^0} \tag{4.18}$$

and the running minimum of the effective potential:

$$\partial_t \rho_0 = -\frac{1}{\lambda_k}\, \partial_t U_k'(\rho)|^{\rho=\rho_k^0}. \tag{4.19}$$

The wave function renormalization Z_k can be extracted from the effective action as:

$$\partial_t Z_k = \lim_{p\to 0} \partial_{\vec{p}^2}\, \partial_t \frac{\delta\Gamma_k}{\delta\tilde{\phi}(-p)\delta\phi(p)}|^{\rho=\rho_k^0}, \tag{4.20}$$

The flow equations for the damping coefficient Y_k can be calculated by the projection

$$\partial_t Y_k = -i \lim_{p\to 0} \partial_{p_0}\, \partial_t \frac{\delta\Gamma_k}{\delta\tilde{\phi}(-p)\delta\phi(p)}|^{\rho=\rho_k^0}, \tag{4.21}$$

and the flow of the relativistic coefficient X_k can be extracted from:

$$\partial_t \tilde{X}_k = -\frac{1}{2} \lim_{p\to 0} \partial^2_{p_0}\, \partial_t \frac{\delta\Gamma_k}{\delta\tilde{\phi}(-p)\delta\phi(p)}|^{\rho=\rho_k^0}. \tag{4.22}$$

4.2 Flow and fixed points

Dimensionless quantities

As explained in section 3.4, we define the static dimensionless coefficients

$$\rho_k^0 = k^{d-2+\eta_Z}\rho, \tag{4.23}$$

$$\lambda_k = k^{4-d-2\,\eta_Z}\lambda, \tag{4.24}$$

and introduce the rescaled frequency and spatial momenta

$$x = Y q_0, \tag{4.25}$$

$$\vec{q}^2 = y\, k^2. \tag{4.26}$$

Y is the dimensionless damping coefficient:

$$Y_k = k^{2-\eta_Z}\, Y. \tag{4.27}$$

The dimensionless form of the relativistic coefficient $\tilde{X}_k$ is:

$$\tilde{X}_k = k^{2-\eta_Z}\, \tilde{X}. \tag{4.28}$$

As before in the non-relativistic case, we define a comparison coefficient between the two involved dynamic coefficients:

$$\kappa = \frac{\tilde{X}}{Y^2}. \tag{4.29}$$

Note that, different to the non-relativistic coefficient $\alpha = \frac{X}{Y}$, the damping appears quadratical. This due to the different order of frequencies the coefficients appear with in the propagators. In case the time scale related to the two different dynamic coefficients diverges at the same rate approaching the critical point, their scaling exponents are related to the dynamic critical exponent as

$$-\eta_{\tilde{X}} + 2\,z = 0, \tag{4.30}$$
$$-\eta_Y +, z = 0, \tag{4.31}$$

where the scaling exponents of the dynamic coefficients are defined as:

$$\eta_{\tilde{X}} = -\partial_t \ln(\tilde{X}), \tag{4.32}$$
$$\eta_Y = -\partial_t \ln(Y). \tag{4.33}$$

If the time scale related to one of the dynamic coefficients would diverge faster than the other while approaching the critical point, which would mean one dynamic term would generate a larger dynamic critical exponent z characterizing the scaling behavior of the frequency dependence of the spectral function than the other, that coefficient will dominate the dynamic behavior in the critical region as discussed in section 3.4:

$$\eta_Y > \frac{1}{2}\,\eta_{\tilde{X}} \;:\; \kappa \xrightarrow{k\to 0} 0, \tag{4.34}$$
$$\eta_Y = \frac{1}{2}\,\eta_{\tilde{X}} \;:\; \kappa \xrightarrow{k\to 0} \text{const}, \tag{4.35}$$
$$\eta_Y < \frac{1}{2}\,\eta_{\tilde{X}} \;:\; \kappa \xrightarrow{k\to 0} \infty. \tag{4.36}$$

The flow of the comparison coefficient κ can be calculated from the scaling exponents of the dynamic coefficients (4.32) and (4.33) as:

$$\partial_t \kappa = \kappa \left(2\,\eta_Y - \eta_{\tilde{X}}\right). \tag{4.37}$$

Flow equations and fixed point solutions

The frequency integrations can be performed again using the residue theorem, while the spatial integration are straight forward polynomial integrations due to the form of the cutoff function (3.26).
The calculations result in the following flow equations for the dimensionless static quantities:

$$\partial_t \rho = (2 - d - \eta_Z)\,\rho + T\,v_d\,\frac{12}{d\,(2+d)}\,\frac{2+d-\eta_z}{(1+2\,\rho\,\lambda)^2}, \tag{4.38}$$

$$\partial_t \lambda = (d - 4 + 2\eta_Z)\,\lambda + T\,v_d\,\lambda^2\,\frac{72}{d\,(2+d)}\,\frac{2+d-\eta_z}{(1+2\,\rho\,\lambda)^2}, \tag{4.39}$$

$$\eta_Z = T\,v_d \frac{(2+d)\,\lambda^2 \rho}{(1+2\rho\lambda)^2}. \tag{4.40}$$

The static equations (4.38)-(4.40) again decouple from all the dynamic coefficients. We can solve them for fixed points independently of the dynamic equations. In three spatial dimensions and with the Temperature set to $T = 1$, the fixed point values for the density ρ and the coupling λ at the stable Wilson-Fisher fixed point are:

$$\rho_C = 0.025 \tag{4.41}$$

$$\lambda_C = 7.991. \tag{4.42}$$

The static critical behavior is qualitatively similar to the discussions in section 3.6.
For the scaling exponents of the dynamic coefficients we get:

$$\eta_{\tilde{X}} = 2 - \eta_Z + T\,v_d\,\lambda^2\,\rho\,\frac{36}{d\,(2+d)}\,\frac{(2+d-\eta_z)\left(1+\kappa^2\,(1+2\,\rho\,\lambda)^2\right)}{\kappa\,(1+2\,\rho\,\lambda)^5} \tag{4.43}$$

$$\eta_Y = 2 - \eta_Z + T\,v_d\,\lambda^2\,\rho\,\frac{36}{d\,(2+d)}\,\frac{(2+d-\eta_z)\,(3+2\,\kappa\,(1+2\,\rho\,\lambda))}{(1+2\,\rho\,\lambda)^4} \tag{4.44}$$

Inserted into equation (4.37), the flow equation for the comparison coefficient becomes:

$$\partial_t \kappa = (2 - \eta_Z)\,\kappa + T\,v_d\,\lambda^2\,\rho\,\frac{36}{d\,(2+d)}\,\frac{(2+d-\eta_z)\,(1+\kappa\,(1+2\,\rho\,\lambda))\,(1+5\,\kappa\,(1+2\,\rho\,\lambda))}{(1+2\,\rho\,\lambda)^5}. \tag{4.45}$$

Calculating the fixed point value of the dynamic equation (4.45) in three spatial dimensions for a temperature set to $T = 1$ and evaluated at the

static fixed point values (4.41) and (4.42) shows a behavior quite different from the non-relativistic system:

$$\kappa_C = -0.019. \tag{4.46}$$

The dynamic scaling exponent z at this dynamical fixed point is:

$$z = 2.13. \tag{4.47}$$

Instead of a dominance of the damping Y over the unitary coefficient and the related vanishing of the comparison coefficient between the two, we now see a "locking" between both quantities, indicating that the times scales of the dynamics related to both of these coefficients are diverging at the same rate in the vicinity of the critical point.
While the non-vanishing value of κ related to this locking is not a problem in general, the negative sign of it is. The negative sign can result either from a negative relativistic coefficient $\tilde{X}$ or a complex damping coefficient Y. Solving the flow equations (4.38) - (4.40) and (4.45) for a set of initial conditions that lead the flow close to the fixed point, we see that the former is the case. Figures 4.1 - 4.3 show the flow of the dynamic coefficients, and the relativistic coefficient $\tilde{X}$ indeed crosses the zero axis.
This is problematic for several reasons. From a physical perspective, the relativistic coefficient $\tilde{X}$ relates to the inverse effective speed of light of of the system. This can be seen directly from the dispersion relation:

$$q_0 = \pm \frac{1}{\sqrt{\tilde{X}_k}} \omega(\vec{q}). \tag{4.48}$$

With $\omega(\vec{q})$ as defined in equation (4.13). This matches the usual relativistic energy momentum relation with $\sqrt{\frac{Z_k}{\tilde{X}_k}}$ assuming the role of the speed of light c. Therefore, we would not expect the coefficient $\tilde{X}_k$ to become negative.
Additionally, the change of the sign of $\tilde{X}$ will change the pole structure of the propagators in a way that both the retarded and the advanced propagator have poles with negative and positive imaginary parts of the frequencies. If we perform the Fourier transformation back to the temporal domain, we see that both propagators are now non-vanishing for positive and negative differences $t - t'$ in their time arguments, contrary to their definitions (2.13) and (2.14).

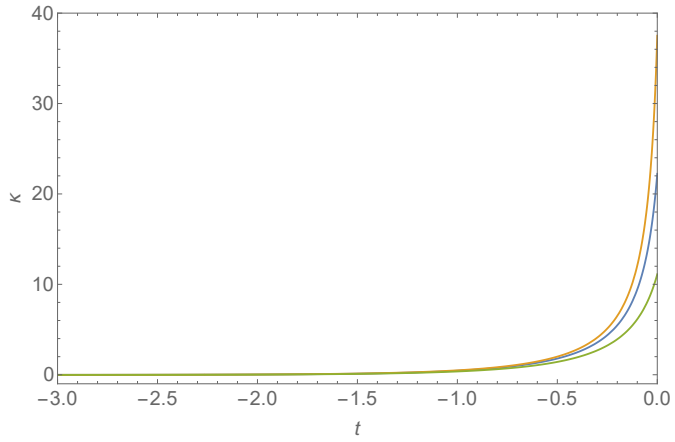

Figure 4.1: The flow of the comparison coefficient κ in three dimensions, evaluated at the ρ and λ values of the Wilson-Fisher fixed point for three different sets of initial values for $\tilde{X}$ and Y. The system flows towards $\kappa = 0$ regardless of the initial values. The exact examination of the fixed point values of κ reveals that its flow will stop slightly below zero.

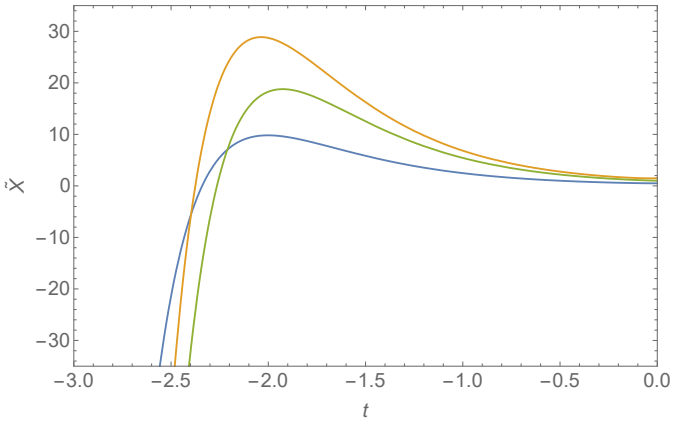

Figure 4.2: The flow of the dimensionless, relativistic coefficient $\tilde{X}$ in three dimensions, evaluated at the ρ and λ values of the Wilson-Fisher fixed point for three different sets of initial values. Increasing at the start, the values of the dimensionless relativistic coefficient will fall below zero fast, independent of the initial conditions.

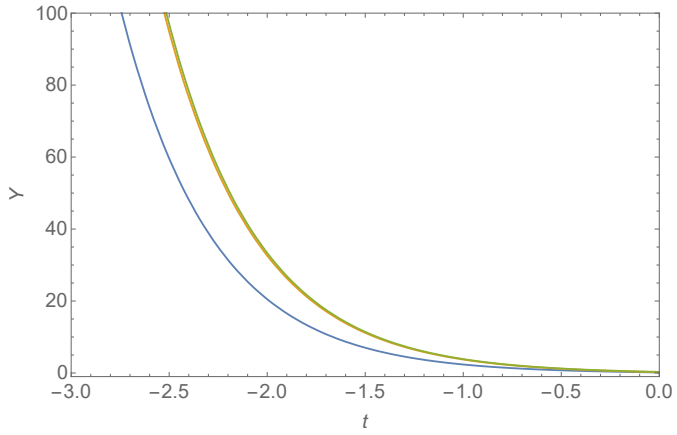

Figure 4.3: The flow of the dimensionless damping Y in three dimensions, evaluated at the ρ and λ values of the Wilson-Fisher fixed point for three different sets of initial values.

4.3 Extended truncation

In this section we examine the effect of higher order terms in the time derivative expansion on the dynamic critical behavior in general and the unphysical values of κ we discovered so far in particular. For this purpose we extend our ansatz to include terms of time derivative up to order five:

$$\Gamma_k^{Extended}[\psi,\tilde{\psi}] = \Gamma_k[\psi,\tilde{\psi}] + \int_x \{\tilde{\psi}(x)\left[-\tilde{X}_k'\,\partial_t^4 + i\,Y_k'\,\partial_t^3 + i\,Y_k''\,\partial_t^5\right]\psi(x)\}. \tag{4.49}$$

This is not systematic in the sense of an expansion in canonic dimensions, as we would have to include higher order spatial gradient, field and mixed terms as well. It is sufficient as an indicator of the effect of higher order frequency terms on the critical dynamic behavior. As a regulator function, we again choose the spatial, optimized cutoff (3.26).
As the additional terms do not appear in the microscopic action (4.4), the initial values of their coefficients have to be zero.

The projections on the new coefficients included in (4.49) are

$$\partial_t Y'_k = -\frac{i}{3!} \lim_{p\to 0} \partial^3_{p_0}\, \partial_t \frac{\delta\Gamma_k}{\delta\tilde{\phi}(-p)\delta\phi(p)}|^{\rho=\rho^0_k}, \tag{4.50}$$

$$\partial_t Y''_k = -\frac{i}{5!} \lim_{p\to 0} \partial^5_{p_0}\, \partial_t \frac{\delta\Gamma_k}{\delta\tilde{\phi}(-p)\delta\phi(p)}|^{\rho=\rho^0_k}, \tag{4.51}$$

$$\partial_t \tilde{X}'_k = -\frac{1}{4!} \lim_{p\to 0} \partial^4_{p_0}\, \partial_t \frac{\delta\Gamma_k}{\delta\tilde{\phi}(-p)\delta\phi(p)}|^{\rho=\rho^0_k}, \tag{4.52}$$

with the related scaling coefficients

$$\eta_{Y'} = -\partial_t \ln(Y'), \tag{4.53}$$

$$\eta_{Y''} = -\partial_t \ln(Y''), \tag{4.54}$$

$$\eta_{\tilde{X}'} = -\partial_t \ln(\tilde{X}'). \tag{4.55}$$

Again, we define dimensionless forms of the new dynamic coefficients:

$$Y'_k = k^{2-\eta_Z}\, Y', \tag{4.56}$$

$$Y''_k = k^{2-\eta_Z}\, Y'', \tag{4.57}$$

$$\tilde{X}'_k = k^{2-\eta_Z}\, \tilde{X}'. \tag{4.58}$$

And in the same manner as before, we define new comparison coefficients for the additional dynamic coefficients:

$$\kappa_2 = \frac{\tilde{X}'}{Y^4}, \tag{4.59}$$

$$\tau = \frac{Y'}{Y^3}, \tag{4.60}$$

$$\tau_2 = \frac{Y'}{Y^5}. \tag{4.61}$$

Their flow equations are related to the dynamic scaling exponents (4.53) - (4.55) by:

$$\partial_t \kappa_2 = \kappa_2 \left(4\,\eta_Y - \eta_{\tilde{X}'}\right), \tag{4.62}$$

$$\partial_t \tau = \tau \left(3\,\eta_Y - \eta_{Y'}\right), \tag{4.63}$$

$$\partial_t \tau_2 = \tau_2 \left(5\,\eta_Y - \eta_{Y''}\right). \tag{4.64}$$

The static equations are not influenced by these changes in the truncation, equations (4.38) - (4.40) are still valid. This allows to evaluate the dynamic

equations at the fixed point values (4.41) and (4.42) and solve them for fixed points separately from the static equations. The frequency integrations necessary for the calculation of the dynamic flow equations become rather involved now. Instead of applying the residue theorem, we perform the integrals numerically. The following table shows the fixed point values for the comparison coefficients (4.59)-(4.61) at the different orders of time derivative terms included:

	κ	τ	κ_2	τ_2	z
$O(\partial_t^2)$	-0.0195	-	-	-	2.1301
$O(\partial_t^3)$	-0.0192	-0.0094	-	-	2.1279
$O(\partial_t^4)$	-0.0193	-0.0093	0.0029	-	2.1283
$O(\partial_t^5)$	-0.0195	-0.0094	0.0029	0.0010	2.1273

We can see that the changes to the coefficient κ are only very minor with each additional time derivative term added to the truncation. This indicates that the unphysical behavior of the coefficient κ at the fixed point can not be explained by a mere lack of time derivative terms included in the approximation.

4.4 Cutoff functions

In this section we will examine the influence of two different cutoff functions on the critical behavior of the system. We will use the ansatz (4.7) for the effective action, as already in section 4.1.
First we will use a spatial exponential cutoff as shown in section 3.2:

$$R_k(\vec{q}) = Z_k\, \vec{q}^2\, \frac{e^{-\frac{\vec{q}^2}{k^2}}}{1 - e^{-\frac{\vec{q}^2}{k^2}}}, \tag{4.65}$$

With this cutoff, we decide to perform the spatial integrations numerically while we still perform the frequency integrations via the residue theorem. The fixed point values with these cutoffs are

$$\rho_C = 0.0325, \tag{4.66}$$
$$\lambda_C = 10.1011, \tag{4.67}$$
$$\kappa_C = -0.0231. \tag{4.68}$$

The static and dynamic fixed point values show only minor quantitative changes, while the main issue of the negative dynamic coefficient κ still

holds.
As a second cutoff function, we will use a frequency dependent exponential cutoff of the form

$$R_k(\vec{q}) = \left(-\tilde{X}_k\, q_0^2 + Z_k\, \vec{q}^2\right) \frac{e^{\tilde{X}\, q_0^2 - \frac{\vec{q}^2}{k^2}}}{1 - e^{\tilde{X}\, q_0^2 - \frac{\vec{q}^2}{k^2}}}. \tag{4.69}$$

Note that all frequency dependencies of the cutoff function have to be accompanied by an appropriate dynamic coefficient to allow for scaling behavior. It will still regularize the infrared divergences appearing in calculations for systems close to the critical point. This cutoff function has the advantage that it conserves Lorentz invariance. For a system at non-vanishing temperature this will not be relevant at the critical point, where Lorentz invariance will be broken by the thermal fluctuations. It can affect the flow at scales much larger than the temperature though, where the effects of thermal fluctuations will be minor.
More importantly, if we would include the full Bose-Einstein distribution function (2.101) in our calculations, this cutoff allows to include the fixed point corresponding to second order phase transitions both at non-vanishing as well as vanishing temperatures. For the structure of the so called Quantum Phase Transitions at zero temperature, the consequences of the Lorentz invariance of the system are crucial for its critical behavior. Through the restrictions of Lorentz symmetry, the value of the dynamic coefficient X_k is locked to the one of the wave function renormalization Z_k for all scales, therefore fixating the dynamic critical exponent to $z = 1$. The system can be mapped to a classical, static O(N) symmetric system in $D = d + 1$ dimensions then, which has been discussed in, for example, the references [71] and [77].
While the critical behavior at exactly vanishing temperature is well understood, it is not a physically relevant situation per se, as zero temperature is not accessible experimentally. The intriguing question in this context is if and how the zero temperature fixed point influences areas of the phase diagram of the system for very low temperatures, inducing critical behavior in the sense of a maybe finite, but very large correlation length and time compared to all remaining scales involved.
The cutoff function (4.69) in combination with a full distribution function (2.101) allows us to describe systems at all temperatures in one set up and is therefore suitable to examine possible critical regions in the phase diagram at very low temperature due to the influence of the fixed point related to the quantum phase transition.

The cutoff function (4.69) combined with a classical approximation of the distribution function will change the static fixed point values ρ_c and λ_c for a system of three spatial dimensions and temperature set to one only slightly compared to the former calculations using purely spatial cutoff functions, delivering

$$\rho_C = 0.0337, \tag{4.70}$$
$$\lambda_C = 10.4464. \tag{4.71}$$

The changes in the fixed point value of the comparison coefficient κ are more significantly compared to the results using the spatial exponential cutoff function (4.65), the frequency dependent cutoff function still does not influence its unphysical negative sign though

$$\kappa_C = -0.0180. \tag{4.72}$$

All spatial and frequency integrations have been performed numerically.
So while the implementation of the four dimensional cutoff function (4.69) does not solve the problem of the negative dynamic comparison coefficient, it does open up the opportunity to examine the transition from quantum to thermal critical phenomena due to its conservation of Lorentz invariance.

4.5 Non-relativistic limit

The cause of the unphysical behavior of the relativistic system defined by the action (4.1) is not clear yet. In the former sections, we employed different technical improvements on the setup without observing any significant changes in this regard.
A different explanation would be the possibility of a physical effect crucial for the dynamic critical behavior that is not taken into account by our truncation.
One possible candidate are the effects of particle number conservation in the non-relativistic limit of the system. Even if including those into our calculations will not explain the unphysical behavior seen in section 4.2 - 4.4, it is sill worthwhile to explore the effects of particle number conservation as it is not clear a priori if they effect the critical physics in general. While the effective mass does vanish at the critical point the length scale of the involved momenta does as well.
We examine two different methods to formulate an action which allows for a straight forward inclusion of the non-relativistic form in the ansatz for the

effective average action.
The first one is based on separating the field into a complex field and a phase factor. In the non-relativistic limit the complex field is supposed to change slow over time compared to the mass scale, while the phase factor will oscillate rapidly. A discussion of this approach can be found e.g. in reference [11].
Starting at the relativistic action (4.1) with pointlike interactions,

$$S[\psi] = \int_x \left\{ \frac{1}{2}\,\psi(x)\,\left[\partial_t^2 - \nabla^2 + m^2\right]\psi(x) + \frac{\lambda}{4!}\psi(x)^4 \right\}, \tag{4.73}$$

we transform our field as

$$\psi(x) = \sqrt{2}\,\Re\left[\varphi(x)e^{-i\,m\,t}\right] = \frac{1}{\sqrt{2}}\,\left[\varphi(x)e^{-i\,m\,t} + \varphi^*(x)e^{i\,m\,t}\right], \tag{4.74}$$

where the new field $\varphi(x)$ is complex valued.
The action (4.73) then becomes

$$\begin{aligned} S[\varphi,\varphi^*] = \frac{1}{4}\int_x & \left\{ e^{-2\,i\,m\,t}\,\varphi(x)\,\hat{A}\,\varphi(x) + e^{2\,i\,m\,t}\,\varphi^*(x)\,\hat{A}^\dagger\,\varphi^*(x) + 2\,\varphi(x)^*\hat{A}\,\varphi(x) \right\} \\ + \frac{\lambda}{4\cdot 4!}\int_x & \left\{ e^{-4\,i\,m\,t}\,\varphi(x)^4 + 4\,e^{-2\,i\,m\,t}\,\varphi(x)^2\,\left(\varphi(x)\,\varphi^*(x)\right) + 6\,\left(\varphi(x)\,\varphi^*(x)\right)^2 \right\} \\ + \frac{\lambda}{4\cdot 4!}\int_x & \left\{ 4\,e^{2\,i\,m\,t}\,\left(\varphi(x)^*\right)^2\,\left(\varphi(x)\,\varphi(x)^*\right) + e^{4\,i\,m\,t}\,\left(\varphi^*(x)\right)^4 \right\}. \end{aligned} \tag{4.75}$$

where we performed one partial integration and define the derivative operator $\hat{A}$ and its conjugate $\hat{A}^\dagger$ as:

$$\hat{A} = \partial_t^2 - 2\,i\,m\,\partial_t - \nabla^2, \tag{4.76}$$

$$\hat{A}^\dagger = \partial_t^2 + 2\,i\,m\,\partial_t - \nabla^2. \tag{4.77}$$

Note that even though the action (4.75) is built from a complex field now, we of course still only have the Z_2 symmetry of the original relativistic action (4.73) as several terms break a possible $U(1)$ symmetry.
If we now assume that in a non-relativistic situation, the field $\varphi(x)$ will be slow moving compared to the mass scale,

$$|m\partial_t\varphi(x)| >> |\partial_t^2\varphi(x)|, \tag{4.78}$$

the derivative operators become

$$\hat{A} \to -2\,i\,m\,\partial_t - \nabla^2, \tag{4.79}$$

$$\hat{A}^\dagger \to 2\,i\,m\,\partial_t - \nabla^2. \tag{4.80}$$

This leads to a quadratic dispersion relation as we would expect in the non-relativistic limit.
Additionally, the phase factors $e^{\pm i m t}$ will oscillate fast compared to the changes of the field $\varphi(x)$. Therefore the time integral over all terms containing factors of $e^{\pm i m t}$ will vanish in the action. These are exactly the terms breaking the $U(1)$ symmetry of the action. The remaining action in this limit is:

$$S[\varphi, \varphi^*] = \int_x \left\{ \frac{1}{2} \varphi(x)^* \left[-2\, i\, m\, \partial_t - \nabla^2 \right] \varphi(x) + \frac{\lambda}{16} \left(\varphi(x)\, \varphi^*(x) \right)^2 \right\}. \tag{4.81}$$

After a simple rescaling of the fields and the coupling constant,

$$\varphi(x) \to \frac{1}{\sqrt{m}} \varphi(x), \tag{4.82}$$

$$\lambda \to 8\, m^2\, \tilde{\lambda}, \tag{4.83}$$

the action matches exactly the non-relativistic action (3.1) discussed in chapter 3:

$$S[\varphi, \varphi^*] = \int_x \left\{ \varphi(x)^* \left[-i\, \partial_t - \frac{1}{2\, m} \nabla^2 \right] \varphi(x) + \frac{\tilde{\lambda}}{2} \left(\varphi(x)\, \varphi^*(x) \right)^2 \right\}. \tag{4.84}$$

So an ansatz for the effective average action based on the reformulation (4.75) of the relativistic microscopic action will indeed contain all necessary terms to allow the transition to a non-relativistic system during the functional renormalization group flow, enabling a change from a linear to a quadratic dispersion relation as well as the establishment of an $U(1)$ symmetry related to particle number conservation.
The action (4.75) is unfortunately very inconvenient to handle during the calculations of the flow due to the presences of the explicitly time dependent phase factors.

Therefore, we focus on a second, different approach based on the ideas discussed in reference [29]. We reformulate the action (4.1) in a Hamiltonian form, introducing the conjugate momentum field $\pi(x)$ as a second field variable:

$$S[\psi, \pi] = \int_x \left\{ -\pi(x)\, \partial_t \psi(x) + \frac{1}{2} \left[\pi(x)^2 + \psi(x)\, \omega^2(\vec{\nabla})\, \psi(x) \right] + \frac{\lambda}{4!} \psi(x)^4 \right\}. \tag{4.85}$$

We used the shorthand notation $\omega^2(\vec{\nabla}) = -\vec{\nabla}^2 + m^2$. As the action is quadratic in the conjugate momentum field $\pi(x)$, integrating it out in the path integral is straight forward, ending up again at path integral over the field $\psi(x)$ only, weighted with the action (4.1). Both formulations are equivalent.
In the next step, we express the two real fields included in the action (4.85) through a single complex field:

$$\psi(x) = \frac{\sqrt{2}}{\sqrt{\omega(\vec{\nabla})}} \Re\left[\varphi(x)\right] = \frac{1}{\sqrt{2\,\omega(\vec{\nabla})}}\,\left(\varphi(x) + \varphi^*(x)\right), \tag{4.86}$$

$$\pi(x) = \sqrt{2\,\omega(\vec{\nabla})}\,\Im\left[\varphi(x)\right] = (-i)\,\frac{\sqrt{\omega(\vec{\nabla})}}{\sqrt{2}}\,\left(\varphi(x) - \varphi^*(x)\right). \tag{4.87}$$

Inserting these into the action (4.85) results in:

$$\begin{aligned} S[\varphi,\varphi^*] = &\int_x \left\{-\varphi^*(x)\,\partial_t\varphi(x) + \varphi^*(x)\,\omega(\vec{\nabla})\varphi(x)\right\} \\ &+ \int_x \left\{\frac{\lambda}{8\,\omega^2(\vec{\nabla})}\left[\frac{1}{12}\,\varphi(x)^4 + \frac{1}{3}\,\varphi(x)^3\,\varphi^*(x) + \frac{1}{2}\,\left(\varphi(x)\,\varphi^*(x)\right)^2\right]\right\} \\ &+ \int_x \left\{\frac{\lambda}{8\,\omega^2(\vec{\nabla})}\left[\frac{1}{3}\,\varphi(x)\,\left(\varphi^*(x)\right)^3 + \frac{1}{12}\,\left(\varphi^*(x)\right)^4\right]\right\}. \end{aligned} \tag{4.88}$$

Again, the action adopts the Z_2 symmetry of the original form (4.1) while a possible $U(1)$ symmetry is broken by four of the interaction terms.
In the non-relativistic limit, where the mass becomes much larger than the involved momenta, the dispersion relation in the action will change from the linear form in (4.88) to a quadratic form:

$$\omega(\vec{p}^2) = \sqrt{p^2 + m^2} = m + \frac{\vec{p}^2}{2\,m} + O(\left(\frac{\vec{p}^2}{m^2}\right)^2). \tag{4.89}$$

To allow a possible $U(1)$ symmetry and therefore particle number conservation to emerge during the flow, we have to ensure that our ansatz includes separate flowing coefficients for the different interaction terms in the action (4.88).
The reformulation (4.88) of the original action avoids the inconvenient time dependent phase factors found in the action (4.75), and the dynamic part is reduced to a simple linear time derivative term as found in the non-relativistic action (3.1). This simple dynamic form comes at the cost of a rather involved,

non-polynomial, spatial gradient structure. Therefore, we have to allow arbitrary spatial momentum dependencies in our ansatz, demanding for a more sophisticated truncation scheme for the spatial gradients than a polynomial expansion.
We take the approximation scheme introduced in the references [16] and [5] as the starting point of our truncation. It is based on the exact equation

$$\Gamma^{(s+1)}(\{p_i\}, 0, \phi_0) = \partial_{\phi_0}\Gamma^{(s)}(\{p_i\}, \phi_0). \tag{4.90}$$

The functions $\Gamma^{(n)}(\{p_i\}, 0, \phi_0)$ are the functional derivatives of the effective action withe respect to n fields with different momentum arguments, evaluated at the constant field configuration ϕ_0.
The infinite hierarchy of flow equations is then truncated by assuming that the internal momentum dependence of the vertex functions above a certain order n can be neglected. This will produce a closed set of flow equations for the vertex functions up to order n with all their momentum dependencies conserved. The vertex functions of order $n+1$ and $n+2$ involved in these flow equations can be calculated from the order n vertex functions by using (4.90).
Our focus lies on the critical behavior of the second propagator functions, therefore it is sufficient to resolve full momentum dependence only up to order $n = 2$. To test the convergence of this approximation scheme, higher order of n should be implemented later on.
As we only need to resolve the full spatial momentum dependencies to capture the non-relativistic limit of the action (4.88), we can additionally expand the effective average action in the fields and time derivatives as before. The lowest order ansatz then is of the form

$$\begin{aligned}
\Gamma_k[\phi,\phi^*] = &\int_x \Big\{-\phi^*(x)\, X_k(\vec{\nabla})\, \partial_t\phi(x) + \phi^*(x)\, \omega_k(\vec{\nabla})\phi(x)\Big\} \\
&+ \int_x \left\{\phi(x)^3\, \lambda_k^a(\nabla)\, \phi(x) + \phi(x)^2\, \left[g_k^a(\nabla)\phi(x)\right]\, \left[h_k^a(\nabla)\phi(x)\right]\right\} \\
&+ \int_x \left\{\phi(x)^3\, \lambda_k^b(\nabla)\, \phi^*(x) + \phi(x)^2\, \Big[g_k^b(\nabla)\phi(x)\Big]\, \Big[h_k^b(\nabla)\phi^*(x)\Big]\right\} \\
&+ \int_x \left\{\phi(x)^2\, \phi^*(x)\, \lambda_k^c(\nabla)\, \phi^*(x) + \phi(x)^2\, \left[g_k^c(\nabla)\phi^*(x)\right]\, \left[h_k^c(\nabla)\phi^*(x)\right]\right\} \\
&+ \int_x \left\{\phi(x)\, \left(\phi^*(x)\right)^2\, \lambda_k^d(\nabla)\, \phi^*(x) + \phi(x)\, \phi^*(x)\, \Big[g_k^d(\nabla)\phi^*(x)\Big]\, \Big[h_k^d(\nabla)\phi^*(x)\Big]\right\} \\
&+ \int_x \Big\{\left(\phi^*(x)\right)^3\, \lambda_k^e(\nabla)\, \phi^*(x) + \left(\phi^*(x)\right)^2\, \left[g_k^e(\nabla)\phi^*(x)\right]\, \left[h_k^e(\nabla)\phi^*(x)\right]\Big\}.
\end{aligned} \tag{4.91}$$

With $\phi(x) = \langle\varphi(x)\rangle$. The functions $\lambda_k^i(\vec{\nabla})$ as well as $\omega_k(\vec{\nabla})$ and $X_k(\vec{\nabla})$ are even functions in the gradients, while the functions $g_k^i(\nabla)$ and $h_k^i(\nabla)$ are odd.
To produce real time correlations functions, we have to translate the action (4.88) as well as the ansatz for the related effective average action (4.91) into Keldysh form as described in section 2.3, using equation (2.55).
The calculation of the flow equations produced by the resulting ansatz is numerically significantly more challenging than the equations of the truncations used so far. Unfortunately, at the date this thesis is handed in the calculations are still ongoing for this reason.

Chapter 5

Effects of conserved quantities on the dynamic critical behavior

As mentioned before, the dynamics of conserved quantities can be of crucial relevance for the overall dynamic critical behavior, while not straightforward to implement in the truncation schemes introduced so far. Fortunately, the Langevin representation formulated in section 3.8 can be utilized to employ a approximation treating the conserved quantity as an independent, auxiliary field. While a mesoscopic approximation itself, this approach could shed light on possible implementations of the dynamics of conserved quantities on a microscopic level.
This approach as a mesoscopic, effective description of the effects of conserved quantities on the dynamic critical behavior has been a well discussed subject in past research. The different possibilities of general dynamic behavior and interaction between physical and auxiliary field have been separated into universality classes in the paper [47]. These universality classes have subsequently been extensively studied in the context of the perturbative renormalization group, see [24], [18], [36] and [83] for a past and very recent examples.
We will approach the most basic model of a conserved quantity coupled to a field following a relaxational Langevin equation as described in section 3.8 using the functional renormalization group. This Model has been used to describe, for example, the critical dynamics of mobile impurities [55, 56, 41], structural phase transitions [45] and long wavelength fluctuations near the QCD critical point [6, 80].

It turns out that the hitherto existing perturbative renormalization group studies of this model, as in references [43], [44], [35], [19] and [2], disagree on the existence of a specific scaling region in the plane of spatial dimensions and field components of the order parameter. We confirmed the existence as well as determined the extend of this so called anomalous scaling region by means of the functional renormalization group, published in reference [70].

5.1 Coupling a conserved auxiliary field to the Langevin equation

Starting point is the representation of our system as a Langevin equation as explained in section 3.8:

$$\partial_t \psi_i(x) = -D \frac{\delta H_{GL}[\psi]}{\delta \psi_i(x)} + \xi_i(x). \tag{5.1}$$

The coefficient D is again proportional to the inverse relaxation time of the ψ field.
We will now introduce an additional, auxiliary field

$$\partial_t \psi_i(x) = -D \frac{\delta \tilde{H}_{GL}[\psi, \nu]}{\delta \psi_i(x)} + \xi_i(x), \tag{5.2}$$

$$\partial_t \nu(x) = D_\nu \nabla^2 \frac{\delta \tilde{H}_{GL}[\psi, \nu]}{\delta \nu(x)} + \xi_\nu(x) \tag{5.3}$$

This new field represents the density of the conserved quantity of which we would like to approximate the dynamic behavior. The coefficient D_ν characterizes the inverse time scale of the diffusion of this newly introduced field ν.
The function $\xi_\nu(x)$ is again a gaussian distributed random noise function with the properties:

$$\langle \xi_\nu(x) \rangle = 0, \tag{5.4}$$

$$\langle \xi_\nu(x)\, \xi_\nu(y) \rangle = -2\, D_\nu\, T \nabla^2\, \delta^4(x-y). \tag{5.5}$$

If we take the integral over all spatial dimensions of the system over equation (5.3), we see that the right hand side vanishes due to Gauss theorem, except for the noise function:

$$\int_{\vec{x}} \partial_t \nu(x) = \int_{\vec{x}} \xi_\nu(x). \tag{5.6}$$

Averaging on both sides of the equations yields

$$\partial_t E(t) = \partial_t \int_{\vec{x}} \langle \nu(x) \rangle = 0. \tag{5.7}$$

So the quantity $E(t) = \int_{\vec{x}} \langle \nu(x) \rangle$ is indeed conserved over time, while its microscopic equivalent $\int_{\vec{x}} \nu(x)$ will change over time only by the random noise $\xi_\nu(x)$. The strength of this noise is directly proportional to the temperature. We specify the new Hamiltonian to be

$$\tilde{H}_{GL}[\psi, \nu] = H_{GL}[\psi] + \int_x \left\{ \frac{1}{2}\, \nu^2(x) + \frac{1}{2}\, \gamma\, \nu(x)\, \psi^2(x) \right\} \tag{5.8}$$

with new coefficient γ indicating the strength of the coupling between the ψ and ν fields and the original Ginzburg-Landau Hamiltonian

$$H_{GL}[\psi] = \int_x \left\{ \frac{1}{2}\, (\nabla \psi(x))^2 + V(\psi^2) \right\}, \tag{5.9}$$

$$V(\psi^2) = \frac{1}{2}\, m^2\, \psi^2(x) + \frac{\tilde{\lambda}}{4!}\, \left(\psi^2(x)\right)^2. \tag{5.10}$$

$$\tag{5.11}$$

The physical meaning of the auxiliary field $\nu(x)$ becomes clear if we examine the extremal conditions of this new Hamiltonian:

$$\frac{\delta\, \tilde{H}_{GL}[\psi, \nu]}{\delta\, \psi_i(x)} = -\nabla^2 \psi_i(x) + m^2\, \psi_i(x) + \frac{\tilde{\lambda}}{3!}\, \psi_i(x)\, \psi^2(x) + \gamma\, \nu(x) \psi_i(x) = 0, \tag{5.12}$$

$$\frac{\delta\, \tilde{H}_{GL}[\psi, \nu]}{\delta\, \nu(x)} = \nu(x) + \frac{1}{2}\, \gamma\, \psi^2(x) = 0. \tag{5.13}$$

We see that the through the second equation, the auxiliary field is fixed at the minimum of the Hamiltonian to

$$\nu(x) = -\frac{1}{2}\, \gamma\, \psi^2(x). \tag{5.14}$$

So the auxiliary field and therefore the conserved density resembles the square of the order parameter field ψ. This is of course only exact true at the minimum of the Hamiltonian, i. e. at the equilibrium configurations of the Langevin equations (5.2) and (5.3). As we aim to calculate equilibrium correlation functions to answer dynamic questions in the linear response regime around thermal equilibrium, this should suffice as an approximation of the dynamics of a conserved order parameter squared ψ.
If we insert condition (5.14) into the first equation for the minimum, we restore the minimal condition for the original Ginzburg-Landau Hamiltonian:

$$-\nabla^2\psi_i(x) + m^2\,\psi_i(x) + \frac{\lambda}{3!}\,\psi_i(x)\,\psi^2(x) = 0, \tag{5.15}$$

with a shifted interaction constant:

$$\lambda = 3!\left(\frac{\tilde{\lambda}}{3!} - \frac{\gamma^2}{2}\right) \tag{5.16}$$

This indicates that the static behavior of the system, defined by the minimum of the Hamiltonian, will not change due to the coupling of the auxiliary field except for a shift of the interaction constant. The coupling of the field $\nu(x)$ in this fashion is a dynamic matter only, as intended.
To get an impression of the dynamics of the new field, we again linearize the equations of motion in the fields $\psi(x)$ and $\nu(x)$ around the minimum of the Hamiltonian and ignore the noise functions, so we acquire a easily solvable set of differential equations. After performing a spatial Fourier transformation, the solutions to these linearized equations are

$$\delta\psi(t,\vec{p}) = \delta\psi_i\, e^{-\frac{\omega(\vec{p})}{D}t} + \gamma\,\psi_0\,D_\nu\,\delta\nu_i\,\frac{e^{-\frac{\omega_\nu(\vec{p})}{D_\nu}t} - e^{-\frac{\omega(\vec{p})}{D}t}}{D\,\omega_\nu(\vec{p}) - D_\nu\,\omega(\vec{p})}, \tag{5.17}$$

$$\delta\nu(t,\vec{p}) = \delta\nu_i\, e^{-\frac{\omega_\nu(\vec{p})}{D_\nu}t}. \tag{5.18}$$

where $\delta\psi$ and $\delta\nu$ between the fields and their respective minimal values, ψ_0 is the minimum value of the ψ field and we used the shorthand notations:

$$\omega(\vec{p}) = \vec{p}^2 + m^2 + \lambda\,\frac{\psi_0^2}{2}, \tag{5.19}$$

$$\omega_\nu(\vec{p}) = \vec{p}^2. \tag{5.20}$$

It can be directly seen that these solutions produce a conserved quantity:

$$\int_{\vec{x}} \delta\nu(x) = \delta\nu(t,\vec{p}=0) = \delta\nu_i. \tag{5.21}$$

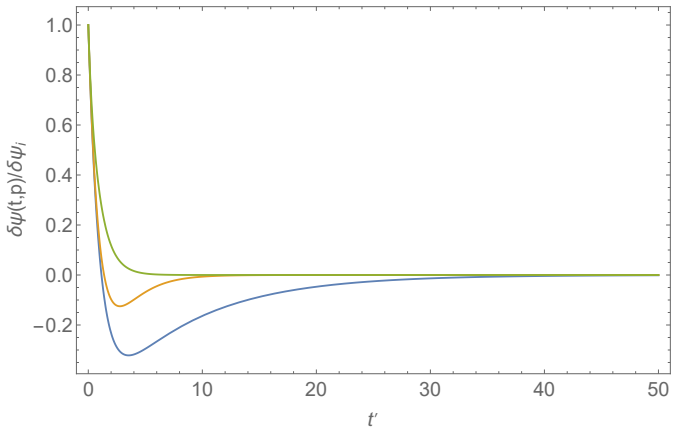

Figure 5.1: The plot shows the relative changes of the perturbation of the ψ field from its minimal value compared to its initial perturbation over the dimensionless time $t' = \frac{\omega(\vec{p})}{D}t$. All involved constants as well as the spatial momenta are set to the same value for all three curves, except for the damping coefficient D, which is chosen such that the ratio $\frac{D}{D_\nu}$ is 0.1 (green), 1 (blue) and 4 (orange).

In figures 5.1 and 5.2 the solutions (5.17) and (5.18) are shown for different ratios of the time scales related to damping and diffusion. For a large ratio $\frac{D}{D_\nu}$, the perturbation to the auxiliary field ν persists notably longer in the system as the perturbation to the field ψ. For a small ratio $\frac{D}{D_\nu}$, the perturbation of the field ψ outlives the perturbation to the auxiliary field ν correspondingly.

5.2 Ansatz and projections

Following the same steps as in section 2.3, we can construct a generating functional for correlation functions of the coupled Langevin equations (5.2)

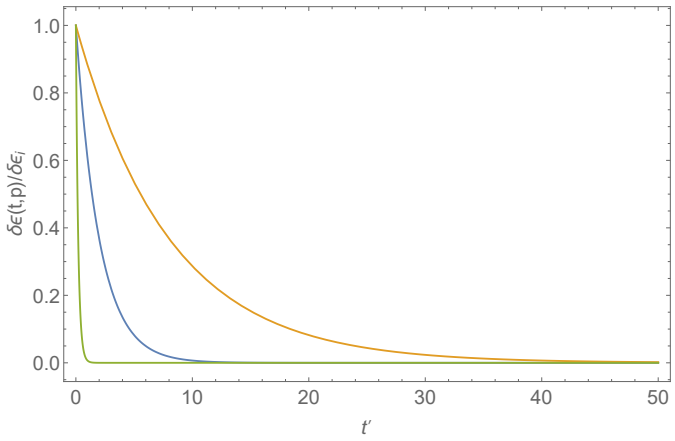

Figure 5.2: The plot shows the relative changes of the perturbation of the ν field from its minimal value compared to its initial perturbation over the dimensionless time $t' = \frac{\omega(\vec{p})}{D}t$. All involved constants as well as the spatial momenta are set to the same value for all three curves, except for the damping coefficient D, which is chosen such that the ratio $\frac{D}{D_\nu}$ is 0.1 (green), 1 (blue) and 4 (orange).

and(5.3) in form of a path integral weighted with the action

$$\begin{aligned} S[\psi,\tilde{\psi},\nu,\tilde{\nu}] = &\int_x \left\{\tilde{\psi}_i(x)\ \left[D\,\partial_t - \nabla^2\right]\ \psi_i(x) + \tilde{\psi}_i(x)\,\psi_i(x)\,\partial_{\psi^2}V(\psi^2)\right\} \\ &+ \int_x \left\{\gamma\,\tilde{\psi}_i(x)\,\psi_i(x)\,\nu(x) - T\,D\,\tilde{\psi}^2(x)\right\} \\ &+ \int_x \left\{\tilde{\nu}(x)\ \left[D_\nu\,\partial_t - \nabla^2\right]\ \nu(x) - \frac{\gamma}{2}\,\tilde{\nu}(x)\,\nabla^2\psi^2(x) + T\,D_\nu\,\tilde{\nu}(x)\,\nabla^2\tilde{\nu}(x)\right\} \end{aligned} \tag{5.22}$$

Our ansatz for the effective average action again includes the lowest order in fields and gradients compatible with the terms included in the initial action (5.22):

$$\begin{aligned} \Gamma_k[\phi,\tilde{\phi},\epsilon,\tilde{\epsilon}] = &\int_x \left\{\tilde{\phi}_i(x)\ \left[Y_k\,\partial_t - Z_k\,\nabla^2\right]\ \phi_i(x) + \tilde{\phi}_i(x)\,\phi_i(x)\,\partial_{\phi^2}U_k(\phi^2)\right\} \\ &+ \int_x \left\{\gamma_k\,\tilde{\phi}_i(x)\,\phi_i(x)\,\epsilon(x) - T\,Y_k\,\tilde{\phi}^2(x)\right\} \\ &+ \int_x \left\{\tilde{\epsilon}(x)\ \left[Y_k^\epsilon\,\partial_t - Z_k^\epsilon\,\nabla^2\right]\ \epsilon(x) - \frac{\gamma_k}{2}\,\tilde{\epsilon}(x)\,\nabla^2\phi^2(x) + T\,Y_k^\epsilon\,\tilde{\epsilon}(x)\,\nabla^2\tilde{\epsilon}(x)\right\} \end{aligned} \tag{5.23}$$

with the field averages

$$\phi(x) = \langle \psi(x) \rangle, \tag{5.24}$$
$$\epsilon(x) = \langle \nu(x) \rangle. \tag{5.25}$$

For the potential we choose again

$$U_k(\rho) = \frac{\lambda_k}{2} \left(\rho(x) - \rho_k^0 \right)^2, \tag{5.26}$$

As a regulator function, the optimized cutoff for the ϕ sector is applied. It will turn out that a cutoff function in the ϕ sector is sufficient to regularize any infrared divergences of the theory, so there is no cutoff function necessary for the ϵ sector.
To simplify the notation in regard of taking field derivatives, we formulate a superfield χ containing the auxiliary field ϵ as well as all N components of the field ϕ together with the corresponding response field:

$$\chi(x) = (\epsilon(x), \phi(x)), \tag{5.27}$$
$$\tilde{\chi}(x) = \left(\tilde{\epsilon}(x), \tilde{\phi}(x) \right) \tag{5.28}$$

Propagators and vertex functions

The propagators produced by the ansatz (5.23), evaluated at vanishing sources, are

$$G_k^R(q_0,\vec{q}) =$$
$$-\begin{pmatrix} i\,q_0\,Y_k^\epsilon + Z_k^\epsilon \vec{q}^2 & \gamma_k\sqrt{2\rho}\,\vec{q}^2 & 0 & ... \\ \gamma_k\sqrt{2\rho} & i\,q_0\,Y_k + Z_k\vec{q}^2 + \partial_\rho U_k(\rho) + 2\,\rho\,\partial_\rho^2 U_k(\rho) & 0 & ... \\ 0 & 0 & i\,q_0\,Y_k + Z_k\vec{q}^2 + \partial_\rho U_k(\rho) & ... \\ ... & ... & ... & ... \end{pmatrix}^{-1}, \tag{5.29}$$

$$G_k^A(q_0,\vec{q}) =$$
$$-\begin{pmatrix} -i\,q_0\,Y_k^\epsilon + Z_k^\epsilon \vec{q}^2 & \gamma_k\sqrt{2\rho}\,\vec{q}^2 & 0 & ... \\ \gamma_k\sqrt{2\rho} & -i\,q_0\,Y_k + Z_k\vec{q}^2 + \partial_\rho U_k(\rho) + 2\,\rho\,\partial_\rho^2 U_k(\rho) & 0 & ... \\ 0 & 0 & -i\,q_0\,Y_k + Z_k\vec{q}^2 + \partial_\rho U_k(\rho) & ... \\ ... & ... & ... & ... \end{pmatrix}^{-1}, \tag{5.30}$$

$$iF_k(q_0,\vec{q}) =$$
$$G_k^R(q_0,\vec{q}) \begin{pmatrix} -2\,T\,Y_k^\epsilon\vec{q}^2 & 0 & 0 & ... \\ 0 & -2\,T\,Y_k & 0 & ... \\ 0 & 0 & -2\,T\,Y_k & ... \\ ... & ... & ... & ... \end{pmatrix} G_k^A(q_0,\vec{q}). \tag{5.31}$$

The remaining entries abbreviated by the dots are zero, except for the diagonal elements. These are identical to the $(3,3)$ element for each matrix.
For the vertex function we use the matrix notation

$$\left(\frac{\delta\Gamma_k^{\tilde{\chi}\chi}(q_2,q_3)}{\delta\chi_l(q_1)}\right)_{ij} = \frac{\delta^3\Gamma_k[\phi,\tilde{\phi},\epsilon,\tilde{\epsilon}]}{\delta\,\chi_l(q_1)\,\delta\,\tilde{\chi}_i(q_2)\delta\,\chi_j(q_3)}. \tag{5.32}$$

For the following set of vertex functions, similar to the propagator functions, all matrix elements abbreviated by the dots are zero except for the diagonal

elements, which are identical to the element $(3,3)$:

$$\frac{\delta\Gamma_k^{\chi\chi}(q_2,q_3)}{\delta\tilde{\chi}_1(q_1)} = \begin{pmatrix} 0 & 0 & 0 & ... \\ 0 & \gamma_k\ (\vec{q_2}+\vec{q_3})^2 & 0 & ... \\ 0 & 0 & \gamma_k\ (\vec{q_2}+\vec{q_3})^2 & ... \\ ... & ... & ... & ... \end{pmatrix}, \tag{5.33}$$

$$\frac{\delta\Gamma_k^{\chi\tilde{\chi}}(q_2,q_3)}{\delta\chi_1(q_1)} = \frac{\delta\Gamma_k^{\tilde{\chi}\chi}}{\delta\chi_1(p)} = \begin{pmatrix} 0 & 0 & 0 & ... \\ 0 & \gamma_k & 0 & ... \\ 0 & 0 & \gamma_k & ... \\ ... & ... & ... & ... \end{pmatrix}, \tag{5.34}$$

$$\frac{\delta\Gamma_k^{\chi\chi}(q_2,q_3)}{\delta\tilde{\chi}_2(q_1)} = \begin{pmatrix} 0 & \gamma_k & 0 & ... \\ \gamma_k & 3\sqrt{2\rho}\,\partial_\rho^2 U_k(\rho) & 0 & ... \\ 0 & 0 & \sqrt{2\rho}\,\partial_\rho^2 U_k(\rho) & ... \\ ... & ... & ... & ... \end{pmatrix}, \tag{5.35}$$

$$\frac{\delta\Gamma_k^{\tilde{\chi}\chi}(q_2,q_3)}{\delta\chi_2(q_1)} = \begin{pmatrix} 0 & \gamma_k\ (\vec{q_1}+\vec{q_3})^2 & 0 & ... \\ \gamma_k & 3\sqrt{2\rho}\,\partial_\rho^2 U_k(\rho) & 0 & ... \\ 0 & 0 & \sqrt{2\rho}\,\partial_\rho^2 U_k(\rho) & ... \\ ... & ... & ... & ... \end{pmatrix}, \tag{5.36}$$

$$\frac{\delta\Gamma_k^{\chi\tilde{\chi}}(q_2,q_3)}{\delta\chi_2(q_1)} = \begin{pmatrix} 0 & \gamma_k & 0 & ... \\ \gamma_k\ (\vec{q_1}+\vec{q_2})^2 & 3\sqrt{2\rho}\,\partial_\rho^2 U_k(\rho) & 0 & ... \\ 0 & 0 & \sqrt{2\rho}\,\partial_\rho^2 U_k(\rho) & ... \\ ... & ... & ... & ... \end{pmatrix}. \tag{5.37}$$

For the last set of vertex functions appearing in the relevant diagrams, all entries abbreviated by the dots vanish:

$$\frac{\delta\Gamma_k^{\chi\chi}(q_2,q_3)}{\delta\tilde{\chi}_3(q_1)} = \begin{pmatrix} 0 & 0 & \gamma_k & \dots \\ 0 & 0 & \sqrt{2\rho}\,\partial_\rho^2 U_k(\rho) & \dots \\ \gamma_k & \sqrt{2\rho}\,\partial_\rho^2 U_k(\rho) & 0 & \dots \\ \dots & \dots & \dots & \dots \end{pmatrix}, \tag{5.38}$$

$$\frac{\delta\Gamma_k^{\tilde{\chi}\chi}(q_2,q_3)}{\delta\chi_3(q_1)} = \begin{pmatrix} 0 & 0 & \gamma_k\,(\vec{q_1}+\vec{q_3})^2 & \dots \\ 0 & 0 & \sqrt{2\rho}\,\partial_\rho^2 U_k(\rho) & \dots \\ \gamma_k & \sqrt{2\rho}\,\partial_\rho^2 U_k(\rho) & 0 & \dots \\ \dots & \dots & \dots & \dots \end{pmatrix}, \tag{5.39}$$

$$\frac{\delta\Gamma_k^{\chi\tilde{\chi}}(q_2,q_3)}{\delta\chi_3(q_1)} = \begin{pmatrix} 0 & 0 & \gamma_k & \dots \\ 0 & 0 & \sqrt{2\rho}\,\partial_\rho^2 U_k(\rho) & \dots \\ \gamma_k\,(\vec{q_1}+\vec{q_2})^2 & \sqrt{2\rho}\,\partial_\rho^2 U_k(\rho) & 0 & \dots \\ \dots & \dots & \dots & \dots \end{pmatrix}. \tag{5.40}$$

It is notable that this basic truncation already produces momentum dependent vertex functions. This is due to the spatial gradients in the Langevin equation (5.3), and the necessity to represent them in the truncation to ensure the conservation of $E(t)$ is preserved.

Projections and dimensionless coefficients

The coefficients of the ϕ sector can be calculated as in the previous chapters:

$$\partial_t U_k'(\rho) = \frac{1}{\sqrt{2\rho}} \lim_{p\to 0} \partial_t \frac{\delta\Gamma_k}{\delta\tilde{\chi}_2(p)}, \tag{5.41}$$

$$\partial_t \tilde{\lambda}_k = \left[\partial_\rho \partial_t U_k'(\rho)\right] |_{\epsilon=0}^{\rho=\rho_k^0}, \tag{5.42}$$

$$\partial_t \rho_k^0 = -\frac{1}{\tilde{\lambda}_k} \partial_t U_k'(\rho)|_{\epsilon=0}^{\rho=\rho_k^0}, \tag{5.43}$$

$$\partial_t Z_k = \lim_{p\to 0} \partial_{\vec{p}^2} \partial_t \frac{\delta\Gamma_k}{\delta\tilde{\chi}_3(-p)\delta\chi_3(p)}|_{\epsilon=0}^{\rho=\rho_k^0}, \tag{5.44}$$

$$\partial_t Y_k = -i \lim_{p\to 0} \partial_{p_0} \partial_t \frac{\delta\Gamma_k}{\delta\tilde{\chi}_3(-p)\delta\chi_3(p)}|_{\epsilon=0}^{\rho=\rho_k^0}. \tag{5.45}$$

The coefficients of the ϵ sector are derived by the equations:

$$\partial_t \gamma_k = \frac{1}{2\sqrt{\rho_k^0}} \lim_{p\to 0} \partial_t \frac{\delta\Gamma_k}{\delta\tilde{\chi}_2(-p)\delta\chi_1(p)}|_{\epsilon=0}^{\rho=\rho_k^0}, \tag{5.46}$$

$$\partial_t Z_k^\epsilon = \lim_{p\to 0} \partial_{\vec{p}^2} \partial_t \frac{\delta\Gamma_k}{\delta\tilde{\chi}_1(-p)\delta\chi_1(p)}|_{\epsilon=0}^{\rho=\rho_k^0}, \tag{5.47}$$

$$\partial_t Y_k^\epsilon = -i \lim_{p\to 0} \partial_{p_0} \partial_t \frac{\delta\Gamma_k}{\delta\tilde{\chi}_1(-p)\delta\chi_1(p)}|_{\epsilon=0}^{\rho=\rho_k^0}. \tag{5.48}$$

As before, we will introduce dimensionless quantities

$$\rho_k^0 = k^{d-2+\eta_Z} \rho, \tag{5.49}$$

$$\tilde{\lambda}_k = k^{4-d-2\,\eta_Z} \tilde{\lambda}, \tag{5.50}$$

$$Y_k = k^{2-\eta_Z}\, Y, \tag{5.51}$$

$$\gamma_k = k^{\frac{d}{2}-2+\eta_Z+\frac{\eta_\epsilon}{2}}\, \gamma, \tag{5.52}$$

$$Y_k^\epsilon = k^{2-\eta_\epsilon}\, Y^\epsilon. \tag{5.53}$$

The anomalous dimensions of the ϕ and ϵ sector are defined as

$$\eta_Z = -\partial_t \ln(Z_k), \tag{5.54}$$

$$\eta_\epsilon = -\partial_t \ln(Z_k^\epsilon). \tag{5.55}$$

We also define the shifted interaction coefficient

$$\lambda = \tilde{\lambda} - \gamma^2, \tag{5.56}$$

with the flow equation

$$\partial_t \lambda = \partial_t \tilde{\lambda} - 2\gamma \partial_t \gamma. \tag{5.57}$$

5.3 Flow equations

The frequency as well as spatial momentum integrations involved in the flow equations can calculated analytically again. The static flow equations in the ϕ sector are:

$$\partial_t \rho = (2 - d - \eta_Z)\ \rho + 2\, v_d\, T\, \left[3\, \frac{2}{d\ (2+d)}\, \frac{(2+d-\eta_Z)}{(1+2\,\rho\,\lambda)^2} + (N-1)\ \frac{2}{d\ (2+d)}\ (2+d-\eta_Z) \right], \tag{5.58}$$

$$\partial_t \lambda = (d - 4 + 2\,\eta_Z)\ \lambda + 2\, v_d\, T\, \lambda^2\, \left[9\, \frac{4}{d\ (2+d)}\, \frac{(2+d-\eta_Z)}{(1+2\,\rho\,\lambda)^3} + (N-1)\ \frac{4}{d\ (2+d)}\ (2+d-\eta_Z) \right], \tag{5.59}$$

$$\eta_Z = 16\, \frac{v_d}{d}\, T\, \rho\, \lambda^2\, \frac{1}{(1+2\,\rho\,\lambda)^2}. \tag{5.60}$$

We see that the static flow equations of the ϕ sector decouple form the ϵ sector if we express them in the shifted coupling strength (5.56). This agrees with the discussion in section 5.1.
The flow equations for the coefficients related to the auxiliary field ϵ are:

$$\begin{aligned} \partial_t \gamma = & \left(\frac{d}{2} - 2 + \eta_Z + \frac{\eta_\epsilon}{2} \right) \gamma \\ & + 2\, v_d\, T\, \gamma\ \left(\lambda + \gamma^2 \right)\ \left[3\, \frac{4}{d\ (2+d)}\, \frac{(2+d-\eta_Z)}{(1+2\,\rho\,\lambda)^3} + (N-1)\ \frac{4}{d\ (2+d)}\ (2+d-\eta_Z) \right], \end{aligned} \tag{5.61}$$

$$\eta_\epsilon = -\,2\, v_d\, T\, \gamma^2\, \left[\frac{4}{d\ (2+d)}\, \frac{(2+d-\eta_Z)}{(1+2\,\rho\,\lambda)^3} + (N-1)\ \frac{4}{d\ (2+d)}\ (2+d-\eta_Z) \right] \tag{5.62}$$

The flow equation for the diffusion coefficient Y^ϵ vanishes exactly. This is a consequence of its general structure, as it is contains the vertex function

$$\frac{\delta \Gamma_k^{\chi\chi}(q, -q-p)}{\delta \tilde{\chi}_1(p)} \propto \vec{p}^2. \tag{5.63}$$

This leads to a proportionality to the external spatial momentum squared of the whole diagram. As the projection on the diffusion coefficient Y_k^ϵ does not involve any derivatives with respect to the external spatial momenta, the diagram will vanish in the limit $p \to 0$. This conclusion is independent of the truncation scheme, as the proportionality of the vertex function to the

external spatial momenta is a consequence of the gradients on the right hand side of the Langevin equation (5.3) for the auxiliary field, which ensure the conservation of $E(t)$.
For this reason, the dimensionful diffusion coefficient Y_k^ϵ can be set to one to simplify the calculations of the flow equations. Note that the dimensionless diffusion coefficient Y^ϵ does change with the renormalization group scale, but in a trivial way:

$$\partial_t Y^\epsilon = (\eta_\epsilon - 2)\ Y^\epsilon. \tag{5.64}$$

This puts strong restrictions on possible scaling behavior of the ϵ sector. The only possibility the combination $iY_k^\epsilon + Z_k^\epsilon \vec{q}^2$ can exhibit scaling behavior of the form shown in (2.3) is if the dynamic scaling coefficient fulfills the condition

$$z = 2 - \eta_\epsilon. \tag{5.65}$$

We define a comparison coefficient between the two dynamic scales analogous to the ones in the previous chapters. As it will turn out to be necessary during the fixed point analysis, a form for the coefficient is chosen that can capture both possible cases of one dynamic scale dominating over the other as well as a locking between both:

$$\kappa = \frac{1}{1 + \frac{Y}{Y^\epsilon}} = \frac{1}{1 + \frac{Z_k^\epsilon Y_k}{Z_k}}. \tag{5.66}$$

The flow equation for this coefficient is

$$\partial_t \kappa = \kappa\ (1 - \kappa)\ (\eta_Y + \eta_\epsilon - 2)\,. \tag{5.67}$$

The equation for the scaling exponent of the dimensionless damping coefficient Y appearing in this flow equation is

$$\begin{aligned}\eta_Y = 2 - \eta_Z + \frac{2\, v_d\, T}{\rho}\ &\left[\frac{2}{d\ (2+d)}\ \frac{(2 + d - \eta_Z)}{(1 + 2\,\rho\,\lambda)^2} + \frac{2}{d\ (2+d)}\ (2 + d - \eta_Z)\right] \\ &- 2\,\frac{2\, v_d\, T}{\rho}\, h\left(\rho\ \left(\lambda + \gamma^2\right), \gamma^2\, \rho\, \frac{1-\kappa}{\kappa}, \frac{1-\kappa}{\kappa}, \eta_Z\right)\end{aligned} \tag{5.68}$$

The function $h(\omega_1, \omega_2, \omega_3, \eta)$ used here is

$$
\begin{aligned}
h(\omega_1,\omega_2,\omega_3,\eta) =& \frac{1}{(1+\omega_1)^2}\Big[\frac{(1+\omega_1)\;(\omega_2+(1+\omega_3))}{1+\omega_1-\omega_2+\omega_3+\omega_1\,\omega_3} \\
&+\left(\frac{2}{d}-1\right)\,{}_2F_1\left(1,\frac{d}{2},\frac{d+2}{2},\frac{\omega_2}{\omega_1+1}-\omega_3\right) \\
&-\frac{d}{d+2}\;(\omega_2+2\omega_3)\;{}_2F_1\left(1,\frac{d+2}{2},\frac{d+4}{2},\frac{\omega_2}{\omega_1+1}-\omega_3\right) \\
&-\frac{d+2}{d+4}\,\omega_3^2\,{}_2F_1\left(1,\frac{d+4}{2},\frac{d+6}{2},\frac{\omega_2}{\omega_1+1}-\omega_3\right) \\
&-\frac{\eta}{2}\Big\{\left(\frac{2}{d}-1\right)\,{}_2F_1\left(1,\frac{d}{2},\frac{d+2}{2},\frac{\omega_2}{\omega_1+1}-\omega_3\right) \\
&-\frac{d}{d+2}\;(\omega_2+2\omega_3-1)\;{}_2F_1\left(1,\frac{d+2}{2},\frac{d+4}{2},\frac{\omega_2}{\omega_1+1}-\omega_3\right) \\
&-\frac{d+2}{d+4}\;(\omega_3-\omega_2-2\omega_3)\;{}_2F_1\left(1,\frac{d+4}{2},\frac{d+6}{2},\frac{\omega_2}{\omega_1+1}-\omega_3\right) \\
&+\frac{d+6}{d+8}\,\omega_3^2\,{}_2F_1\left(1,\frac{d}{2},\frac{d+2}{2},\frac{\omega_2}{\omega_1+1}-\omega_3\right)\Big\}\Big] \qquad (5.69)
\end{aligned}
$$

The functions ${}_2F_1\,(x_1,x_2,x_3,x_4)$ are the hypergeometric functions, defined and explained for example in reference [1].

5.4 Fixed point solutions and scaling regions

In this section we will discuss the fixed point structure of the flow equations derived in the last section. All actual calculations will be performed at temperature $T=1$. The flow equations order into three different groups, the static equations of the ϕ and ϵ sector and the dynamic equation.
The static flow equations of the ϕ sector decouple from the dynamic coefficients and those related to the auxiliary field ϵ and can therefore be solved separately for fixed points. The fixed point and stability properties of this static $O(N)$ model are well discussed, for example in references [25] and [14]. Examples for the cases $N=2$ and $N=1$ can be found in chapters 3 and 4. Using the fixed point values of the static ϕ sector, we can solve the static ϵ sector, which is still decoupled from the dynamic equations. To finally solve the dynamic flow equation (5.67), the fixed point values of the coefficients of both static sectors are necessary.
There a four possible fixed point solutions for the system. The stability of these fixed points is solely determined by the number N of field components

of the ϕ field and the number d of spatial dimensions.

- The first case is the decoupled scaling region, characterized by the vanishing of the coupling γ between the two sectors at the fixed point. The two Langevin equations (5.2) and (5.3) will decouple then, and the equation for the ϕ fields will reduce exactly to those of the universality class of Model A. So in this phase, the dynamics will be purely relaxational. A discussion of the $N = 1$ case of Model A in the context of the functional renormalization group can be found in reference [20].

In case of a non-vanishing coupling between the two sectors, i.e. $\gamma_C > 0$, we find three possible types of dynamics. Either one of the time scales of the relaxational dynamics of the ϕ sector or the diffusive dynamics of the ϵ sector can dominate, or both types of dynamics can act on the same time scale.

- In the weak scaling region, the comparison coefficient κ vanishes at the fixed point:

$$\kappa_C = 0. \tag{5.70}$$

  The time scale related to the relaxational dynamic of the ϕ sector dominates over the scale of the diffusive dynamics of the ϵ sector. Therefore, if the temperature of the system is close to its critical temperature, perturbations of the ϵ sector will diffuse effectively instantaneous back to the equilibrium state compared to the time scale of the relaxation of perturbations in the ϕ sector. The dynamic scaling exponent is given by:

$$z = \eta_Y \tag{5.71}$$

- In the strong scaling region, the comparison coefficient κ assumes a non-vanishing value smaller than one at the fixed point:

$$0 < \kappa_C < 1. \tag{5.72}$$

  Perturbations relax back to equilibrium on the same time scale in the ϕ sector as they diffuse in the ϵ sector. Both types of dynamics are relevant for the dynamic critical behavior. The dynamic scaling exponent is given by:

$$z = \eta_Y = 2 - \eta_\epsilon. \tag{5.73}$$

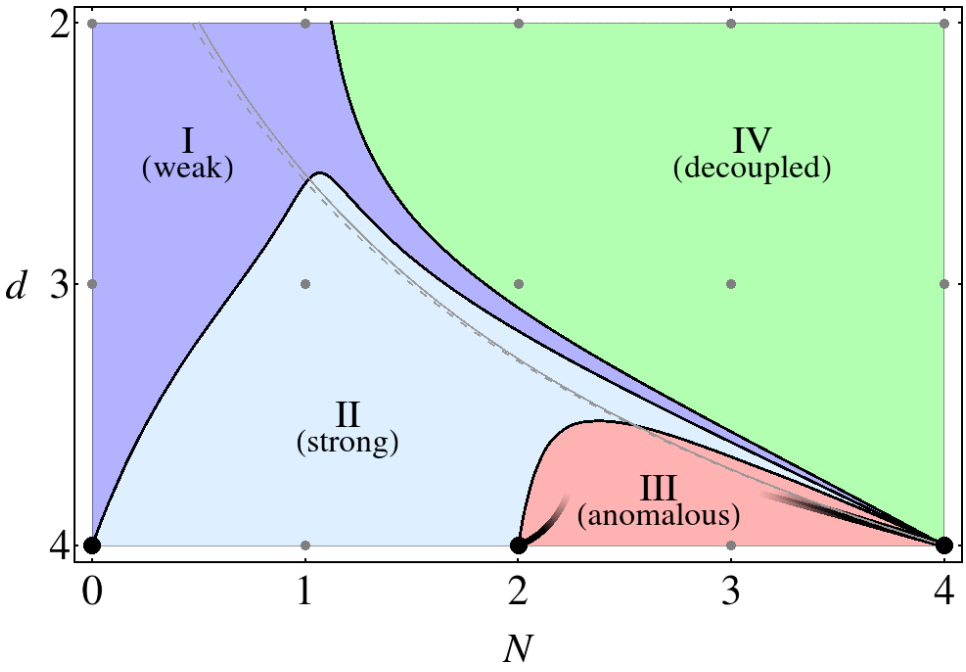

Figure 5.3: The different scaling regions I - IV in the (N, d) plane for the N component scalar field with a coupled conserved quantity, adopted from reference [70]. The thick lines represent results of a perturbative renormalization group approach to second order in the ϵ expansion from reference [35], the thin line represents results to first order in the ϵ expansion from reference [18].

- In the anomalous scaling region, the comparison coefficient κ assumes the value one at the fixed point:

$$\kappa_C = 1. \tag{5.74}$$

  In this case, the critical dynamic behavior is characterized by diffusion processes. The relaxation of the ϕ sector occurs effectively instantaneous on the time scale of the diffusive dynamics of the ϵ sector if the system is close to the critical point. The dynamic scaling exponent is given by:

$$z = 2 - \eta_\epsilon. \tag{5.75}$$

All four cases of critical dynamic behavior can be found for appropriate values of the spatial dimensions d and the number of field components of

the ϕ field N. The different areas of dynamic critical behavior in the (N, d) plane are shown in figure 5.3. It is notable that perturbative renormalization group approaches, for example in reference [34] or [18], could not conclusively determine the existence and possible region of anomalous scaling in the (N, d) plane.
The following table shows the fixed point values for the stable fixed point of one exemplary (N, d) point in each region:

Scaling Region	N	d	γ_C	κ_C	η_Y	η_ϵ	z
Decoupled	2	3	0	0	2.027	0	2.027
Weak	1	2	2.879	0	2.151	-0.064	2.151
Strong	1	3	2.190	0.176	2.059	-0.059	2.059
Anomalous	3	3.9	0.341	1	2.002	-0.003	2.003

In the figures 5.4 and 5.5 the flow of the coupling γ between the sectors and the comparison coefficient κ is shown for these four exemplary points in the (N, d) plane. The initial values are chosen such that all coefficients except the ones shown in the figures start already at their fixed point values and therefore do not change with the renormalization group scale. Note that as the (N, d) point representing the anomalous scaling region is very close to the $d = 4$ line, where the gaussian fixed point is the stable one in the static ϕ sector, the coefficients exhibit only very small changes with the renormalization group scale. Accordingly, the scaling exponents at this (N, d) point differ only slightly from those of the non-interacting case emerging at the gaussian fixed point.

5.5 General dynamic universality classes

The universality class of Model C discussed in the former section describes the dynamics of a non-conserved order parameter coupled to a conserved auxiliary field. In this section we provide a general formulation of the universality classes of Model A to Model F in terms of the closed time path action in Keldysh form. These universality classes cover the dynamics of conserved and non-conserved order parameters independently and coupled to a conserved auxiliary field, taking into account possible non-vanishing Poisson brackets between the order parameter and auxiliary field as well [27].
All these possible dynamics formulated in one combined Langevin equation yields:

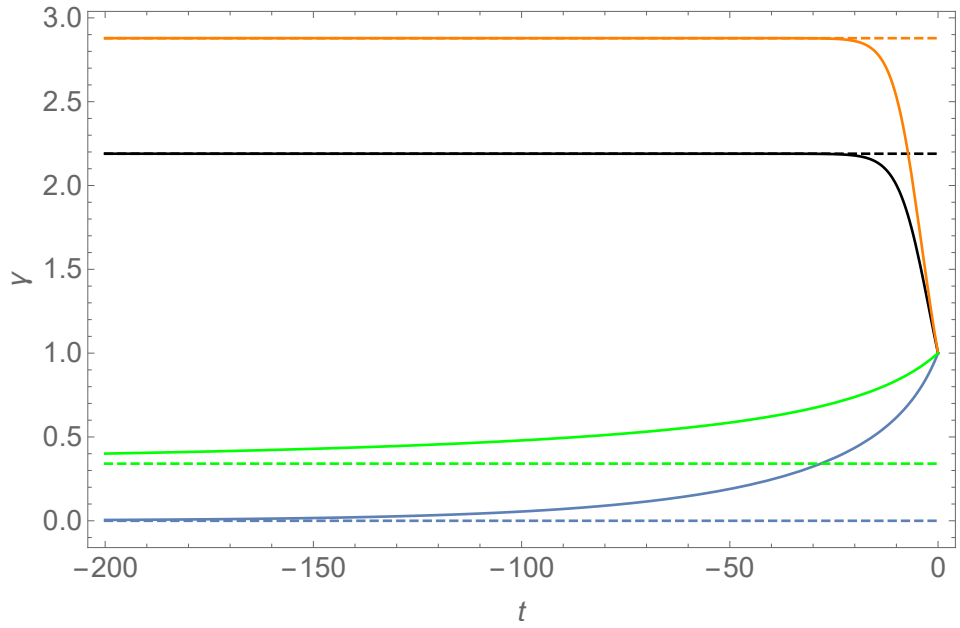

Figure 5.4: The flow of the dimensionless coupling γ between the ϕ and ϵ sector. The four different scaling regions are represented through $N = 2$, $d = 3$ for the decoupled scaling region (blue), $N = 1$, $d = 2$ for the weak scaling region (orange), $N = 1$, $d = 3$ for the strong scaling region (black) and $N = 3$, $d = 3.9$ for the anomalous scaling region (green). The dashed lines show the corresponding fixed point values γ_C. The initial values of all coefficient but γ are set to their fixed point values.

$$\begin{aligned}\partial_t\psi(x) = &- D\,(m^2\,\psi(x) - Z_1\,\nabla^2\psi(x) + Z_2\,\nabla^4\psi(x) - Z_3\,\nabla^2\psi(x)^3 + \frac{\lambda}{3!}\,\psi(x)^3 \\ &+ \gamma_1\,\nu\,\psi(x) - \gamma_2\,\nabla^2\,\nu(x)\,\psi(x)) + i\,g\,\psi(x)\,(Z_\nu\,\nu(x) + \frac{1}{2}\,\gamma_1\,\psi(x)^2) + \xi(x)\end{aligned} \tag{5.76}$$

for the order parameter and the equation

$$\partial_t\nu(x) = D_\nu(Z_\nu\,\nabla^2\nu(x) + (\gamma_1 + \gamma_2)\,(\nabla\psi(x))^2 + (\gamma_1 + \gamma_2)\,\psi(x)\,\nabla^2\psi(x)) + \xi_\nu(x) \tag{5.77}$$

for the auxiliary field. The noise functions have the properties

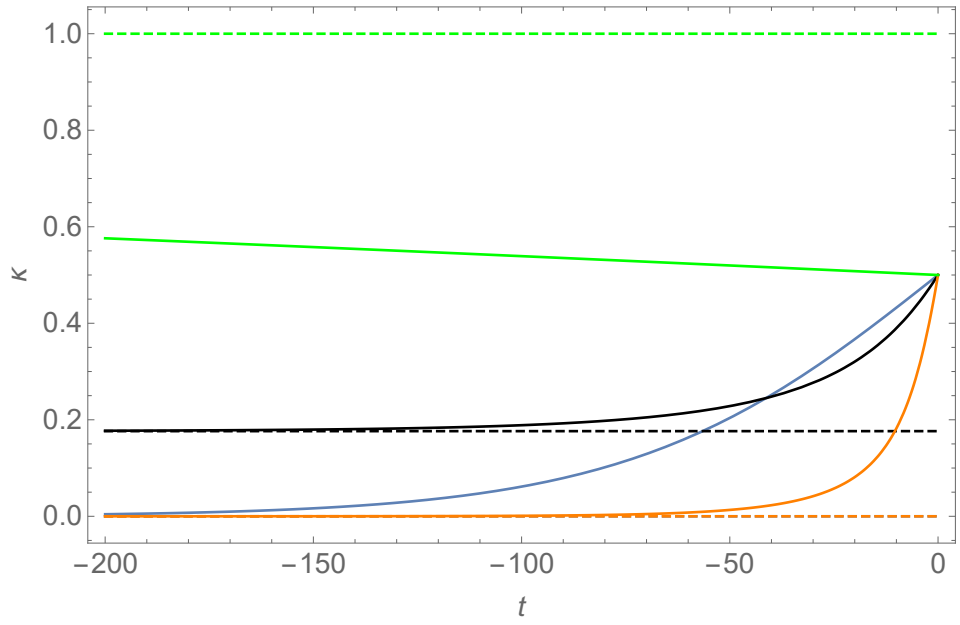

Figure 5.5: The flow of the comparison coefficient κ measuring the competition of the time scales of the diffusive and relaxational dynamics. The four different scaling regions are represented through $N = 2$, $d = 3$ for the decoupled scaling region (blue), $N = 1$, $d = 2$ for the weak scaling region (orange), $N = 1$, $d = 3$ for the strong scaling region (black) and $N = 3$, $d = 3.9$ for the anomalous scaling region (green). The dashed lines show the corresponding fixed point values γ_C. The initial values of all coefficient but κ are set to their fixed point values.

$$\langle \xi(x) \rangle = 0, \tag{5.78}$$

$$\langle \xi(x)\, \xi(y) \rangle = 2\, \Re(D)\, T\, \left(\delta - (1-\delta)\nabla^2\right)\, \delta^4(x-y) \tag{5.79}$$

$$\langle \xi_\nu(x) \rangle = 0, \tag{5.80}$$

$$\langle \xi_\nu(x)\, \xi_\nu(y) \rangle = -2\, \Re(D_\nu)\, T \nabla^2\, \delta^4(x-y). \tag{5.81}$$

In the cases of Model E and F, the field is considered to be complex, as well as the relaxation coefficient D. There are extended versions of the Models A to D named as Model A+ to D+, where the field and relaxation coefficients are assumed to be complex as well [36]. Apart from that, all coefficients are considered to be real.

The averages over the Langevin equations (5.77) and (5.77) can again be formulated as a path integral weighted by the following action:

$$\begin{aligned} S[\psi,\tilde{\psi},\nu,\tilde{\nu}] = \int_x \Big[& \tilde{\psi}(x)\,(Y\,\partial_t\psi(x) + m^2\psi(x) - Z_1\nabla^2\psi(x) + Z_2\nabla^4\psi(x) - Z_3\nabla^2\psi(x)^3 + \frac{\lambda}{3!}\psi(x)^3 \\ & + \gamma_1\,\nu(x)\,\psi(x) - \gamma_2\,\nabla^2\nu\,\psi(x) + i\,g\,Z_\nu\,\nu(x)\psi(x) + \frac{1}{2}\,i\,g\,\gamma_1\psi(x)^3) \\ & + \tilde{\nu}(x)\,(Y_\nu\,\partial_t\nu(x) - Z_\nu\nabla^2\nu - \frac{1}{2}\,(\gamma_1+\gamma_2)\,\nabla^2\psi(x)^2) \\ & - \Re(Y)\,\tilde{\psi}(x)\,(\delta - (1-\delta)\,\nabla^2)\,\tilde{\psi}(x) + \Re(Y_\nu)\,\tilde{\nu}(x)\,\nabla^2\tilde{\nu}(x) + c.c.\Big] \end{aligned} \tag{5.82}$$

As usual we used $Y = \frac{1}{D}$ and $Y_\nu = \frac{1}{D_\nu}$. This action can be used as the basis of functional renormalization group calculations involving all or any combination of critical dynamics associated to the universality classes of Model A to F. The following table shows the coefficients that are non-zero in each single one of these models:

	m^2	λ	Z_2	Z_3	γ_1	γ_2	g	δ
Model A	$\neq 0$	$\neq 0$	0	0	0	0	0	1
Model B	0	0	$\neq 0$	$\neq 0$	0	0	0	0
Model C	$\neq 0$	$\neq 0$	0	0	$\neq 0$	0	0	1
Model D	0	0	$\neq 0$	$\neq 0$	0	$\neq 0$	0	0
Model E	$\neq 0$	$\neq 0$	0	0	0	0	$\neq 0$	1
Model F	$\neq 0$	$\neq 0$	0	0	$\neq 0$	0	$\neq 0$	1

We can also categorize the interaction terms involved in each of these models:

	$\tilde{\phi}\phi^3$	$\tilde{\phi}\nabla^2\phi^3$	$i\tilde{\phi}\phi^3$	$\tilde{\phi}\nu\phi$	$i\tilde{\phi}\nu\phi$	$\tilde{\phi}\nabla^2(\nu\phi)$	$\tilde{\nu}\nabla^2\phi^2$
Model A	λ	0	0	0	0	0	0
Model B	0	Z_3	0	0	0	0	0
Model C	λ	0	0	γ_1	0	0	γ_1
Model D	0	Z_3	0	0	0	γ_2	γ_2
Model E	λ	0	0	0	$Z_\nu g$	0	0
Model F	λ	0	$g\gamma_1$	γ_1	$Z_\nu g$	0	γ_1

Chapter 6

Conclusions

Starting in Chapter 2, we introduced the established method of the real time functional renormalization group as a tool for the computation of real time correlation functions. We discussed the incorporation of the initial density matrix of thermal equilibrium by utilizing the specific properties of the equilibrium state. The role of the so called quantum vertices appearing in the real time formulation of the functional renormalization group has been examined and found to be irrelevant for the computation of propagators in thermal equilibrium.

In chapter 3, dynamic critical phenomena in a system on non-relativistic, interacting bosons were investigated applying the framework introduced earlier. The competition between the time scales of relaxational and unitary dynamics was examined and the relaxational dynamic was found to be dominant in the vicinity of the critical point. Integrating out the fast modes in the functional renormalization group flow also led to the built up of terms inducing a gaussian noise on the equations of motion, acting effectively as a heat bath to the slow modes not yet integrated out. The results match those of the dynamic universality class of Model A in the classification scheme of Halperin and Hohenberg. The actual dynamic universality class of the non-relativistic bose gas is commonly assumed to be Model E, which can not be distinguished from Model A at the current level of the truncation applied in this work. The extension of the truncation scheme to include possible fixed points of Model E might be an interesting endeavor.

Chapter 4 engaged in examination of the dynamic critical properties of the relativistic $O(N)$ model by again applying the framework established in chap-

ter 2. We found relaxational dynamics and a noise term building up during the functional renormalization group flow similar to the results encountered in the non-relativistic system discussed in chapter 3. The time scale of the relaxational dynamics however did not dominate the scale of the relativistic dynamics in the vicinity of the fixed point. The relativistic coefficient adopts a unphysical negative sign at the fixed point. While the ratio of the dimensionless coefficients related to the relativistic and relaxational dynamics is rather small, it could not be identified as an artefact of the truncation so far. We improved the truncation by extending the expansion of the effective average action in the time derivatives by several orders, observing no significant changes in the quantitative results. This indicates a sufficient convergence of the gradient expansion in the time derivatives, yet it does not explain the unphysical sign change of the relativistic coefficient. The results likewise proofed to be stable under the application of two different regulator functions.
A possible physical reason to this result could be the negligence of the non-relativistic limit and the effects of particle number conservation associated with it in our truncation scheme. We proposed an ansatz and truncation scheme to take the non-relativistic limit into account. Independent of the resolution of the mentioned issues, the possible relevance of the non-relativistic limit for the critical dynamics is an intriguing question we address in our current work. A further subject of future work could be the investigation of quantum critical effects at non-vanishing temperatures. The frequency dependent regulator function discussed in this chapter, which conserves Lorentz invariance, combined with the framework introduced in chapter 2, as it takes all quantum fluctuations into account, appears as a suitable starting point to address this question.

In chapter 5, we investigated the universality class of Model C as an example of an effective theory including the dynamics of a conserved quantity. Applying the functional renormalization group, we were able to determine the existence and extend of the so called anomalous scaling region in the phase diagram of Model C. This resolves a question that could to date not be conclusively addressed by perturbative renormalization group approaches. Further work could include the treatment of additional dynamic universality classes in the Halperin and Hohenberg categorization scheme by the functional renormalization group. We provided a description of the Models A to F in the Keldysh action employed in the real time functional renormalization group approach.
As we have noted in chapter 3, out truncation scheme is at the current state

not able to distinguish between the dynamic universality classes of Halperin and Hohenberg involving the dynamics of conserved quantities. An additional interesting task would therefore be the direct implementation of the dynamics of conserved quantities in our truncation scheme without the introduction of an auxiliary field as an effective description.

Acknowledgments

First of all I would like to thank Prof. Jürgen Berges for his guidance, patience and constant support during the last three years. His enthusiasm and scientific curiosity are nothing less than inspiring, and I greatly appreciate the advice he provided in professional as well as private matters.

I furthermore want to express my deep gratitude to David Mesterházy for the time and efforts he spent to answer my every question, encourage my ideas and support my work in all possible aspects.

I would like to thank David Mesterházy, Leticia F. Palhares and Yuya Tanizaki for the fruitful collaboration.

I would also like to thank Kirill Boguslavskii, Jean-Sebastien Gagnon, Daniil Gelfand, Lutz Goergen, Florian Hebenstreit, Onirban Islam, Valentin Kasper, Gerald Langhanke, David Mesterházy, Niklas Müller, Sebastian Ohmer, Asier P. Orioli, Leticia F. Palhares, Alexander Rothkopf, Sören Schlichting, Dénes Sexty, Naoto Tanji, Benjamin Wallisch and Thorsten Zöller for interesting discussions, a pleasant work atmosphere and an overall great time during the last three years.

For the thorough proof reading of this thesis and plenty of helpful suggestions I thank Florian Kehrle, Alexander Knetsch, Christoph Maurer, David Mesterházy, Asier P. Orioli and Matthias Sattig.

Special thanks goes to Julia Butt for the patience, motivation and advice provided in the last years.

Finally, I would like to thank my family for their constant, loving and unconditional support.

List of Figures

Bibliography

[1] M. Abramowitz and I. A. Stegun. *Handbook of Mathematical Functions*, volume 55. 1965.

[2] V. K. Akkineni and U. C. Täuber. Nonequilibrium critical dynamics of the relaxational models C and D. *Phys. Rev. E - Stat. Nonlinear, Soft Matter Phys.*, 69(3 2):1–23, 2004.

[3] S. Albeverio and H.-K. R. *Mathematical Theory of Feynman Path Integral*. Springer Verlag, 1976.

[4] C. Bagnuls and C. Bervillier. Exact renormalization group equations: an introductory review. *Phys. Rep.*, 348(1-2):91–157, jul 2001.

[5] F. Benitez, J.-P. Blaizot, H. Chaté, B. Delamotte, R. Méndez-Galain, and N. Wschebor. Nonperturbative renormalization group preserving full-momentum dependence: Implementation and quantitative evaluation. *Phys. Rev. E*, 85(2):026707, feb 2012.

[6] B. Berdnikov and K. Rajagopal. Slowing out of equilibrium near the QCD critical point. *Phys. Rev. D*, 61(10):105017, apr 2000.

[7] J. Berges. Introduction to Nonequilibrium Quantum Field Theory. page 131, 2004.

[8] J. Berges. Nonequilibrium Quantum Fields: From Cold Atoms to Cosmology. 2015.

[9] J. Berges and T. Gasenzer. Quantum versus classical statistical dynamics of an ultracold Bose gas. *Phys. Rev. A - At. Mol. Opt. Phys.*, 76(3), 2007.

[10] J. Berges and G. Hoffmeister. Nonthermal fixed points and the functional renormalization group. *Nucl.\ Phys.*, B813:383, 2009.

[11] J. Berges and J. Jaeckel. Far from equilibrium dynamics of Bose-Einstein condensation for Axion Dark Matter. *arXiv Prepr. arXiv1402.4776*, page 18, 2014.

[12] J. Berges and D. Mesterhazy. Introduction to the nonequilibrium functional renormalization group. *Nucl.\ Phys.\ Proc.\ Suppl.*, 228:37–60, 2012.

[13] J. Berges, S. Schlichting, and D. Sexty. Dynamic critical phenomena from spectral functions on the lattice. *Nucl.\ Phys.*, B832:228–240, 2010.

[14] J. Berges, N. Tetradis, and C. Wetterich. Non-perturbative renormalization flow in quantum field theory and statistical physics, 2002.

[15] J.-P. Blaizot and E. Iancu. The Quark-Gluon Plasma: Collective Dynamics and Hard Thermal Loops. 2001.

[16] J. P. Blaizot, R. Méndez-Galain, and N. Wschebor. Non-perturbative renormalization group calculation of the scalar self-energy. *Eur. Phys. J. B*, 58(3):297–309, 2007.

[17] I. Boettcher, J. M. Pawlowski, and S. Diehl. Ultracold atoms and the Functional Renormalization Group. *Nucl. Phys. B - Proc. Suppl.*, 228:63–135, 2012.

[18] E. Brézin and C. De Dominicis. Field-theoretic techniques and critical dynamics. II. Ginzburg-Landau stochastic models with energy conservation. *Phys. Rev. B*, 12(11):4954–4962, dec 1975.

[19] P. Calabrese and A. Gambassi. Aging at Criticality in Model C Dynamics. page 13, 2002.

[20] L. Canet and H. Chaté. Non-perturbative Approach to Critical Dynamics. page 13, 2006.

[21] L. Canet, B. Delamotte, D. Mouhanna, and J. Vidal. Nonperturbative renormalization group approach to the Ising model: A derivative expansion at order 4. *Phys. Rev. B*, 68(6):064421, aug 2003.

[22] K.-c. Chou, Z.-b. Su, B.-l. Hao, and L. Yu. Equilibrium and nonequilibrium formalisms made unified. *Phys. Rep.*, 118(1-2):1–131, feb 1985.

[23] W. T. Coffey and Y. P. Kalmykov. *The Langevin Equation: With Applications to Stochastic Problems in Physics, Chemistry and Electrical Engineering*. World Scientific, 2012.

[24] C. De Dominicis, E. Brézin, and J. Zinn-Justin. Field-theoretic techniques and critical dynamics. I. Ginzburg-Landau stochastic models without energy conservation. *Phys. Rev. B*, 12(11):4945–4953, 1975.

[25] B. Delamotte. An introduction to the nonperturbative renormalization group. *Lect. Notes Phys.*, 852:49–132, 2012.

[26] S. Diehl, H. Gies, J. M. Pawlowski, and C. Wetterich. Renormalization flow and universality for ultracold fermionic atoms. *Phys. Rev. A - At. Mol. Opt. Phys.*, 76(5), 2007.

[27] I. E. Dzyaloshinskii and G. E. Volovick. Poisson brackets in condensed matter physics. *Ann. Phys.*, 125:67, 1980.

[28] A. Einstein. Über die von der molekularkinetischen Theorie der Wärme geforderte Bewegung von in ruhenden Flüssigkeiten suspendierten Teilchen. *Ann. Phys.*, 322(8):549–560, 1905.

[29] T. S. Evans. The Condensed Matter Limit of Relativistic QFT. page 13, 1995.

[30] R. P. Feynman and A. R. Hibbs. *Quantum Mechanics and Path Integrals*, volume 13. 1965.

[31] S. Floerchinger. Functional renormalization and ultracold quantum gases. (June), 2009.

[32] S. Floerchinger and C. Wetterich. Functional renormalization for Bose-Einstein Condensation. 2008.

[33] S. Floerchinger and C. Wetterich. Superfluid Bose gas in two dimensions. *Phys. Rev. A - At. Mol. Opt. Phys.*, 79(1):1–10, 2009.

[34] R. Folk and G. Moser. Critical dynamics of model C resolved. *Phys. Rev. Lett.*, 91(3):030601, jul 2003.

[35] R. Folk and G. Moser. Critical dynamics of stochastic models with energy conservation (model C). *Phys. Rev. E. Stat. Nonlin. Soft Matter Phys.*, 69(3 Pt 2):036101, mar 2004.

[36] R. Folk and G. Moser. Critical dynamics: a field-theoretical approach. *J. Phys. A. Math. Gen.*, 39(24):R207–R313, 2006.

[37] F. Freire, D. F. Litim, and J. M. Pawlowski. Gauge invariance and background field formalism in the exact renormalisation group. *Phys. Lett. Sect. B Nucl. Elem. Part. High-Energy Phys.*, 495(1-2):256–262, 2000.

[38] R. Gersch, J. Reiss, and C. Honerkamp. Fermionic functional renormalization-group for first-order phase transitions: A mean-field model. *New J. Phys.*, 8, 2006.

[39] R. Gezzi, T. Pruschke, and V. Meden. Functional renormalization group for nonequilibrium quantum many-body problems. *Phys. Rev. B - Condens. Matter Mater. Phys.*, 75(4):1–14, 2007.

[40] H. Gies. Introduction to the functional RG and applications to gauge theories. *Lect. Notes Phys.*, 852:287–348, 2012.

[41] G. Grinstein, S.-k. Ma, and G. F. Mazenko. Dynamics of spins interacting with quenched random impurities. *Phys. Rev. B*, 15(1):258–272, jan 1977.

[42] E. P. Gross. Structure of a quantized vortex in boson systems. *Nuovo Cim. Ser. 10*, 20(3):454–477, 1961.

[43] B. Halperin, P. Hohenberg, and S.-k. Ma. Calculation of Dynamic Critical Properties Using Wilson's Expansion Methods. *Phys. Rev. Lett.*, 29(23):1548–1551, 1972.

[44] B. I. Halperin, P. C. Hohenberg, and S. K. Ma. Renormalization-group methods for critical dynamics: I. Recursion relations and effects of energy conservation. *Phys. Rev. B*, 10(1):139–153, 1974.

[45] B. I. Halperin and C. M. Varma. Defects and the central peak near structural phase transitions. *Phys. Rev. B*, 14(9):4030–4044, nov 1976.

[46] P. C. Hohenberg. Existence of Long-Range Order in One and Two Dimensions. *Phys. Rev.*, 158(2):383–386, jun 1967.

[47] P. C. Hohenberg and B. I. Halperin. Theory of dynamic critical phenomena. *Rev. Mod. Phys.*, 49(3):435, 1977.

[48] S. G. Jakobs, V. Meden, and H. Schoeller. Nonequilibrium functional renormalization group for interacting quantum systems. *Phys. Rev. Lett.*, 99(15):1–4, 2007.

[49] A. Kamenev. *Field Theory of Non-Equilibrium Systems.* Cambridge University Press, 2011.

[50] J. I. Kapusta and C. Gale. *Finite-Temperature Field Theory: Principles and Applications.* Cambridge University Press, 2006.

[51] T. Kloss and P. Kopietz. Nonequilibrium time evolution of bosons from the functional renormalization group. *Phys. Rev. B*, 83(20):205118, 2011.

[52] L. Kofman, A. Linde, and A. A. Starobinsky. Reheating after inflation. *Phys. Rev. Lett.*, 73:3195, 1994.

[53] P. Kopietz, L. Bartosch, and F. Schütz. *Introduction to the Functional Renormalization Group.* Springer, 2010.

[54] J. M. Kosterlitz and D. J. Thouless. Ordering, metastability and phase transitions in two-dimensional systems. *J. Phys. C Solid State Phys.*, 6(7):1181–1203, 2002.

[55] U. Krey. On the critical dynamics of a disordered system. *Phys. Lett. A*, 57(3):215–216, jun 1976.

[56] U. Krey. On the critical dynamics of disordered spin systems. *Phys. B+C*, 86-88:615–617, jan 1977.

[57] L. P. Pitaevskii. VORTEX LINES IN AN IMPERFECT BOSE GAS. *Sov. Phys. JETP-USSR*, 13(2):451–454, 1961.

[58] N. P. Landsman and C. G. van Weert. Real and Imaginary Time Field Theory at Finite Temperature and Density. *Phys.\ Rep.*, 145:141, 1987.

[59] M. Le Bellac. *Thermal Field Theory.* Cambridge University Press, 2000.

[60] A. J. Leggett. Bose-Einstein condensation in the alkali gases: Some fundamental concepts, 2001.

[61] D. S. Lemons. Paul Langevin's 1908 paper "On the Theory of Brownian Motion". *Am. J. Phys.*, 65(1908):1079, 1997.

[62] D. F. Litim. Optimisation of the exact renormalisation group. *Phys. Lett. B*, 486(1-2):92–99, jul 2000.

[63] D. F. Litim. Derivative expansion and renormalisation group flows. *J. High Energy Phys.*, 2001(11):059–059, nov 2001.

[64] D. F. Litim. Optimized renormalization group flows. *Phys. Rev. D*, 64(10):105007, oct 2001.

[65] D. F. Litim. Critical exponents from optimised renormalisation group flows. *Nucl. Phys. B*, 631(1-2):128–158, jun 2002.

[66] D. F. Litim and D. Zappalà. Ising exponents from the functional renormalization group. *Phys. Rev. D*, 83(8):085009, apr 2011.

[67] S.-K. Ma. *Modern Theory of Critical Phenomena.* Westview Press, 2000.

[68] P. C. Martin, E. D. Siggia, and H. A. Rose. Statistical dynamics of classical systems. *Phys. Rev. A*, 8(1):423–437, 1973.

[69] N. D. Mermin and H. Wagner. Absence of Ferromagnetism or Antiferromagnetism in One- or Two-Dimensional Isotropic Heisenberg Models. *Phys. Rev. Lett.*, 17(22):1133–1136, nov 1966.

[70] D. Mesterházy, J. H. Stockemer, L. F. Palhares, and J. Berges. Dynamic universality class of Model C from the functional renormalization group. *Phys. Rev. B*, 88(17):174301, 2013.

[71] D. Mesterházy, J. H. Stockemer, and Y. Tanizaki. From quantum to classical dynamics: The relativistic O(N) model in the framework of the real-time functional renormalization group. *Phys. Rev. D*, 92(7):076001, oct 2015.

[72] D. S. Mitrinovic and J. Keckic. *The Cauchy Method of Residues: Theory and Applications (Mathematics and its Applications).* 1984.

[73] E. Nakano, V. Skokov, and B. Friman. Transport coefficients of O(N) scalar field theories close to the critical point. *Phys.\ Rev.*, D85:96007, 2012.

[74] E. Noether. Invariant variation problems. *Transp. Theory Stat. Phys.*, 1(3):186–207, jan 1971.

[75] J. M. Pawlowski and N. Strodthoff. Real time correlation functions and the functional renormalisation group. pages 1–20, 2015.

[76] R. D. Pisarski and F. Wilczek. Remarks on the chiral phase transition in chromodynamics. *Phys. Rev. D*, 29(2):338–341, jan 1984.

[77] S. Sachdev. *Quantum Phase Transitions*. Cambridge University Press, 2011.

[78] J. Sengers. Thermodynamic Behavior of Fluids Near the Critical Point. *Annu. Rev. Phys. Chem.*, 37:189–222, 1986.

[79] L. M. Sieberer, a. Chiocchetta, a. Gambassi, and S. Diehl. Thermodynamic Equilibrium as a Symmetry of the Schwinger-Keldysh Action. pages 1–20, 2015.

[80] D. Son and M. Stephanov. Dynamic universality class of the QCD critical point. *Phys. Rev. D*, 70(5):056001, sep 2004.

[81] M. A. Stephanov. QCD phase diagram: an overview. page 15, dec 2006.

[82] Y. Tanizaki. Fermionic functional renormalization group with multiple regulators and the BCS-BEC crossover. *arXiv Prepr. arXiv1402.0283*, page 18, 2014.

[83] U. C. Täuber. *Critical Dynamics: A Field Theory Approach to Equilibrium and Non-Equilibrium Scaling Behavior*. Cambridge University Press, 2014.

[84] N. Tetradis and C. Wetterich. Critical exponents from the effective average action. *Nucl. Phys. B*, 422(3):541–592, jul 1994.

[85] S.-Y. Wang. Nonequilibrium Phenomena in Quantum Field Theory: From Linear Response to Dynamical Renormalization Group. page 150, oct 2001.

[86] C. Wetterich. The average action for scalar fields near phase transitions. *Zeitschrift fur Phys. C Part. Fields*, 57(3):451–469, 1993.

[87] J. Zinn-Justin. *Quantum Field Theory and Critical Phenomena*. Oxford University Press, 2002.